Doctor of Philosophy

A Study on the Effect of Intake Port Modification to Improve the In-Cylinder Flow Characteristics of Small Motorcycle Engine

The Graduate School

of the University of Ulsan

Department of Mechanical Engineering

Bambang Wahono

A Study on the Effect of Intake Port Modification to Improve the In-Cylinder Flow Characteristics of Small Motorcycle Engine

Supervisor: Prof. Lim, Ocktaeck

A Dissertation

Submitted to

the Graduate School of the University of Ulsan

In partial Fulfillment of the Requirements

for the Degree of

Doctor of Philosophy

by

Bambang Wahono

Department of Mechanical Engineering

University of Ulsan, Republic of Korea

December 2020

A Study on the Effect of Intake Port Modification to Improve the In-Cylinder Flow Characteristics of Small Motorcycle Engine

This certifies that the dissertation of Bambang Wahono is approved.

Committee Chair	**Prof. Park, Kyu Yeol**
Committee Member	**Prof. Lee, Sang Wook**
Committee Member	**Prof. Lee, Yoon Ho**
Committee Member	**Dr. Lee, Young Jae**
Committee Member	**Prof. Lim, Ocktaeck**

Department of Mechanical Engineering

University of Ulsan

December 2020

ABSTRACT

A Study on the Effect of Intake Port Modification to Improve the In-Cylinder Flow Characteristics of Small Motorcycle Engine

Department of Mechanical Engineering
Bambang Wahono

The in-cylinder flow is one of the important factors that affect the quality of air-fuel mixture in engine. One parameter that affect the in-cylinder flow is intake port design. In this study the effect of intake port modification was investigated to improve the flow characteristics of small motorcycle engine. An experimental system with a steady flow bench for a variety of valve lifts at two pressure drops of 300 and 600 mmH_2O was installed and a simulation model based on CFD method was setup. Moreover, the modification of intake port based on the flow direction and inclination angle were investigated to improve the flow characteristic of small motorcycle engine. Looking at the results, the intake port with 15º and 30º increase the flow coefficient compared to the original port of 2.46% and 6% respectively. The increase of pressure drops increases the flow velocity by two times to 100 m/s and make the vortex core to move closer to the cylinder axis. Increase in pressure drop at the beginning of valve lift appeared to have no effect on the swirl ratio until the valve lift reached 5 mm. However, the swirl ratio got a 25% reduction when the valve lift reached 6.25 mm. The flow velocity maximum of the tangential port is almost double compared to the all helical models at 60 m/s. The tangential port with all inclination angle has same flow velocity maximum of 60 m/s in the center of cylinder. However, the port 30º has a more even distribution of velocity magnitude in all directions compared to other models. In the vertical plane, the greatest flow velocity occurs at the 6.46 mm valve lift at port 30º and 15º at 78.5 m/s on the upper side of the cylinder near the intake port. Compared to other models, port 30º has the most turbulent kinetic energy, length scale and kinematic viscosity with an increase of 9.55%, 4.65% and 15.25% respectively compared to the original port. Based on this case study, the tangential port 30º is the most optimal port compared to other models where this port has a better increase in flow velocity and vortices which results in increased turbulence in the cylinder. The increased turbulence is expected to result in a more homogeneous mixing of air-fuel in the cylinder engine.

Keywords: Small motorcycle engine, in-cylinder flow, CFD, steady state flow bench, inclination angle, flow direction.

ACKNOWLEDGEMENT

I would like to express my sincere gratitude to my advisor Professor Ocktaeck Lim for his continuous support of my Ph.D. study, for his generous advice, invaluable guidance, and constant encouragement in making this research possible. I would also like to express my thanks to the Graduate School of Mechanical and Automotive Engineering, University of Ulsan.

My sincere thanks go to all members of Smart Powertrain Laboratory especially Ardhika Setiawan and Muhammad Khristamto Aditya Wardana. I will always appreciate your valuable support during my experimental and simulation setup. Many special thanks go to members of Internal Combustion Engine Laboratory and the Director of Research Centre for Electrical Power and Mechatronics, LIPI Bandung for their excellent co-operation, inspirations, and supports during this study. Special thanks go to Program for Research and Innovation in Science and Technology (Riset-Pro) Ministry of Research, Technology and Higher Education of the Republic of Indonesia for providing me the opportunity, approval, and support to pursue my Ph.D. at University of Ulsan.

I acknowledge my sincere indebtedness and gratitude to my parents (Bapak Trisno Suwito and Ibu Ngatiyem) for their love, dream, and sacrifice throughout my life. I acknowledge the sincerity of my parents-in-law (Bapak Abdullah rohimahullah and Ibu Siti Romlah), who consistently encouraged me to carry on my higher studies in Korea. I am also grateful to my wife (Sa'idatul Abadiyah) and my daughters (Rumaysho, Tsuroyya and Maryam) for their sacrifice, patience, and understanding that were inevitable to make this work possible. I cannot find the appropriate words that could properly describe my appreciation for their devotion, support, and faith in my ability to attain my goals. Special thanks should be given to my supervisory committee members. I would like to acknowledge their comments and suggestions, which was crucial for the successful completion of this study.

TABLE OF CONTENTS

LIST OF FIGURES

LIST OF TABLES

ABBREVIATION AND NOMENCLATURES

AMR	adaptive mesh refinement
B	Bore
BTDC	Before top dead center
CA	Crank angle
CAD	Computer aided design
CCV	Cycle-to-cycle variations
CFD	Computational fluid dynamics
CI	Compression ignition
CR	Compression ratio
DOHC	Dual overhead cam
DISI	Direct injection spark ignition
EGR	Exhaust gas recirculation
EVO	Exhaust valve open
GCI	Gasoline compression ignition
GVSTD	Guide vane swirl and tumble device
HSPIV	High speed particle image velocimetry
HWA	Hot wire anemometry
IVC	Intake valve closure
IVECO	Industrial Vehicles Corporation
IVO	Intake valve opening
K	Conductivity

LDA	Laser doppler anemometry
LES	Large eddy simulation
MVL	Maximum valve lifts
NVO	Negative valve overlap
OHV	Overhead valves
POD	Proper orthogonal decomposition
PCC	Partial cell in cartesian coordinator
RMS	Root-mean-square
RSTM	Reynolds stress turbulence model
SI	Spark ignition
SOHC	Single overhead cam
STL	Stereolithography
TDC	Top dead center
PIV	Particle image velocimetry
PISO	Pressure implicit with splitting of operators
RNG	Renormalized group
SR	Swirl ratio
TKE	Turbulent kinetic energy
TR	Tumble ratio
TRx	cross tumble about x coordinate
TRy	normal tumble about y coordinate
Ym	mass fraction of species m

$\omega_1, \omega_2, \omega_3$	angular speed of the flow about the center of mass in the x, y, z direction
L_1, L_2, L_3	the angular momentum about the x, y, and z axis
I_1, I_2, I_3	the moment inertia about the x, y, and z axis
ε	turbulence dissipation rate
$c\mu$	turbulence model constant
le	the turbulent length scale
ρ	density
μ	viscosity
τ	Reynolds stress
S	source term
δij	Kronecker delta
σ	Viscous stress tensor
Dfm	mass diffusion coefficient
aTDC	after top dead center
bTDC	before top dead center
A_v	inner curtain area of valve, m^2
Aseat	valve inner seat area, m^2
Cd `	discharge coefficient, dimensionless
Cp	specific heat, J/kgK
C_f	flow coefficient, dimensionless
D_v	valve diameter, m
D	intake valve seat diameter, m

L_v	valve lift, m
$\dot{m}_a$	actual mass flow rate, kg/s
$\dot{m}_i$	ideal mass flow rate, kg/s
N	engine speed, rpm
P	pressure, MPa
Patm	pressure, MPa
Po	stagnation pressure, MPa
P_c	gas pressure [Pa]
P_{in}	intake pressure, MPa
Pr	Prandtl number, dimensionless
R	ideal gas constant, kJ/mol·K
R_{air}	universal gas constant for air, kJ/mol·K
Re	Reynolds number, dimensionless
Sc	Schmidt number, dimensionless
T_{in}	intake temperature, K
T	temperature, K
To	stagnation temperature, K
V	volume [m^3]
V_d	displacement volume, cm^3
u_i	velocity component i, m/s
u_p	mean piston speed, m/s
γ	ratio of specific heats, dimensionless

Q	measured volume flow rate, m^3/s
Vo	velocity in the head, m/s
ΔP	pressure drop, mmH_2O
Ø	transported variable, dimensionless
Df	diffusion coefficient, dimensionless
k	turbulent kinetic energy, m^2/s^2
ε	turbulent dissipation, m^2/s^3

1. INTRODUCTION

1.1 Background

In the last few decades, engine designers around the world have been challenged to produce engines that have good performance and low emissions [1–7]. Some ways by many researchers to meet this challenge are the use of alternative fuels [8–12], optimizing the combustion process [13][4][14][6] and redesigning engine components [15–18]. Some researchers have been done the research to improve the performance and decrease the emission by using alternative fuels such as Jatropha biodiesel fuel and soybean biodiesel. Other researchers have succeeded in improving engine performance by optimizing combustion processes such as lean burn combustion method [14], fuel injection strategy method [14], the exhaust gas recirculation (EGR) method [4][19–23] and higher compression ratio [13]. Another interesting research is to redesign engine components such as modification of piston [16], exhaust manifold [17], combustion chamber [15] and intake manifold [18].

Intake manifold is still an interesting subject of study because it plays an important role in the development of modern internal combustion engines, especially to improve engine efficiency [24]. The intake port is an integral part of the intake manifold that is directly connected to the cylinder. The intake port is one of the important components of engine intake system which structures directly affect the process of turbulence, the distribution of air velocity and the entering of air volume to the cylinder [25]. The development of the design of the intake port is one of the most important things in reducing exhaust emissions and improving engine performance. However, it is difficult to obtain low emission levels in the engine because it is not easy to make optimal mixture formations in the cylinder [26]. Utilizing the flow process generated by the intake port is one of the most important ways to improve the mixing process. Therefore, good knowledge about the air motion in the cylinder and how to design the intake port that able to create the optimal mixture formation is needed [27].

In the literature, some studies related to the using of new design of intake manifold have been conducted by many researchers. For example, Gustavo *et. al.* [24] investigated numerically and experimentally effect of the runners geometries variation of intake manifold to improve the volumetric efficiency. They reported that numerically that the manifold with a new runner model which has a length of 0.30 m increases the volumetric efficiency 4% greater

than the original model. They also reported experimentally manifold with a new runner model at 3500 rpm increasing volumetric efficiency by 6%. Yang *et.al*. [28] have been conducted the study about the effect of variation split intake port of three engine model to improve the engine volumetric efficiency using steady flow bench and compared with computational fluid dynamics (CFD) simulations. They reported that engine which has a more aggressive charge motion in intake port have higher value of tumble ratio and swirl ratio than other models both in experimentally and numerically. Cui *et.al*. [18] developed model of new tangential intake port made by computer aided design (CAD) to with a parametric approach to improve efficiency, traceability, and flexibility. They also use the CFD method to determine the effect of structural parameters on the intake port performance. They reported that variations in structural parameters made the large-scale vortex intensities and flow capacities change more regularly. Huang et.al. [29] have conducted research experimentally on the effect of elliptical and circular intake ports on the flow evolution on a single cylinder reciprocating motorcycle engine with particle image velocimetry (PIV). They reported that both models of the intake port began to form a vortex around the middle area of the cylinder during the intake stroke. However, the vortex disappears during the compression stroke on the circular intake port, while the vortex made in the cylinder with elliptical intake port continues to develop into tumble motion. They also reported that the turbulence intensity and the averaged tumble ratio of the engine with elliptic intake port bigger than the engine with the circular intake port. The engine performance also was increased with the elliptic intake port. Adomeit *et.al*. [30] investigated evolution of cyclic fluctuations and the charge motion generation by high speed particle image velocimetry (HSPIV) at two different intake port designs, high tumble port and filling port equipped with the tumble plates in turbo charged DI SI engine. They reported that a filling port design have similar behavior with tumble port design which provides slightly more tumble. However, the tumble appeared to be smaller in port design without tumble plates at the end of compression stroke. Ali jemni *et. al*. [31] have been conducted a study numerically and experimentally about the effects of two intake manifolds on the in-cylinder flows in heavy duty IVECO engine. The first manifold has an unspecified geometrical shape while the second manifold has an optimal filling geometry. They reported that it is possible to know the characteristics of turbulence and flow structure in the cylinder so that the effectiveness of the intake system geometry can be well studied. Falfari *et.al* [32] have been conducted a study about the effect of squish area and head shape on the formation of tumble flow and turbulence kinetic energy on a small motorcycle engine. They reported that the highest turbulence was

obtained in the combustion chamber which had a less squish area close to the spark plug at the time of ignition. Falfari *et.al*. [33] also have been analyzed the effect of the compression ratio, the intake duct angle and the piston shape on small motorcycle engine. However, the squish area and the head shape were kept constant. The goal of this study is to find out which parameters are the most dominant in accelerating combustion to find the optimal set-up. They reported that the most influencing parameter for the combustion speed was the duct of intake. They also report that reducing the compression ratio only affects the rate of change tumble to a level lower than the average turbulence in the cylinder. Kim et.al. [34] have been conducted the effect of variation of intake port design parameters on the swirl that is produced within a diesel engine. They reported that a key factor in producing a high swirl ratio is to control the direction of the flow of air entering through the intake valve seat. Moreover, the bypass near the inlet valve seat changes the swirl flow. In addition, the use of bypass was an effective method for increasing the swirl ratio without sacrificing the mass flow rate.

In mentioned studies, researchers numerically and experimentally investigated the flow characteristics for many designs of intake port. However, very few researches which investigate the effect of variation of intake port inclination and effects of the modification of tangential and helical intake port based on the flow direction on in-cylinder flow engine, especially on small motorcycle engines. Moreover, small motorcycle engines contain small space making it more difficult to visualize and analyze the flow characteristics than large engines. Therefore, an in-depth investigation to provide a better understanding of the flow characteristics mainly based on the variation of the intake port inclination and modification of the tangential and helical intake port on a small motorcycle engine is needed. In addition, the stability of the flow characteristics is also studied to ensure that the results obtained are optimal. This work is expected to act as a basis for visualizing the in-cylinder flow fields and optimizing the internal combustion engine combustion chamber in small motorcycle engines, especially in motorcycles.

1.2 Approach

In this thesis, the cylinder head of four-stroke and four-valves single-cylinder small motorcycle engine 125 cm^3 was examined. Any calculation of port flow in the small motorcycle engine was based on one dimensional characteristic for all ports. In this study, pressure drops used to perform the tests was chosen based on the criteria of Reynolds number. Two pressure

drops and chosen to confirm the flow motion were 300 and 600 mmH_2O. Then, a torque meter for steady-state flow bench was taken to measure the flow.

Firstly, the geometry and 3D design of the intake port must be well prepared. Many designs of the intake port parameters give affects to the flow characteristics on the in-cylinder engine [35]. Among these design parameters, the various of the intake port inclination and the various tangential and helical intake port modifications based on the flow direction were chosen as the numerical and experimental parameter to be investigated. To analyze the effect of these design parameters on the airflow rate, the various of the intake port inclination and the various tangential and helical intake port modifications based on the flow direction were installed on the cylinder head. The variation of intake port inclination is -15º, 0º, 15º and 30º. These intake port models will be compared with original intake port (11.5º). The various helical intake port modifications based on the flow direction are helical intake port with same direction, helical intake port with opposite direction (inward) and helical intake port with opposite direction (outward). These helical intake port modifications will be compared with the tangential intake port. The prototypes of intake port design used in testing designed with Solid work and manufactured by 3D printing technology. In order to save cost, five types of inclination intake ports and three types helical intake ports, one type tangential intake port and one body deck representing the bottom structure of the cylinder head were separately made. A mounting and positioning structure were assembled to the body deck and it allowed combining different intake ports to form various combinations. Moreover, an inclined flow guiding plane was produced at the entrance of the intake ports in order to better guide the airflow.

Secondly, Preparing the experimental apparatus for steady-state flow benches. Measurement of the inflow rate in steady-state conditions is one of the significant keys that have a big influence on engine power and combustion. The tool to measure the inflow rate is the steady-state flow benches. This tool was made to investigate the intake stroke of the real engine operation. This tool can be explained as follow. The airflow is driven by fan of blower and passes the surge tank, control valve and then laminar flow rate. It enters the engine head at last. The intake valve was set using a micrometer manually and conditioned from valve lift of 2 mm to 6.46 mm (valve lift maximum). The pressure drop between the cylinder head and the atmosphere was set to be constant 300 and 600 mmH_2O during the experiment. The feedback control valve regulates the desired pressure at different valve lift settings by releasing air to the pressure relief valve. So that the pressure between the inlet in the intake port and the bottom of

the cylinder can be kept constant. The pressure transducers and thermocouples are also used to measure the pressure and temperature of the intake air. After that, the angular momentum of the air is changed to rotational force with a honeycomb-type commutator located 1.75 times the diameter under the cylinder head. The rotation force is transmitted by a load cell connected to the commutator [36]. Finally, the air flow rate can be measured properly.

Next step is validating the experiment result with the numerical methods. To investigate the effect of the various of the intake port inclination and the various helical intake port on the flow characteristic and comparing to the original intake port, it is necessary to analyze the in-cylinder flow during the intake stroke. Therefore, the three-dimensional flow numerical simulations were carried out to predict the flow characteristics produced in the cylinder. In this study, the numerical analysis was executed using one of the commercial CFD package, CONVERGE. CONVERGE software requires an input file in the form of surface geometry in the format of stereolithography (STL) created using CAD software. The graphical user interface pre-processor arranges and exports the geometry surface to the CONVERGE solver. The surface definition file recognizes surface geometries with unique boundary areas and the CONVERGE solver during runtime has a function to automatically build mesh volumes. CONVERGE software using an innovative boundary approach was able to eliminate the need for grid computing. Steady-state conditions with open cylinder ends were chosen to be the boundary conditions in this study. In this study, the position of the exhaust valve is closed while the intake valve position of each test is made in the fix position. Air is chosen to be fluid in this steady-state model. The air pressure and temperature are adjusted according to experimental data around 1 bar and 300 K respectively. Whereas the air mixture has a composition of 77% nitrogen and 23% oxygen based on mass and the ideal gas law is used to calculate air density. Everything related to the simulation conditions is controlled in the input file. The renormalized group (RNG) k-ε was chosen as a turbulence model to simulate the flow and solid surface to identify the wall law in CONVERGE. Steady state models for each intake port model are assumed at different mass flow rates. For all models, the temperature in the cylinder is made around 300 K. The discrete Navier-Stokes equation is solved using the implicit discretization procedure on the Cartesian grid. Mass, momentum, and energy conversion equations are chosen as equations commonly used to construct the flow models in cylinder. While, the velocity-pressure coupling problem is solved by using pressure implicit with splitting of operators (PISO) algorithm that is applied with the Rhie-Chow scheme [37].

1.3 Objectives of the study

The present study focuses on investigation of the flow characteristic through the inlet port/valve and the cylinder on small motorcycle engine using numerical simulation and experimental methods. In detail, the objectives of this thesis are:

(i) To investigate experimentally and numerically in-cylinder flows of the original small motorcycle engines under steady-state conditions. This work was conducted on the engine head for several fixed valve lifts at variation of pressure drops.

(ii) To investigate the effect of the intake port geometry based on the flow direction on the in-cylinder flow and comparing to the original intake port

(iii) To analyze the flow visualization patterns during both intake and compression strokes.

(iv) To investigate the intake port velocity distribution around the valve curtain of two valve for varied valve lifts with many models of intake port.

(v) To investigate the effects of the various of the intake port inclination on the small motorcycle engine's breathing characteristics experimentally and numerically. Steady flow benches were conducted to investigate the flow characteristic and flow rate by using torque meter steady flow bench.

1.4 Organization of the thesis

Chapter 1 presents the scope of the thesis and gives a brief explanation to the topic of the research and to put it in context with preceding studies done on the same issue. The improvements are briefly described with the research aims and objectives. In chapter 2, a review of the most important findings of the previous work related to the objectives of the present study is given. This review summarized some studies related to the using of new design of engine component especially intake port both in the experimental works and simulation studies. Based on this review, some issues can be inferred as a starting point for the present study. Chapter 3 explains describes the setup of the steady flow bench with head cylinder of small motorcycles engine. The experimental test and analysis procedures are introduced as well. Furthermore, the detail description of the equations governing the motion of the flow, the numerical procedure, and the solution algorithm are presented to validate the experiment result. Chapter 4 aims to explain the experimental and numerically investigating in-cylinder flows of

a small motorcycle engine under steady-state conditions. The experiment was conducted in the engine head for a variety of fixed valve lifts at two pressure drops (300 and 600 mmH_2O). Besides, this study attempted to analyze the characteristics of in-cylinder flows in a small motorcycle engine by applying CFD methods. Moreover, the evolution of the in-cylinder flow small motorcycle engine was illustrated in this study. Chapter 5 discusses and analyses numerically and experimentally the results of the in-cylinder flow of small motorcycle engines for various intake port modifications based on the flow direction. This study also investigates the intake port velocity distribution with many models of intake port around the valve curtain of two intake valves for varied valve lifts. In addition, this study also analyzed variations inflow motion in-cylinder engine in both horizontal and vertical planes on all intake port models. Moreover, this study also investigates cycle-to-cycle of the tumble ratio and TKE development with some intake port models under motoring conditions to assess stability at the beginning of the developing stage. Chapter 6 discusses and analyses numerically and experimentally the results of the in-cylinder flow of small motorcycle engines based on the variation of the intake port inclination. The variation of intake port inclination is -15º, 0º, 11.5º (original), 15º and 30º. In addition, this study also investigating variations inflow motion in-cylinder engine in both horizontal and vertical planes on all variations of the intake port inclination. Moreover, this study also aimed to investigate the influence of the variation of the intake port inclination on the characteristics of the airflow in-cylinder which is carried out in small motorcycle engines under motoring conditions. Finally, summary and conclusions of this thesis and summarizes experimental and simulation studies and combines understanding of various diagnostics to gain insight into characteristic of engine flow are explained in chapter 7.

2. LITERATURE REVIEW

2.1 Introduction

The purpose of this chapter is to provide an explanation of previous research efforts related to current research. An overview of other relevant research studies is also provided. This review is arranged chronologically to offer insight into how past research efforts have laid the foundation for further studies, including this research effort. This review is detailed so that current research efforts can be appropriately designed to add to the current body of literature and equitably the scope and direction of this research effort. In the beginning part will be explained about the basic of a motorcycle engine including the important parts that are in it and those related to this research. The next section will explain the design of some engine components. Some characteristics of the flow inside the intake port and engine cylinder are also discussed in detail in this chapter. Finally, some of the reviews conducted by previous researchers related to this study are also explained in detail at the end of this chapter.

2.2 Small motorcycle engine

Nearly all motorcycles manufactured lately have gasoline internal combustion engines using either four-stroke or two-stroke engines. In the scope of this thesis, the four-stroke small motorcycle engine will be focused. The small motorcycle engine may have single or two cylinders, the engine capacities typically ranged from about 50 cc to 350 cc normally. The motorcycle has some advantages when compare to automobile such as lower cost price, generally better fuel economy, better performance per dollar, more parking options, advantages in slow or stopped traffic, retains value, customization. These advantages explain why the motorcycle is very popular and the number of this vehicle is increasing day by day, especial in the Southeast Asia countries. Nevertheless, with the increasingly stringent emission laws, the two-stroke engine has begun to be abandoned [38]. In fact, a two-stroke engine has fewer moving parts than a four-stroke engine and produces twice the number of power strokes per revolution. Motorcycle engines that use a four-stroke cycle consist of (1) intake stroke or induction stroke, (2) compression stroke, (3) expansion or power stroke, (4) exhaust stroke. The combustion process occurs when the piston approaches the end of the compression stroke, or top dead center (TDC) of the piston position, between stroke 2 and 3. On the other hand, most motorcycle engine manufacturers can be categorized into two major types namely the gasoline engine (spark ignition (SI) engine) or diesel engine (compression ignition (CI) engine).

Spark ignition (SI) engines are mainly defined by a well-mixed air-fuel charge, which is created by port fuel injection at the stoichiometric air-fuel ratio. Combustion is started by using a spark [39], which proposed flame propagates through the mixture burning fuel and releasing heat. Stoichiometric air-fuel ratios allow improved engine's operating stability and reduced cycle-to-cycle variations as the combustion is more easily started and the flame propagates faster compared to more dilute air-fuel mixtures. While, the combustion process in a CI engine starts when the air-fuel mixture self-ignites due to high temperature in the combustion chamber caused by high compression [39]. In conventional CI engines, fresh air enters the combustion chamber during the intake stroke then compressed at compression stroke, after that fuel is injected when piston position is near TDC. The fuel injected/spray atomizes, evaporates, mixes, and auto-ignites promptly. The heat release is dominated by the speed of evaporation and mixing rather than that of flame propagation as in SI engines. Almost all automotive engines consist of two main parts namely the cylinder block and cylinder head [40]. Both components and supporting systems, such as fuel systems, cooling systems, electrical systems, lubrication systems, etc. are inseparable parts of an engine in a vehicle. Let's look more closely at these support systems, now we will concentrate on the cylinder block and cylinder head.

2.2.1 Cylinder block

Cylinder block, or commonly abbreviated as block, and the main components that are installed on the inside of the block have a vertical hole called a cylinder, where the amount varies (there are 1 cylinder, 2 cylinders, 3 cylinders, etc.). When the cylinder head is mounted, the cylinder head is bolted to the upper surface of the block and closes the top end of the cylinder. Special heat-resistant gaskets, called cylinder head gaskets, are installed between the block surface and cylinder head. Block is usually made of cast iron or aluminum. Block has channels where the cooling flow is used to prevent the engine from getting too hot. There are also channels (galleries) that are printed in the block as a place for oil flow, which functions as the engine lubrication channel. Some components contained in the cylinder block include a crankshaft, flywheel, connecting rod, piston and camshaft.

Crankshaft serves to change the back and forth of the piston into rotary motion. This crankshaft is located at the bottom of the engine block in an area called the crankcase. The crankshaft is supported by the bearing and bearing cap in its place inside the crankcase. This bearing is called the main bearing. Connecting rods, which connect the piston and crankshaft,

are attached to the crankshaft by using number of bearings and caps. These bearings are usually called big end bearings. Meanwhile the flywheel on vehicles that use a manual transmission (gear box) has a large size and weight bolted to the end of the crankshaft. This serves to smooth the work of the engine and provides a driving surface for the clutch. The flywheel gear is mounted on its holder through the machining process. A small gear at the end of the shaft of the starter motor is connected to the flywheel gears when the starter motor is working. This will turn the crankshaft and start the engine. Flywheel on vehicles that use automatic transmissions is commonly called a drive plate. Usually thinner and lighter than manual transmission vehicles. While the connecting rod has a function to move the force that pushes the piston down to the crankshaft, during the process of business steps. Therefore, in order not to break, the connecting rod must be strong. The rod has two places for bearings. Large bearings are placed on the crankshaft and small bearings are placed on the piston. A pin is used to connect the piston to the connecting rod, this pin is called a piston pin or gudgeon pin. Another component called the piston functions to move the combustion pressure of the fuel and air mixture through the connecting rod to the crankshaft. Usually the pistons are equipped with three rings around it. The two main rings are the compression rings. The ring seals the gap between the piston and cylinder wall. The ring is designed to prevent the high-pressure gas from the combustion process flowing through the piston. The third ring on the piston is the oil ring. Its function is to prevent lubricating oil on cylinder walls enter the combustion chamber. A piston ring that has worn out in a vehicle can often be detected through smoking exhaust emissions. This smoke is caused by oil, which successfully exceeds the piston and burns in the combustion process. Gudgeon pin that connects the piston with the connecting rod, allowing the rod to swing inside the piston as a result the lower end of the connecting rod and crankshaft rotate.

The last component in the cylinder block is the camshaft. Camshaft can be placed on the cylinder block or on the cylinder head. Some engines have more than one camshaft. Even so the number of camshafts on the engine is not a problem, as well as the placement. The basic function of the camshaft is to drive the inlet valve and the exhaust valve found on the cylinder head. Camshaft is driven by a set of gears contained in the crankshaft and these gears are called timing gear. Another method is used to rotate the crankshaft by using a timing belt and chain. The camshaft is supported by bearings on the front and rear of the crankcase. This shaft is usually not symmetrical shape, there are protuberances along the shaft. This bulge is called a

cam and there is one for each valve. When the camshaft rotates a small cylindrical object, called a cam follower (or sometimes called a lifter or tappet), follows the shape of the cam, the work moves up and down. If an open valve is an inlet valve, the shape of the cam and its position on the camshaft will ensure that the valve is completely open when the piston moves downward in the cylinder, at the entry step. The shape of the cam ensures that the valve is completely closed in the next cycle. In the same way if the valve opened by the cam is the exhaust valve, the cam will open the exhaust valve when the piston moves up during the exhaust step, ie when the piston moves to the top of the cylinder when the exhaust step; allow the valve to remain closed in subsequent steps[40].

2.2.2 Head cylinder

It was mentioned earlier that the cylinder head insulated the top end of the cylinder. This is not the only function, so this time we will examine its important role in how the engine works. The main function of the cylinder head is to provide a space where the mixture of fuel and air can be burned efficiently. This is done by providing a specially shaped hole or space that is positioned above each cylinder, when the head is bolted to the block. The cylinder head also has channels called ports. Inlet is a channel through a mixture of fuel and air into the combustion chamber. Exhaust channel is used gas channel from inside the combustion chamber into the exhaust system. These inlet and exhaust valves are placed as insulation against the combustion chamber and the exhaust channel, when the valves are in a closed position. The intake manifold and the exhaust manifold, the pipes that supply the fuel mixture and carry used gas out of the cylinder head, are bolted to the side of the cylinder head, so that the pipes are in line with the channel. The valve drive gear is mounted on the top of the cylinder head. Valves can be driven by push rods, as explained earlier in this section, or by other alternatives, where one or more camshafts are mounted directly on the cylinder head which is driven by chains or belts from the end of the crankshaft. When this arrangement is used, the engine is classified as over head camshaft (overhead cam) engine. Some engines are referred to as engine multivalves, this means the engine has more than two valves per cylinder [40].

The cylinder head design has a significant effect on combustion efficiency, and hence engine power output. The head may be flat, in this case the combustion chamber is inside the cylinder or depressed in the piston crown, but usually, the dome inside the cylinder head provides most of the combustion volume. Motorcycles use small valves in various designs:

side valves, overhead valves (OHV) with pushrod operation, single overhead cam (SOHC), and dual overhead cam (DOHC). A cylinder with a desmodromic valve may have three or even four camshafts. SOHC or DOHC cylinder heads will have at least two valves per cylinder (1 inlet and 1 exhaust), but a multi-valve engine may have three (2 inlet and 1 exhaust), or four (2 inlet and 2 exhaust), or even five (3 inlet and 2 exhaust). The cylinder head is the hottest part of the engine and requires adequate cooling, usually air cooling, oil cooling, or liquid cooling. Some motorcycles can be identified by the type of cylinder head, namely the airhead, panhead, oilhead, and even knucklehead. The part of head cylinder is shown in Fig. 2.1.

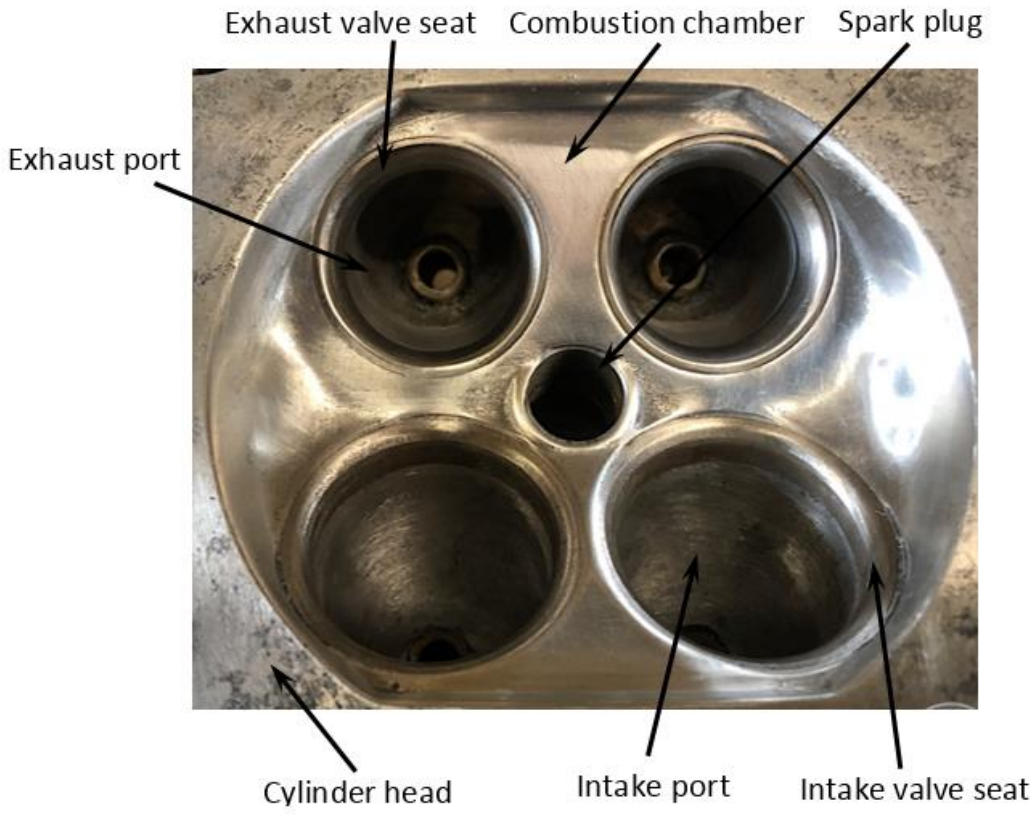

Fig. 2.1. The part of head cylinder [41]

2.3 Improvement of intake port design

In order to improve engine performance specifically related to the development of intake port design, a good understanding of the basics of three-dimensional turbulent flow in intake port and cylinder area is required. This is one of the reasons why there are still many researchers in the world to remain focused on conducting research in this field both experimentally and theoretically. Previous researchers used classic diagnostic techniques to investigate the engine flow field, such as the hot-wire anemometer method (HWA) [42–45]

and PIV [46] to make measurements. Several other methods have also been developed to better understand the flow at the intake and cylinder both experimentally and in simulation such as the use of optical methods with laser-Doppler anemometry (LDA) [47–51], which is carried out in order to avoid flow distortion that can damage the accuracy resulting from physical inspection. Moreover, increasingly rapid developments in the field of computing have made methods to predict the flow of both the intake and cylinder engines with three dimensions more realistic and feasible to apply. This has encouraged the use of computational studies increasingly favored by many researchers in the world [52–54]. The following is an explanation of some improvement of intake port designs.

2.3.1. Intake port shape effect

Intake ports largely determine the performance of internal combustion engines in general and especially motorcycle engine. It has been recognized by the engine designer that engine power output can be increased by increasing the flow characteristics of the induction system. The following are a few examples of studies conducted by several researchers related to the effect of intake port shape on flow characteristics in the engine.

Andras, and Zoltan [55] have investigated the air flow characteristics of the intake port of a diesel engine by numerical simulation. They developed and compared the mathematical model of the engineering problem and their numerical with the actual physical measurements. They reported that they found that a first order finite volume method, the Vijayasundaram flux vector split method with local time-stepping is suitable for computing the flow characteristics, namely the flow and swirl coefficients, accurately. By accuracy its mean that the computed and the measured quantities differ in 0–0.5% and 0.5–10%, respectively, validating their numerical model. Applying subsequently this code and a domain deformation they were able to increase in 1% the flow coefficient under the constraint of a constant swirl number, which is significant since only small modifications were allowed solutions.

Lee *et.al* [56] have investigated the intake port shape for a five-valve engine for the developing of a high efficiency gasoline engine. In this study, they developed intake multivalve cylinder heads which manufactured by using a three-dimensional computer-assisted design program, and steady state flow experiments and flow visualization experiments which performed with these cylinder heads. They reported that the five-valve engines have larger valve opening areas, have larger intake flowrates than the four-valve engines. Moreover, the

flowrates of various port heights show similar values. For the case of low port height, a reduction of flow increase rate characteristics was observed clearly at the high valve lift. At low and middle valve lifts, the intake port with three equal size valves shows better intake flow characteristics than the intake port with two large side valves and one small valve. At high valve lift, however, it shows lower flow characteristics than the others do. They also concluded that the swirl fow of the five-valve engine was observed to be small because the ports were designed symmetrically. The flow visualization tests showed that the five- valve engine of small valve diameter formed more developed tumble flow than the four-valve engine did.

Yoshihara *at.al* [57] describes the key requirements for engine design to generate high tumble flow with high flow coefficient by using both simulation and experiment. It is important that the air flow of tumble is straight and runs along the wall of the combustion chamber near the exhaust valves for high tumble flow efficiency. As a result, better performance can be achieved by changing the layout of the valve angle and the intake port. The generated tumble flow improved by 10%.

2.3.2. Intake valve shape effect

The inlet valve also give effect on the determining the performance of an internal combustion engine, it has been recognised by engine designers that volumetric efficiency, and therefore power output, may be increased by improvement in the flow characteristics of the induction system. Yi ye *et. al.* [58] investigated the effects of the groove shape on the flow characteristics through CFD and experimental investigations. The RNG k–ε turbulence model is used to simulate the pressure distributions of the flow fields inside three notches with their corresponding typical structural grooves in order to analyze the changes of restricted locations along with the openings and, furthermore, to calculate the flow areas of the notches. The accuracy of the employed model is demonstrated by comparing the computational results with the experimental data. They reported that the groove shape has significant effects on the flow characteristics (flow area, discharge characteristic, jet flow angle, steady flow force and throttling stiffness) of spool valve. Variable valve actuation and closed-loop control promise to play a key role in the promotion and control of these advanced combustion modes as explained Modiyani *et.al.* [59]. They reported modulation of intake valve closure timing dictates the effective compression ratio and influences the total amount of charge trapped inside

the cylinder, and in so doing allows manipulation of the in-cylinder reactant concentrations and temperature prior to and during the combustion process.

2.3.3. Valve lift effect

In many cases, the change of valve lift made effect to flow characteristic through the inlet valve and in-cylinder engine. Qin *et. al.* [60] used Large eddy simulation (LES) to calculate the in-cylinder turbulent flow field in a direct injection spark ignition (DISI) engine. The computations are carried out for three different maximum valve lifts (MVL) and throughout 100 consecutive engine cycles. The simulated results as well as corresponding particle image velocimetry (PIV) measurement database are analyzed by the proper orthogonal decomposition (POD) method. Through a new developed POD quadruple decomposition, the instantaneous in-cylinder flow fields are decomposed into four parts, named mean field, coherent field, transition field and turbulent field, respectively. Then the in-cylinder turbulent flow characteristics and cycle-to-cycle variations (CCV) are studied separately upon the four parts flow fields. They reported that each part exhibits its specific characteristics and has close connection with others. The mean part contains more than 50% of the total kinetic energy and the energy cascade phenomenon occurs among the four-part fields; the coherent field part possesses the highest CCV level which dominates CCV of the bulk flow. In addition, it is observed that a change in MVL affects significantly the in-cylinder flow behavior including CCV, especially for the coherent part. Furthermore, the POD analysis demonstrates that at least 25 sample cycles for the mean velocity and 50 sample cycles for the root-mean-square (RMS) velocity are necessary for obtaining converged and correct results in CCV.

Wang *et.al.* [61] investigated the in-cylinder tumble flow characteristics with reduced Maximum Valve Lifts (MVL) and used a modified four-valve Spark-Ignition (SI) test engine. They tested Three different MVL of 6.8 mm, 4.0 mm and 1.7 mm. They reported that the higher MVLs at the phase-averaged flow fields could produce stronger vertical flows which turn more toward to the piston top and finally are possible to form big scale tumble flow structure. Although lower MVLs create a higher tumble ratio when the piston is close to the bottom dead centre (BDC), higher MVLs substantially produce higher tumble ratios when the piston is moving close to the top dead centre (TDC). In terms of kinetic energy, lower MVLs result in higher values including higher total kinetic energy and higher fluctuating energy. Finally, the

vortex centres results demonstrate lower MVLs could enhance cycle-to-cycle variation due to the weakened tumble vortex.

2.3.4. Pressure drop effect

The air flow between the intake valve and its seat has properties similar to the flow through the venturi where the parts converge and diverge. Flow characteristics are determined by the effects of viscous friction, flow separation, and pressure recovery. Separation of flow from the wall is the main factor affecting the discharge coefficient. This causes poor pressure recovery and reduces the discharge coefficient. If a decrease in overall static pressure in the valve is given, pressure recovery tends to increase the discharge coefficient because the velocity in the throat increases with lower pressure. Blair *at.al.* [62] investigated the application of maps of measured discharge coefficients for poppet valves, cylinder ports, and in-pipe throttles within a theoretical simulation of the unsteady gas flow through an internal combustion engine. The maps provided cover both inflow and outflow at the discontinuity being discussed and are displayed as contour maps of the discharge coefficient as some function of the geometrical flow area of that discontinuity and of the pressure ratio across it up to a maximum value of 2.0. They reported that the method of measuring discharge coefficients of valves, ports, etc., over a range of discontinuity area but at a single, low, pressure ratio is quite inadequate for the acquisition of data to accurately guide a theoretical engine simulation package.

2.4 Characteristic of intake port flow

The intake port and intake valve design provide the effect of induction of air flow through the inlet valve. Lifting the intake valve, valve geometry, the area around the valve, and valve timing are some parameters that have a considerable effect on the formation and development of fluid flow in the cylinder [63]. The challenge is to produce the right position from these parameters to achieve optimal engine performance. The structure of flow through the inlet valve there are several models that vary together with changing valve lifts and have three different levels and shown in Fig. 2.2. In low valve lifts, flow flows close to the head and valve seat. While at intermediate valve lifts, the flow is separate from the valve head and at high valve lifts, the flow is separated from the inside edge of the valve seat [40].

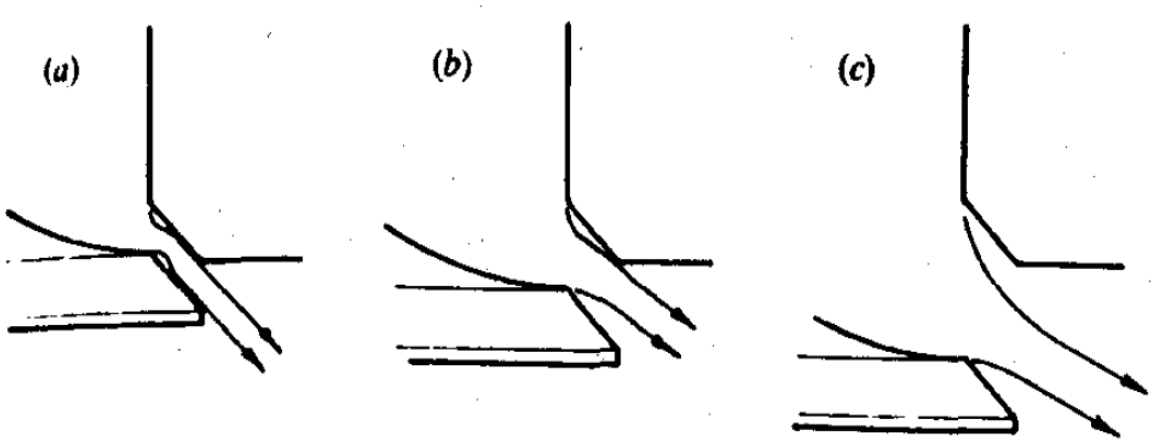

Fig. 2.2. Three air flow structures through the inlet valve: (a) low lift (b) intermediate lift (c) high lift [42]

The performance of the intake port and valve assembly in terms of the air flow capacity induced into the cylinder can be evaluated under steady flow test conditions using a flow rig test. The breathing capacity of the flow through the inlet valve can be evaluated by the following parameters:

2.4.1. Discharge coefficient

The discharge coefficient (C_d) is defined as the ratio of the actual mass flow rate ($\dot{m}_a$) to the ideal mass flow rate ($\dot{m}_i$) and is shown in Equation 1. The discharge coefficient is widely used to check the flow efficiency through various engine components such as valves, ports, and channels and can be measured under steady flow conditions for various pressure and valve lift ratios per diameter (Lv / Dv).

$$C_d = \frac{\dot{m}_a}{\dot{m}_i} \tag{1}$$

Real gas flow effects are used to calculate the ideal mass flow rate using equation 2, where P is pressure, T is temperature, R_{air} is the universal gas constant for air, and γ is the ratio of specific heat. The value of the discharge coefficient and the choice of reference area are linked together, the reference area of the release coefficient is the inner curtain area of valve $A_v = \pi D_v L_v$, where L_v is the valve lift and D_v is the valve diameter. Heywood [40] explained that the valve lift is low when the flow remains close to the head and the valve seat has a high discharge coefficient. While on the middle valve lift, the flow is separated from the valve head on the inside edge of the valve head. A decrease in the discharge coefficient occurs suddenly at this point. Illustration of this explanation can be seen in Figure 2.3.

$$\dot{m}_i = \frac{A_v P_{atm}}{\sqrt{R_{air} T}} \sqrt{\frac{2\gamma}{\gamma - 1} \left(\frac{P}{P_{atm}}\right)^{2/\gamma} \left(1 - \left(\frac{P}{P_{atm}}\right)^{\frac{\gamma-1}{\gamma}}\right)} \quad (2)$$

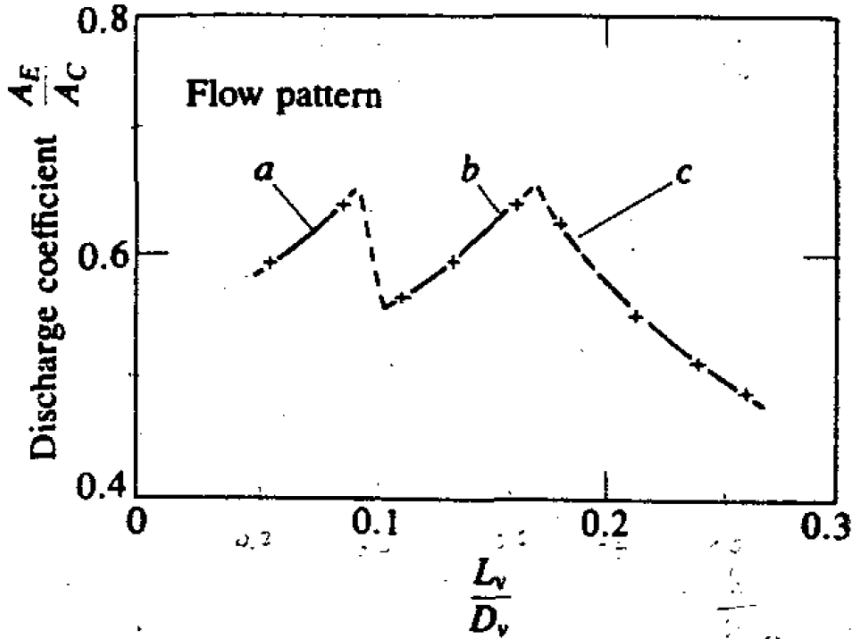

Fig. 2.3. Discharge coefficient values through the inlet valve [42]

2.4.2. Air flow rate

The mass flow rate through the poppet valve is usually explained by the equation for compressive flow through flow restriction that derived from a one-dimensional isentropic flow analysis and the effect of a real gas flow is entered using an experimentally determined discharge coefficient. The air flow rate is related to the upstream stagnation pressure *Po*, and the stagnation temperature *To*, the static pressure downstream of the flow restriction (assumed to be the same as the pressure at the limitation, P_T) and reference area *A*, the valve design characteristics. For flow into the cylinder through the intake valve, *Po* is the intake system pressure *Pi* and P_T, is the cylinder pressure.

2.4.3. Flow coefficient

The flow coefficient (C_f) is defined as the ratio of the actual mass flow rate ($\dot{m}_a$), to ideal mass flow rate, ($\dot{m}_i$), of both intake and exhaust system as calculated by Equation 1, which is similar to the discharge coefficient but the reference area is the valve inner seat area Aseat = $\pi((\text{Dseat})^2)/4$. The flow coefficient has a capability of comparisons at high lift values in the contrast to the discharge coefficient.

2.5 Characteristic of in-cylinder flow

The following are some flow characteristics that give information about what happen inside the engine cylinder and give an effect on mixing air-fuel so that it indirectly affects to the engine performance:

2.5.1. Swirl ratio

The two important terms related to the rotation flow patterns inside the cylinder are swirl ratio and tumble ratio. The definition of swirl ratio is the ratio of the angular speed of the flow about the center of mass in the z-direction, ω_3, to the angular speed of the crankshaft, $\omega_{crankshaft}$, as shown in the Eq 3. Swirl flow is built by bringing the flow from the intake port to the in-cylinder engine with the initial angular momentum and interaction of the intake port, the wall of cylinder engine and face of the piston. Swirl flow can survive throughout the compression process and even into the expansion process.

$$R_s = \frac{\omega_3}{\omega_{crankshaft}} \tag{3}$$

2.5.2. Tumble ratio

As explained in swirl ratio, tumble ratio also one of important terms related to the rotation flow patterns inside the cylinder. The definition of tumble ratio (in the *x*-direction) is the ratio of the angular speed of the flow about the center of mass in the *x*-direction, ω_1, to the angular speed of the crankshaft, $\omega_{crankshaft}$, as shown in the equation 4.

$$TR_x = \frac{\omega_1}{\omega_{crankshaft}} \tag{4}$$

Similarly, the tumble ratio in the *y*-direction is calculated by evaluating the ratio of the angular speed of the flow about the center of mass in the *y*-direction, ω_2, to the angular speed of the crankshaft, $\omega_{crankshaft}$, as shown in equation 5.

$$TR_y = \frac{\omega_2}{\omega_{crankshaft}} \tag{5}$$

The total tumble ratio magnitude can be computed as:

$$TR = \sqrt{{TR_x}^2 + {TR_y}^2} \tag{6}$$

The components of ω_i are calculated from the angular momentum, L_i, and the moment of inertia, I_i, as the following equation:

$$\omega_i = \frac{L_i}{I_i} \tag{7}$$

The tumble ratio generally had to be estimated under transient conditions to give a significant influence on the movement of the piston on the in-cylinder tumble flow [64]. Strength in tumble flow give the effect a good of fuel stratification [65].

2.5.3. Angular momentum

To measure the behavior of the engine system, the in-cylinder angular momentum in the engine cylinder need to be evaluated. The angular momentum, L_k, for a Cartesian system can be expressed as the following equation:

$$L_k = x_i u_j \varepsilon_{ijk} \tag{8}$$

where u_j represents the velocity fields and x_i represents the coordinate system with the axis of rotation at x_i=0, and the Levi-Civita symbol ε_{ijk}, is expressed as:

$$\varepsilon_{ijk} = \begin{cases} 0 \\ +1 \\ -1 \end{cases} \tag{9}$$

and is equal to 0 if any two indice are the same, +1 if *ijk* =123, 231 or 312 and -1 if *ijk* =132, 213 or 321. For a discrete system of cells, the angular momentum about the *x*, *y*, and *z*-axes (L_1, L_2, and L_3) can be calculated using the following equations:

$$\begin{aligned} L_1 &= \sum_{n=1}^{numcells} m_n \left((y_n - y_{cm})w_n - (z_n - z_{cm})v_n\right) \\ L_2 &= \sum_{n=1}^{numcells} m_n \left((z_n - z_{cm})u_n - (x_n - x_{cm})w_n\right) \\ L_3 &= \sum_{n=1}^{numcells} m_n \left((x_n - x_{cm})v_n - (y_n - y_{cm})u_n\right) \end{aligned} \tag{10}$$

where m_n is the mass of each cell; x_n, y_n, and z_n are the coordinates of each cell; u_n, v_n, and w_n are the components of velocity for each cell; and x_{cm}, y_{cm}, and z_{cm} are the center of mass coordinates. CONVERGE uses the center of mass as the rotation center when calculating rotational quantities such as swirl and tumble. For sector cases, x_{cm} = 0 and y_{cm} = 0 (the z axis is the axis of rotation). The moments of inertia about the *x, y* and *z* axes (I_1, I_2, *and* I_3) for a system of cells can be expressed as:

$$I_1 = \sum_{n=0}^{numcells} m_n [(^{y_n} - (^{z_n}]$$
$$I_2 = \sum_{n=0}^{numcells} m_n [(^{z_n} - (^{x_n}] \quad ` \quad (11)$$
$$I_3 = \sum_{n=0}^{numcells} m_n [(^{x_n} - (^{y_n}]$$

2.5.4. Turbulent Kinetic Energy

Turbulent Kinetic Energy (TKE) is the average value of kinetic energy per unit mass in the turbulent flow, which is physically characterized by the measure of the root-mean-square (RMS) from velocity fluctuations. TKE is an in-cylinder flow parameter important in determining turbulent viscosity. There are two sets of factors that could trigger TKE. The first is the exertion of frictions, detachment of flow that happens surrounding the valve vortexes as well as the gradients of significant strain throughout strokes from intake and exhaust. The second is the diminishing tumble during the final stage of the compression stroke. In this study, the turbulence model was analyzed using the renormalized group (RNG) *k-ε* model. There are two equations in the RNG k-ε model: the turbulence kinetic energy (TKE), k, and the turbulent dissipation rate of the TKE, *ε*, [66]. The TKE equation is shown in the following equation:

$$\frac{\partial \rho k}{\partial t} + \frac{\partial \rho u_i k}{\partial x_i} = \tau_{ij} \frac{\partial u_i}{\partial x_j} + \frac{\partial}{\partial x_j} \frac{\mu}{\mathrm{Pr}_k} \frac{\partial k}{\partial x_j} - \rho \varepsilon \quad (12)$$

The equation for the dissipation of turbulent kinetic energy is shown in the following equation:

$$\frac{\partial \rho \varepsilon}{\partial t} + \frac{\partial (\rho u_i \varepsilon)}{\partial x_i} = \frac{\partial}{\partial x_j} \left(\frac{\mu}{\mathrm{Pr}_\varepsilon} \frac{\partial \varepsilon}{\partial x_j} \right) + c_{\varepsilon 3} \rho \varepsilon \frac{\partial u_i}{\partial x_i} + \left(c_{\varepsilon 1} \frac{\partial u_i}{\partial x_j} \tau_{ij} - c_{\varepsilon 2} \rho \varepsilon \right) \frac{\varepsilon}{k} + S - \rho R \quad (13)$$

where ρ is density, ui is velocity component, μ is dynamic viscosity, τij is Reynolds stress, and S is the user-supplied source term. The model constants are given as $c\varepsilon_1$ = 1.42, $c\varepsilon_2$ = 1.68, $c\varepsilon_3$ = -1 and $P_{rk} = P_{r\varepsilon}$ =1.39 [67]. *R* can be expressed by the following equation:

$$R = \frac{C_\mu \eta^3 (1 - \eta/\eta_0)}{(1 + \beta \eta^3)} \frac{\varepsilon^2}{k} \quad (14)$$

The expression for η is:

$$\eta = \frac{k}{\varepsilon} \sqrt{2 S_{ij} S_{ij}} \quad (15)$$

where C_μ = 0.0845, η_0 = 4.38, β = 0.012, and S_{ij} is the mean strain rate tensor [67].

2.5.5. Length scale

To estimate the characteristics of inlet turbulence during a CFD simulation, the physical quantity measure of large eddies that laden with energy within a turbulent flow is required. This measure is called the turbulence length scale. Each eddy scale corresponds to a specific turbulence length scale. Some types of eddy scale that have been standardized are integral length scales, Taylor microscale and Kolmogorov microscale for energy-containing, inertial subrange and dissipation range eddies, respectively. In this study, the integral length scale is used to predict the turbulent length scale. The in-cylinder flow in the engine is turbulent. Therefore, the mixing and transfer rates are larger than the molecular diffusion rate. In order to achieve a good prediction for process in the cylinder, it is important to simulate the turbulence. The integral length scale is a result computed based on the turbulence kinetic energy (TKE), *k*, and the turbulent dissipation rate of the TKE, ε. The equation for the integral length scale, le, is as follows

$$le = {C_\mu}^{3/4} \frac{k^{3/2}}{\varepsilon} \tag{16}$$

where C_μ is a model constant.

2.6 Review of previous studies on engine flow

Due to environmental issues, the regulations for internal combustion engines have become stricter. Therefore, improving performance and decreasing exhaust emissions for internal combustion engines are priorities. Many researchers have suggested ways to improve engine performance and to reduce exhaust emission [2,3,12,40,4–11], which are useful in maintaining the environment and saving energy. The general method to improve the engine performance is by using an appropriate design of several parts of the engine such as intake manifold, exhaust manifold, combustion chamber, and piston. To obtain the optimal performance and minimize emissions, it is important to improve the combustion characteristics of the engine, which means reducing the unburned elements (pollutants) in the exhaust emission. One way to improve combustion characteristics is by achieving a homogeneous mixture in-cylinder, particularly for the stoichiometric operation of the intake port injection system. The homogeneity of the mixture can be improved by using swirl flow and tumble flow at a low-to-medium, controlled in-cylinder directional flow [68–71]. Most of flow structure investigations [63,72,73] focus on the organised structures that can be initially prepared during

the intake process. These structures can be characterised as swirl and tumble motions or a combination of both. The definition of swirl flow is the charge rotation about the cylinder axis, while tumble flow is a rotation orthogonal to the cylinder axis [74][75]. The swirl and tumble flows occur in the cylinder engine simultaneously. In the combustion system, tumble and swirl motions are used together to produce optimal air-fuel mixing. On the other hand, these two motions are used to get fast air-fuel mixing by increasing the level of turbulence and increasing the combustion process. Swirl motion occurs more frequently in diesel engines because diesel engines require high-intensity rotations while tumble motion are found in gasoline engines with a pent roof design. Optimizing the in-cylinder flow motion, including such components as tumble and swirl, is one method of improving the combustion rate and permitting operation at higher compression ratios (CRs) and leaner mixtures [76]. Changes in chamber geometry, injector design, spray targeting, injection pressure, and injection timing can also substantially affect the combustion rate [40].

Therefore, comprehensive knowledge regarding flow structure from the intake port to the engine cylinder is very important to optimize the mixture preparation and combustion process. The flow structure starting from the intake port to the cylinder that occurs during the intake step falls into two classifications, namely the unorganized and organized structure. An irregular structure is a structure where a cylinder is filled with undefined flow. On the other hand, an organized structure is a rotational flow structure formed through the design of the inlet port, inlet valve and cylinder head assembly and piston geometry. Moreover, valve lifts have a very important influence on the formation and development of flow motion in-cylinder engine [63].

There are several methods that can explain the growth of rotational flow. Induction of a large amount of flow over the inlet valve, which is sucked into the cylinder and rotated by the influence of the cylinder wall and piston shape can produce tumble motion. Li *et al*. [77] conducted a study in which they reported that strong tumble flow could be generated where most of it occurred at the bottom of the inlet valve. In other parts, intake port models such as helical or tangential models can produce different swirl movements. The helical model produces a vortex inside the channel port before it enters the cylinder. While the tangential model produces a vortex in the cylinder in the presence of substantial tangential momentum. Mahrous *et al*. [63] conducted a study to determine the effect of using a higher degree of negative valve overlap (NVO) variables on the process of preparing a mixture in the cylinder

at the end of the compression step. They reported that modifications to the swirl and tumble movements in the cylinder were obtained. The breakdown of rotational motion into a form of turbulence during the compression step differs from one movement to another. Vucinic *et al*. [73] investigated the effects of piston motion on tumble flow. They reported that several cases occurred where the tumble structure was destroyed because of the effect of piston movement. Then, the destruction of large-scale structures from tumble will increase the level of turbulence at the end of compression stroke. However, the swirl movement will continue with a weak angular momentum during the compression stroke. Kang *et al*. [78] also concluded that the intensity of turbulence can be doubled because of the effect of the tumble vortex that persists through compression strokes. Some form of piston can also affect the movement of tumble in the cylinder. Xavier and Alain [79] have carried out experimental investigations about the effect of the shape of the piston and cylinder head on the tumble motion in the cylinder. They report that maintaining tumble angular momentum and reducing the process of falling distortion are the most important effects of concave piston design. Huang *et al.* [80] also conducted an experimental investigation and they concluded that a flat crown piston induces a tumble ratio and a higher turbulence intensity than a slightly concave piston. It can be concluded that the rotational flow and flow turbulence characteristics are two important things to design the intake port optimally.

Many researchers have investigated rotating flow in cylinders and their effect on turbulence growth. Kang et al. [78] have analyzed flow structure and have reported that tumble motion does not affect the integral time scale, but the integral length scale increases significantly due to the effect of falling large-scale tumble movements to small scale vortices when the piston approaches the top dead center (TDC). Hill and Zhang [81] also explain that rotational motion is one method to increase the rate of combustion and allow for operations with a better mixture and with a higher compression ratio. However, unwanted higher heat losses occur because of the effect of rotational motion on the transfer of heat convection to the cylinder wall. Another disadvantage is the decrease in volumetric efficiency due to the loss of extra pressure during the intake process. Xavier and Alain [79] also explain that cyclic fluctuations from the average velocity at TDC are almost twice as large without vortices. It has also been shown that vortex movements are effective in holding down cyclic variations with a flat piston while falling movements are effective in increasing this variation and intensity of turbulence. Vucinic et al. [73] conducted a study of flow in the cylinder in which they reported

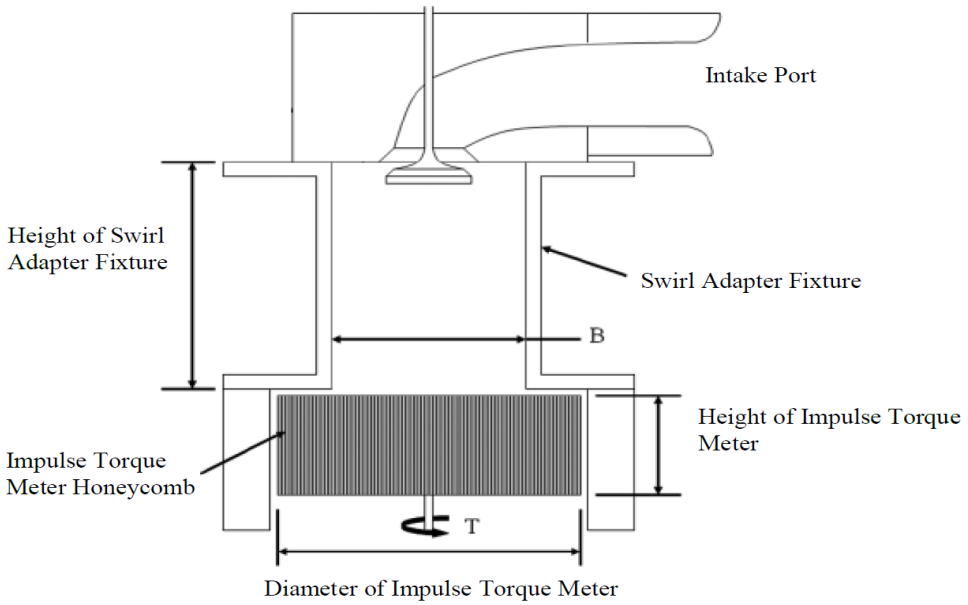

a. Steady state flow benches type torque meter

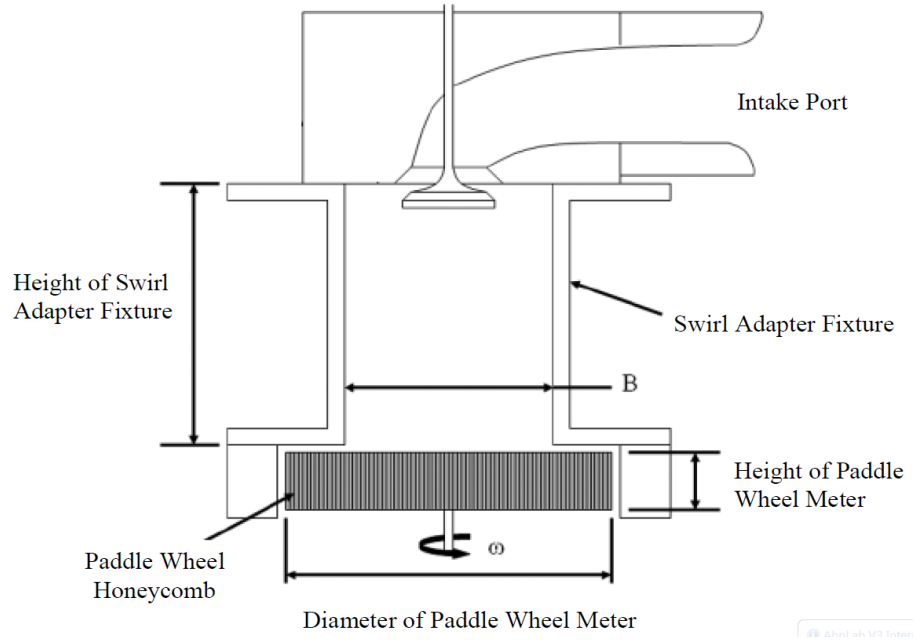

b. Steady state flow benches type paddle wheel anemometer

Fig. 2.4. Two type of steady state flow benches [87]

that when the valve lift was reduced the core of the vortex valve moved closer to the cylinder wall. Ismail et al. [82] also conducted a study related to the effect of changes in the valve lift where when the valve lift and test pressure increase, an increase in air flow rate and exhaust coefficient in the intake manifold and exhaust manifold system. However, when the valve lift reaches the maximum position per diameter ($0.25L_v/D_v$), the air flow rate becomes stable.

The in-cylinder flow motion in an internal combustion engine can be measured using experimental methods such as laser Doppler anemometry (LDA) [83], hot wire anemometry (HWA) [45], particle image velocimetry (PIV) [84][85] and steady state flow benches [86]. HWA and LDA are good tools, but they can only measure a few regions in-cylinder; thus, it is difficult to visualize the whole flow field using them. 3D-PIV gives a full view of the flow structures, but it still has limitations, such as the fact that the sizes of the flow structures are limited by image resolution. There are two types of steady state flow benches to measure rotational flow, namely a torque meter and paddle wheel anemometer [87].

The torque meter method is a steady flow test rig by using a swirl meter torque to measure the torque produced by the flow and then forwarded by the honeycomb element. The illustration of this type is shown in Figure 2.4.a. Paddle wheel anemometer is a type of steady flow test rig using a paddle wheel anemometer to measure the angular velocity of flow. Steady flow test rigs of this type can be seen in Figure 2.4.b. The steady flow rig test method is used to identify rotational motion that produce the characteristics of the intake valve and port on a fixed valve lift.

Another option is to visualize the in-cylinder flow motions in the engine with computational fluid dynamics (CFD). CFD provides detailed flow information about the whole flow field, with high image resolution that may be difficult to achieve using experimental methods. Commercial programs using CFD methods to analyze the flow motion in-cylinder include AVL FIRE [88–90], ANSYSCFX [71], KIVA [91], GT-Power [24], FloWorks [31], STAR-CD [92][27][16], STAR CCM+ [93] and CONVERGE [94–96].

The most difficult challenges in using CFD simulations such as the use of flow structures both starting at the intake port and in the engine cylinder are derived from several things such as the complicated engine geometry associated with the moving piston and some moving valves as well as the difficulty of mesh production and the amount of information generated with every calculation. In addition, numerical simulations require accurate predictions of turbulence modeling and initial conditions, especially in terms of describing the movement of air at the beginning of a calculation [40]. In addition, the movement of air formed in the engine cylinders is three-dimensional, highly volatile and covers a broad spectrum of length and time scale. The turbulence generated in the engine cylinder plays an important role in the complete engine cycle process, directly affecting the general flow structure, as well as

the mixture of air and fuel and combustion stability. The main factor that is important for the flow structure in the cylinder is the formation of large eddy and then broken down into turbulent kinetic energy, which acts as an increase in combustion characteristics. Large-scale analysis and fluctuation in internal combustion engine is important for improving engine performance.

Several studies related to numerical computation studies show that the coefficient difference in the standard k-ε turbulence model is very influential on the prediction of the flow field in the engine cylinder. High order turbulence models have capability to provide better accuracy than other models. On the other hand, improvement of mesh generation and selection of the right scheme can significantly improve the accuracy of the predicted flow field. Bella *et al.* [97] conducted a numerical study related to flow characteristics in a high-performance engine intake system at 12000 rpm during the induction period. They report that code prediction capability is increased in medium and high valve lifts using the renormalization group (RNG) k-ε turbulence model compared to standard k-ε. Nomura *et al.* [98] also conducted a numerical study of turbulent movements in flow cylinders. This method is called the partial cell in cartesian coordinator (PCC) method which was developed using Cartesian coordinates and partial cells in order to reduce the work in preparing input data on geometry. They report that there is a good agreement for the intensity of turbulence and flow patterns with the experimental results. They also explained that related to numerical simulations on the intake port valve for steady and transient conditions with moving valves and pistons. They concluded that the finite element method would provide good capabilities for the analysis of complex shape regions such as intake ports and valves. Choi *et al.* [99] also conducted research on flow fields in cylinders both experimentally with PIV and numerically with Star-CD. In CFD analysis, the Reynolds k-ε high standard and the k-ε RNG model were adopted with tetrahedral, hexahedral, and hybrid mesh to determine the model turbulence model dependencies. The comparison of PIV with CFD results shows that the high standard k-ε Reynolds model is a turbulence model that is more appropriate for low-speed operation than the k-ε RNG model. Payri et al. [93] have conducted research to estimate the three-dimensional flow of intake and compression stroke from a four-valve direct-injection engine with different piston shapes. They reported that the turbulent velocities predicted were quite good compared to the experimental radial and tangential turbulent components measured near TDC. However, for pistons with new models, it was found that strong turbulence speed fluctuations were not sufficiently predictable due to the poor performance of the k-ε model in the presence of strong

shear pressures. They report that the CFD prediction of flow in cylinders is quite accurate where there is an increase in knowledge about air flow characteristics during intake and compression stroke. From many CFD methods, CONVERGE is one of the CFD methods that omits the problem of grid generation from the process of simulation. Unlike other CFD methods, CONVERGE produces a truly orthogonal and structured grid at runtime condition, based on grid control parameters defined by the user. This grid generation method completely removes the need to generate a grid manually [66].

However, experiments are required as a preliminary verification for the steady flow problem. In practices, the preliminary verification is taken by using a steady flow bench [100], by which the measurement is a simplified for studying engine performance. Steady flow bench has become a standard measurement to characterize in-cylinder engine airflows in the automotive industry. Assumptions used in this method include a presumed close relation between steady flow measurements and the results achieved from a running engine cylinder.

Researchers have analyzed the in-cylinder flow motion in large engines using the CFD and experimental method. Abdul Gafoor and Gupta [88] studied the piston bowl geometry and swirl ratio in diesel engines numerically using the AVL FIRE platform. The simulation was performed for a single cylinder of a diesel engine with bore x stroke of 85.73 mm x 82.55 mm, and CR of 17.6. They investigated the effect on swirl ratio of variations in the bowl geometry of the piston. They reported that increasing the turbulent kinetic energy (TKE), together with increasing the swirl ratio, are required for maximum combustion. On the other hand, the combustion will be greatly affected by bowl geometry with a large diameter and shallow depth. Sharma *et al*. [89] developed a methodology to observe the in-cylinder flow and combustion of a diesel engine using AVL FIRE and KIVA-3V. Their simulation was carried out on a constant-speed turbocharged engine with bore x stroke of 102 mm x 116 mm and CR of 16.3, and was conducted for three cases, as follows: naturally aspirated, turbocharged inlet with initial in-cylinder pressure of 1.0 bar, and turbocharged inlet with initial in-cylinder pressure of 1.2 bar. The results showed that at the late of the suction stroke, the values for TKE and the swirl ratio peak were similar for all cases. The results also showed that the peak of the swirl ratio for the three cases was large enough to be considered significant. The value of the swirl ratio peak was around 2.2. The other swirl peak was seen in the early part of the suction stroke of the turbocharged inlet with initial in-cylinder pressure of 1.0 bar. However, the value of this peak is only 0.56. On the other hand, this small peak was not seen in the early part of the suction

stroke in the case of the naturally aspirated and in the case of the turbocharged inlet with initial in-cylinder pressure of 1.2 bar.

Using AVL FIRE, Wu et al. [90] studied the effect of various combustion chamber shapes on the lean combustion process and the cylinder flow of a spark-ignition compressed natural gas (CNG) engine. Their study was carried out on a large engine (190 mm x 210 mm). One kind of the combustion chamber was original chamber and two others were modifications. The extrusion areas of the three types of combustion chambers were 35301.72 mm^2 (original), 42371.12 mm^2, and 36011.13 mm^2. Two of the combustion chambers types were designed with a fixed CR of 10:1. Wu et al. reported that the increased intensity of turbulence can accelerate the speed of flame propagation. The growing trend of TKE in two modification chambers is slightly higher than that of the original chamber. It has been reported that combustion chamber shape has a significant effect on the TKE in-cylinder.

Perini et al. [91] have studied the effectiveness of CFD to analyze the incylinder fluid flows of a light-duty diesel engine with bore x stroke of 82 mm x 90.4 mm. They reported that the results are helpful for combustion model to know the part of in-cylinder flow on ignition in partial combustion mode. Qi et al. [27] have investigated the effect of intake port design on incylinder flow, and they reported that a minor intake port change dramatically affected in-cylinder flow. On the other hand, strong tumble will cause turbulence increase at spark time, which will improve combustion stability. Raj et al. [16] conducted a study on energy-efficient piston configuration for effective air motion using STAR-CD CFD software and compared it with experimental results. In their simulation, they used a two-valve single-cylinder engine with bore x stroke of 87.5 mm x 110 mm and four piston configurations at 1000 rpm. The four piston configurations were flat, inclined, center bowl, and inclined offset bowl. A medium mesh size of 350000 cells was used for these four piston configurations. Compared to the other cases, the center bowl on flat piston showed higher TKE, tumble ratio, turbulent length scale and turbulent intensity. Fang and Singh [94] used CONVERGE to investigate the flow separation for steady-state flow bench simulations. They reported that the study generally showed that the increase in mass flow rate was directly proportional to the increase in valve lift. However, in certain cases, the mass flow rate may reduce when the valve lift increases, due to the separation of turbulent flow motion at the valve seat. It can be estimated when high mesh density is used in the proximity of the walls of the intake port and the valve seat. Addepalli and Mallikarjuna [96] have analyzed the effect of engine operating parameter, inlet

air pressure, engine speed and CR on the level of mixture stratification in four-stroke wall-guided gasoline direct injection (GDI) engines using CONVERGE. They developed an engine parameter named 'stratification index' to measure the mixture stratification, and reported that the mixture stratification in a wall guided GDI engine varied significantly with inlet air pressure and engine speed, but was not significantly affected by CR.

In another work, Binjuwair and Ibrahim [101] evaluated the in-cylinder flow fields of a single-cylinder optical large engine with 88mm bore by using realizable k-ε and Reynolds stress turbulence model (RSTM) against experimental PIV data. Their results showed the realizable k-ε turbulence model as being able to predict qualitative trends of kinetic energy profile of the turbulence but poorly able to predict the average velocity of RSTM fluctuations. Mohammadebrahim et al. [87] investigated flow characteristics in the intake port of a four-valve engine with 78.6mm bore at a steady-state flow bench. Their study aimed at determining the effects of intake adaptor, paddlewheel diameter, adaptor length and diameter, test pressure, asymmetric valves and lifting adaptor roughness on the intensity of swirl and the measured flow coefficients. They reported the intensity of swirl to depend on the adaptor length and pressure. They also concluded intake adapter as one of the most effective parameters for testing flow coefficients. Yang et al. [102] have investigated the in-cylinder flow of a large-bore engine by using six models of modified flow box in steady-state port flow simulations. It reported estimated mass-flow rates to agree within 1% with measured data between intermediate and high valve lifts. At low valve lifts, slightly overpredicted mass-flow rate was observed. Furthermore, Idris Saad and Saiful Bari [103] have used a guide vane swirl and tumble device (GVSTD) in compression ignition (CI) engines with large bore (104 mm) by applying vegetable oils to improve characteristics of the in-cylinder airflow. They reported parameters such as in-cylinder pressure, TKE and velocity to enhance the combustion by breaking-up more fuel molecules, resulting in a better mixing of vegetable oil fuel and air. Then, Yang et al. [28] investigated the intake port of an engine with 86mm bore by comparatively using steady-state flow bench and numerical simulation. They reported the estimated discharge coefficients and swirl-tumble index of steady flow bench to have a good agreement with the results of numerical simulation.

2.7 Summary

This literature review has revealed the various study on the flow field of in-cylinder engine, especially in large engines. Significant progress has been made in this field, both experimental work and simulation studies. However, there are still many areas that need further investigation due to the complexity of the engine. It is unfortunate that most of the research related to this problem is more on large engines and very few researches in this area which explain comprehensively on small motorcycle engines. This is understandable because technically, large engines contain enough spaces to more easily visualize and analyze in-cylinder flow motion than small motorcycle engines. Besides, the existing works provide a less comprehensive and less detailed explanation. Therefore, a comprehensive investigation is needed to provide a better understanding of the cylinder flow field characteristics in small motorcycle engines. This work is expected to act as a basis for visualizing the flow fields in cylinders in small motorcycle engines, especially motorcycles. To fill this gap, some experimental and simulation work will be carried out to identify the important parameters and phenomena related to flow characteristics in order to improve the mixing of fuel-air and finally it can ultimately improve the engine efficiency. A brief explanation of how to obtain targets can be summarized in the effect flowchart as shown in Figure 2.5. Information on the experimental set up and simulation methods that will be applied in this study will be explained in Chapter 3.

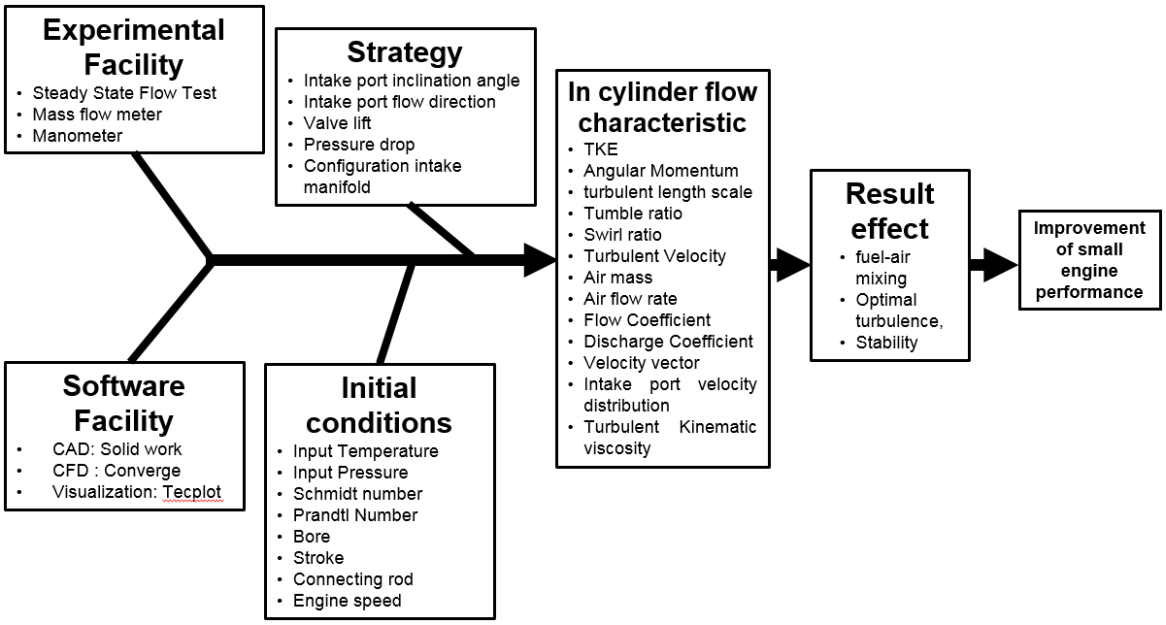

Fig. 2.5 Effect flowchart of the potential strategies to improve the performance of small motorcycles engine

3. EXPERIMENT SET UP AND SIMULATION MODEL

In the previous chapter, a literature review on the flow field of in-cylinder engine both experiment and simulation method include some parameter related to the flow characteristic in-cylinder engine especially on the large engine has been discussed. The research gaps that will be solved have been outlined. This chapter provides the information on the engine experimental details and numerical procedures to identify the important parameters and phenomena related to flow characteristics in order to improve the mixing of fuel-air and finally it can ultimately improve the engine efficiency. In the following section, detail of engine, experiment set up and numerical method are explained.

3.1 Experiment set-up

3.1.1. Rapid prototype of intake port and head cylinder

In this study, a 125 cm^3 single-cylinder gasoline small motorcycle engine with bore-stroke 57 mm x 48.8 mm and four strokes, four valves, and a flat piston was examined. The detailed specifications of the engine are shown in Table 3.1. There are three steps that will be carried out in this study. Firstly, it will be investigated the cylinder head of an original small motorcycle engine. Secondly, the modification of the intake port of this small motorcycle engine with some changes in the shape of the intake port based on the flow direction will also be investigated. Finally, the modification of the inclination of the intake port will also be investigated to complete this study. The cylinder head of an original small motorcycle engine was shown in Fig. 3.1 and the geometrical model of the original small motorcycle engine was shown in Fig. 3.2. The intake port was at the right side and the exhaust port was at the left side, as shown in Fig. 3.2. The flow towards the exhaust port is assumed to be positive and the flow towards the intake port is assumed to be negative.

Many design parameters for the intake port affect the flow characteristics of the in-cylinder engine [35]. Among these design parameters, two modification of intake port will we applied in this study. Firstly, the various helical intake port modifications based on the flow direction were chosen as the numerical and experimental parameters to be investigated. To investigate the effect of these design parameters on the intake flow rate, the various intake port modifications based on flow direction were installed on the cylinder head. The various intake port modifications based on the flow direction are a helical intake port with the same direction,

Fig. 3.1. Cylinder head of small gasoline engine

helical intake port with the opposite direction (inward), and the helical intake port with the opposite direction (outward). These helical intake port modifications will be compared with the tangential intake port as the original intake port. Secondly, the various of the intake port inclination was chosen as the next numerical and experimental parameters to be investigated. To investigate the effect of these design parameters on the intake flow rate, the various the intake port inclination were also installed on the cylinder head. The variation of intake port inclination is -15º, 0º, 15º and 30º. These intake port models will be compared with original intake port (11.5º). The modifications of the intake ports for each test cylinder head configuration are shown in Fig. 3.3 and 3.4. The modification of engine geometry and the surface model was created using SolidWorks and the design prototypes of the intake port used in testing were manufactured by 3D printing technology. In order to save cost, five types of inclination intake ports and three types helical intake ports, one type tangential intake port and one body deck representing the bottom structure of the cylinder head were separately made, as shown in Fig. 3.5 and 3.6. A mounting and positioning structure were assembled to the body deck and it allowed combining different intake ports to form various combinations. Moreover, an inclined flow guiding plane was produced at the entrance of the intake ports in order to better guide the airflow.

Table 3.1. Specifications of the small motorcycle engine.

Parameter	Value
Bore [mm]	57
Stroke [mm]	48.8
Displacement [cm^3]	125
Compression ratio [-]	10.2: 1
Number of valves [-]	4
Diameter intake valve [mm]	22.03
Diameter exhaust valve [mm]	18.75
Maximum lift of intake valve [mm]	6.46
Maximum lift of exhaust valve [mm]	6.42
Intake valve open [º bTDC]	94
Intake valve closed [º aBDC]	70
Exhaust valve open [º bBDC]	57
Exhaust valve closed [º aTDC]	40
Combustion chamber [-]	Pent roof type
Valve train	DOHC 4 valve
Swirl profile	3.11

In other side, the surface geometry was then exported and modified in CONVERGE, one of the packaged commercial software of CFD, to produce an engine model for simulation calculations. This simulation result will be the validation from the experiment result. The measurement of the intake flow rate under a steady-state condition is one of the significant keys that have a big influence on engine power and combustion. Any calculation of port flow in the small motorcycle engine was based on one dimensional characteristic for all ports. In this study, pressure drops used to perform the tests was chosen based on the criteria of Reynolds number. Two pressure drops chosen to confirm the flow motion were 300 and 600 mmH_2O. Moreover, the variation of engine speed i.e. 2000, 3000 and 4000 rpm in some cases used to

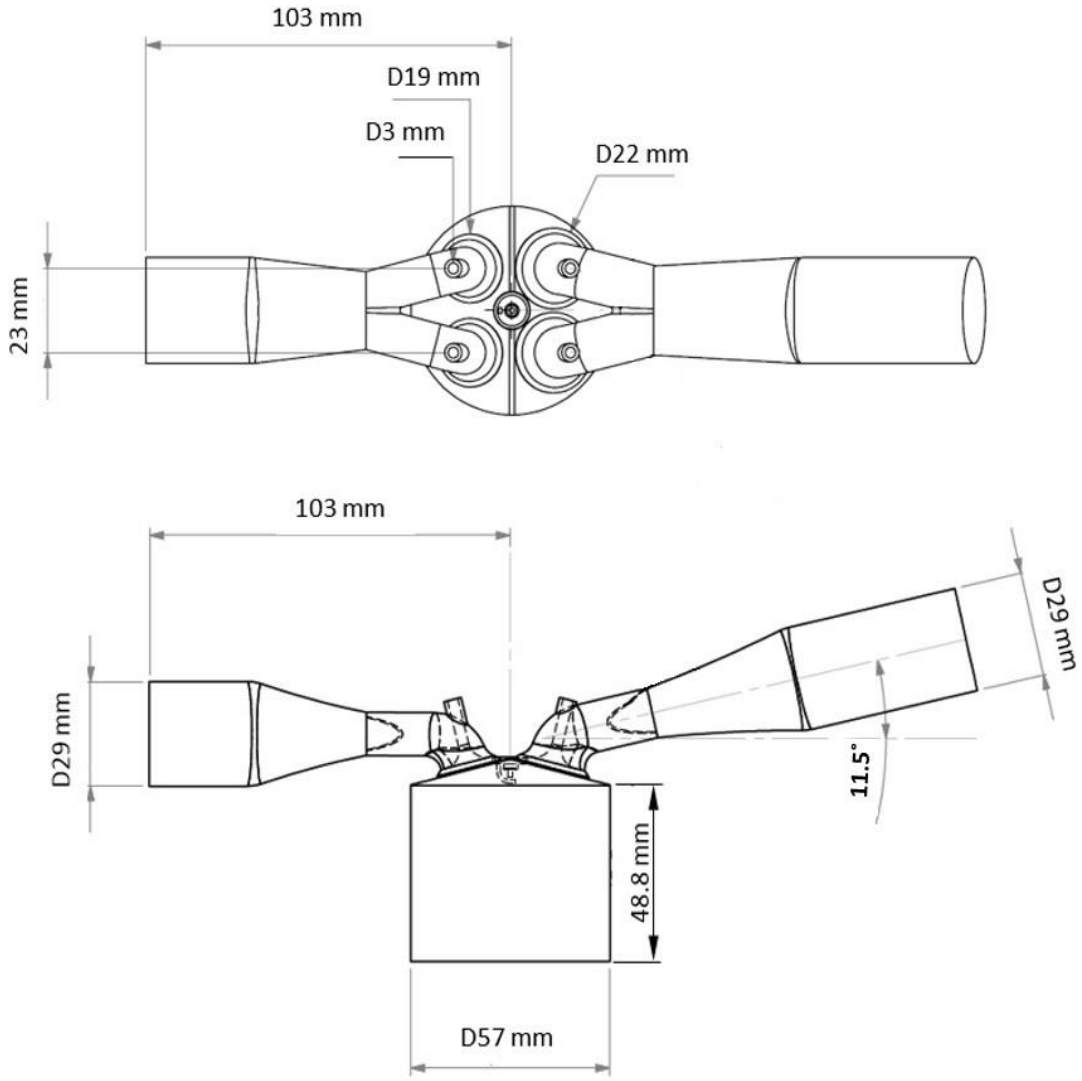

Fig. 3.2. The geometric model of the small motorcycle engine with a tangential intake port

make more comprehensive this explanation. This range of engine speeds was chosen because it reflects the normal operating conditions of a motorcycle used by one passenger in an urban area. Then, a torque meter for steady-state flow bench was taken to measure the flow.

3.1.2. Air flow test rig

The measurement of the intake flow rate under a steady-state condition is one of the significant keys that have a big influence on the engine power and combustion. The steady-state flow bench is a tool to evaluate the resistance of a test piece, e.g., a cylinder head, against

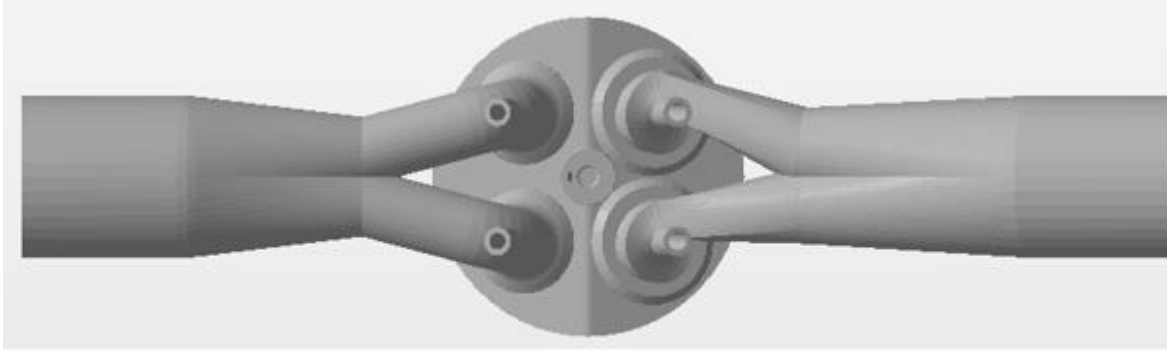

Helical intake port with same direction (model 1)

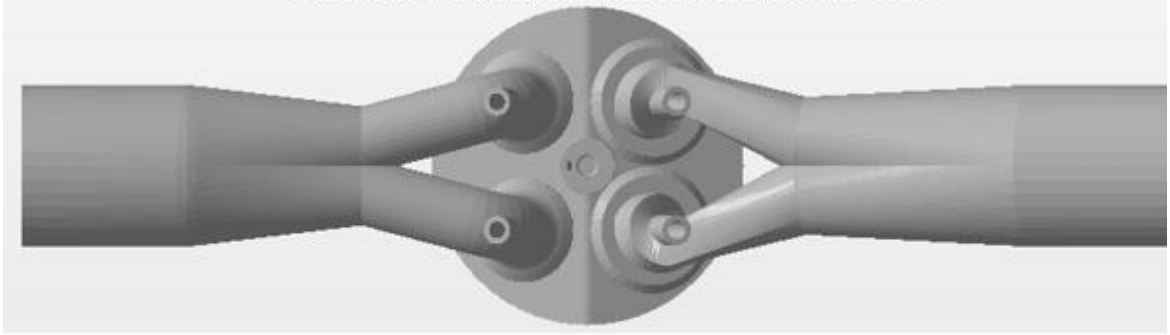

Helical intake port with opposite direction (inward) (model 2)

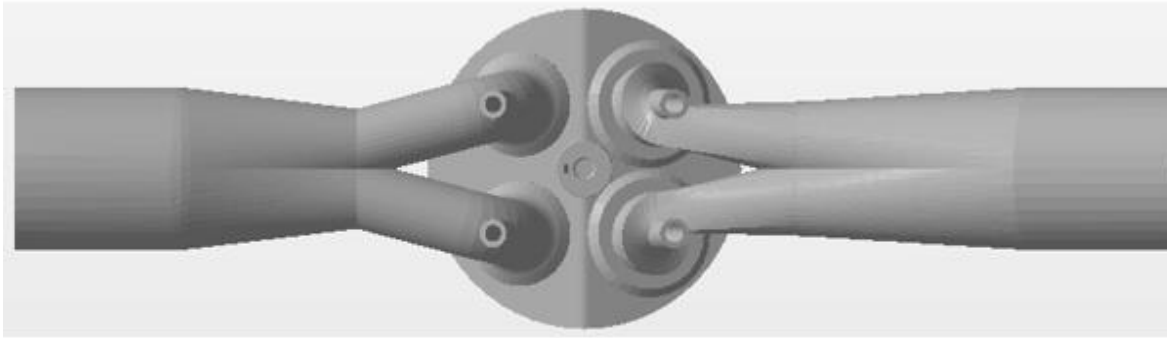

Helical intake port with opposite direction (outward) (model 3)

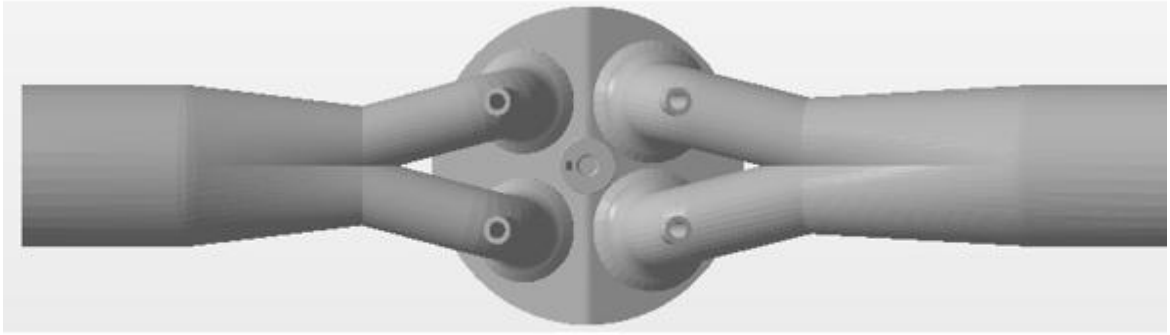

Tangential intake port (model 4)

Fig. 3.3. The various intake port modifications based on the flow direction at 11.5º

airflow. Besides, it is easy to apply and inexpensive to predict the ability of a cylinder head to convert the linear motion of intake flow to a rotational motion. Fig. 3.7 exhibits a schematic of the steady-state flow bench taken in this study and the steady flow test experimental set up was shown in Fig 3.8. This tool was made to investigate the intake stroke of the real engine

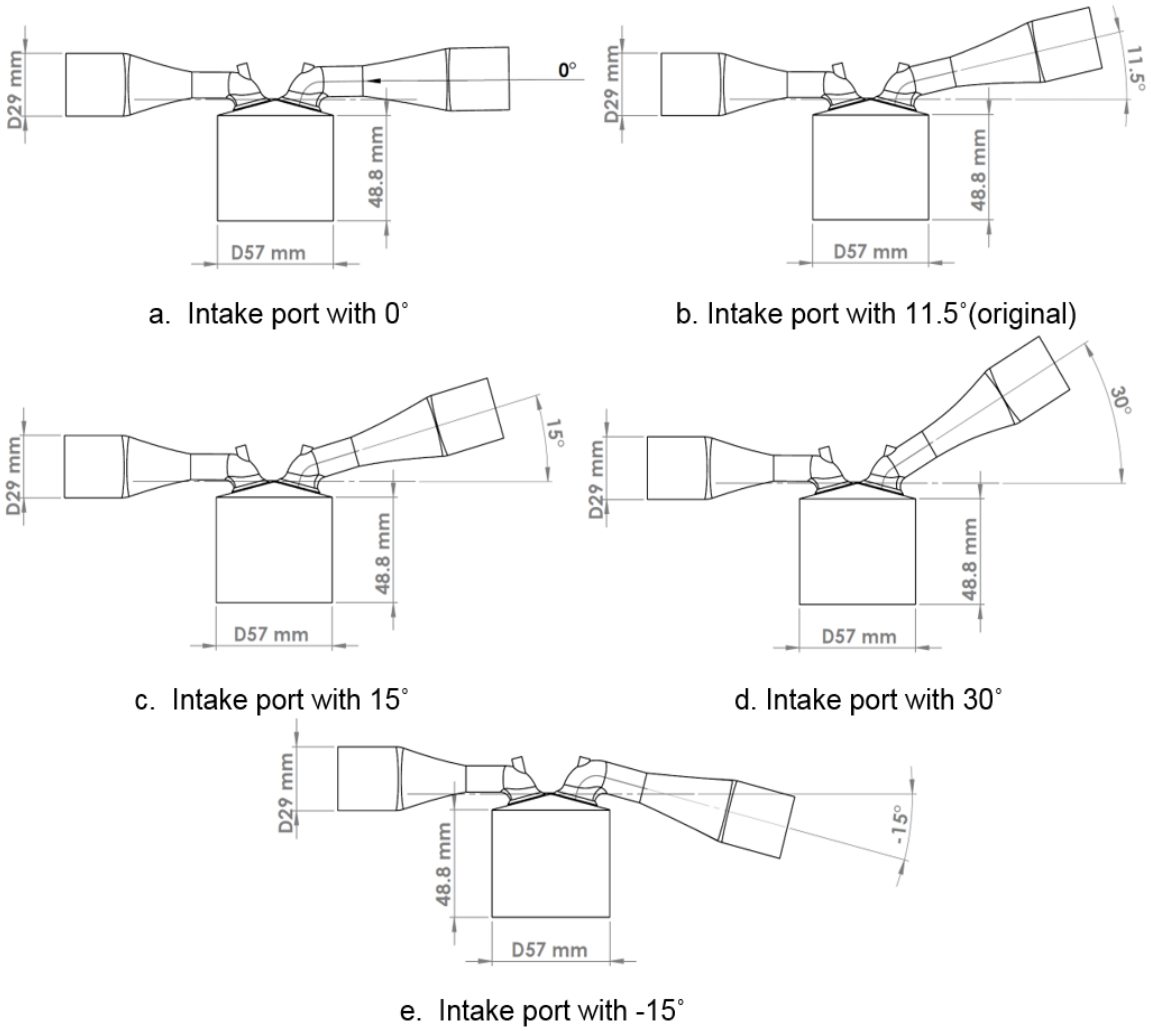

Fig. 3.4. The engine modification with different inclination of intake port

operation. This tool can be explained as follows. First, the air was driven by a blower fan to pass through surge tank, pressure-relief valve and laminar flow rate, and eventually entering the engine head. The intake valve was adjusted manually using a micrometer and positioned at a constant valve lift of 2–6.46mm (maximum valve lift). The measurements were carried out at a constant pressure drop of 300 and 600 mmH_2O across the intake valve. The pressure adjustment required for different valve lift settings was controlled through the feedback controller valve to pressure relief valve. Therefore, the pressure drop between the inlet of the intake port and the lower end of the cylinder can be kept constant so that the pressure drop can

Helical intake port with same direction (model 1)

Helical intake port with opposite direction (inward) (model 2)

Helical intake port with opposite direction (outward) (model 3)

Tangential intake port (model 4)

Body deck representing the bottom structure of the cylinder head

Fig. 3.5. Prototypes of the various intake port modifications based on the flow direction and body deck at 11.5º

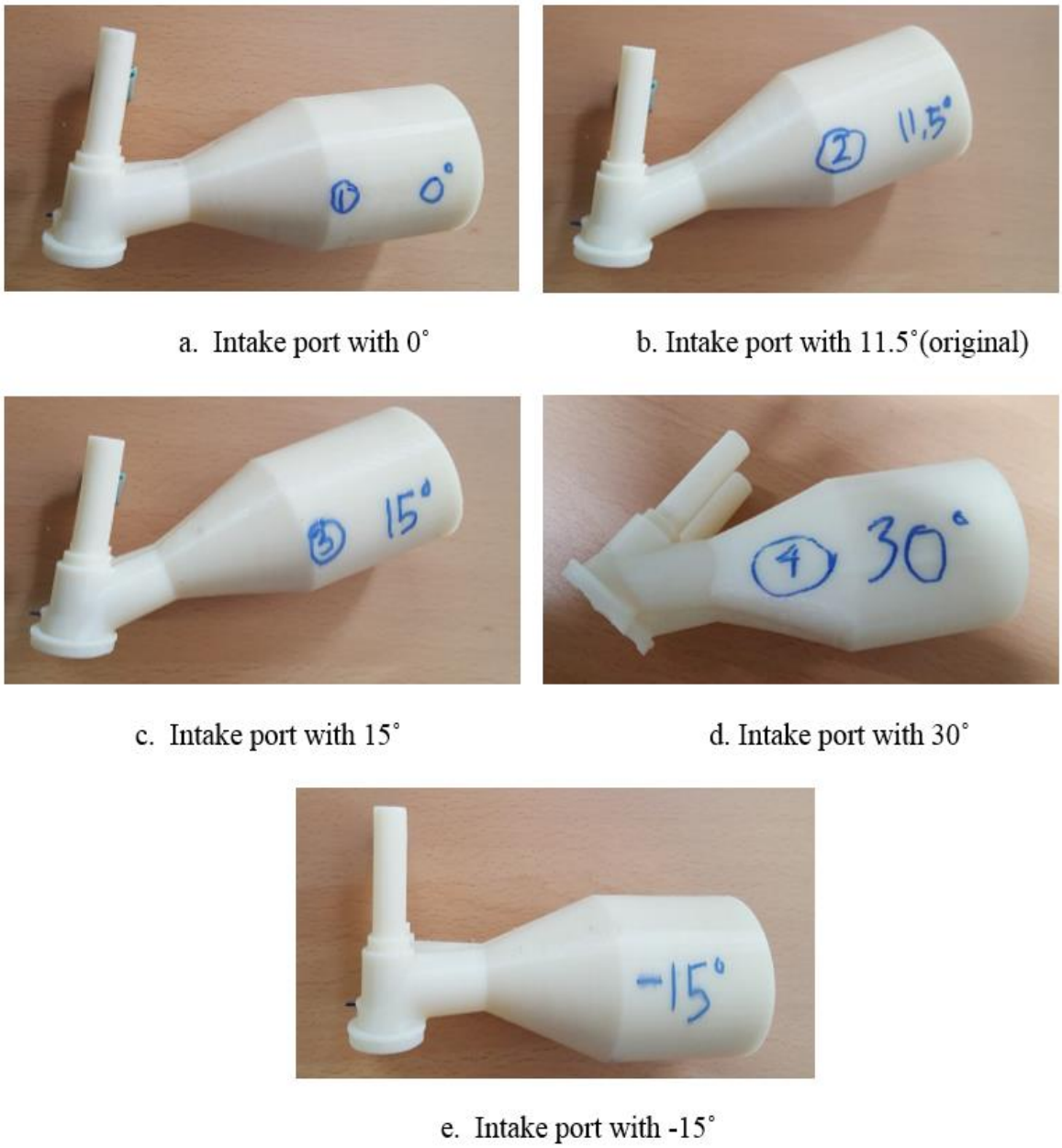

a. Intake port with 0˚ b. Intake port with 11.5˚(original)

c. Intake port with 15˚ d. Intake port with 30˚

e. Intake port with -15˚

Fig. 3.6. Prototypes of various intake ports modification based on the inclination and body deck at 11.5º

confirm enough turbulence. Pressure and temperature of the intake air were measured by pressure transducer and thermocouple, respectively. This tool was also accompanied by a honeycomb-type commutator to convert angular momentum of air into a rotational force. The honeycomb was located from the cylinder head at a depth of 1.75x inner diameter. A load cell connected to the commutator was used to transmit rotational force added by the air to the commutator. Finally, measurements were conducted on airflow rate, forces required to fix commutator to not get rotated, and rotational force with the load cell [36].

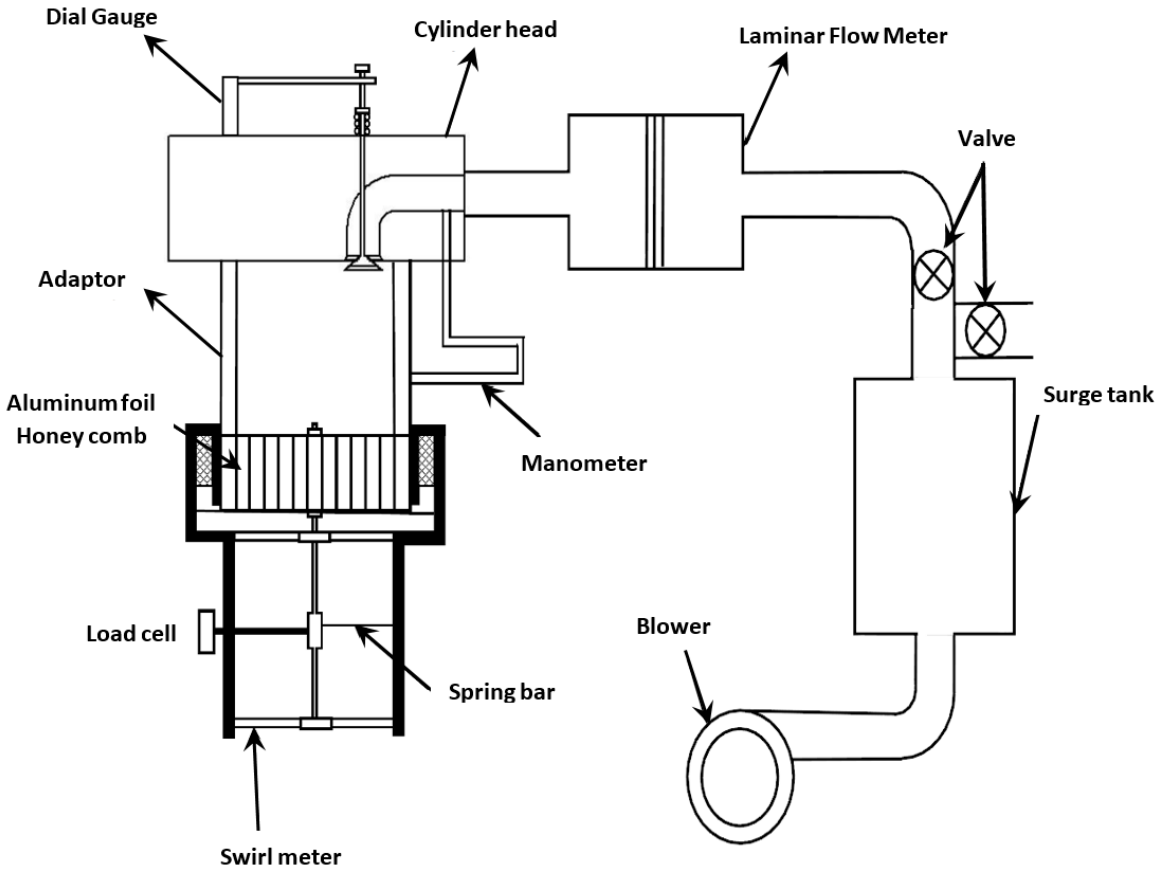

Fig. 3.7. Schematic of the steady-state tests [24]

Fig. 3.8. Steady flow test experimental set up

3.1.3. Evaluation Approach

To provide a good understanding of the suction capability of the small motorcycle engine, the analysis in this study represents the ability to breathe in terms of the flow coefficient. Based on studies conducted in previous research, different definitions have been used for the flow coefficient. However, this study relies on the definition adopted by Xu [104] because it has been used more frequently in the analysis of intake flow by vehicle companies. The flow coefficient, Cf, is defined as follows:

$$C_f = \frac{Q}{A_{seat} x V_o} \tag{17}$$

where Q is the measured volume flow rate, Vo is the velocity in the head and Aseat is the inner seat area. The velocity head is defined as:

$$V_o = \sqrt{\frac{2x\Delta P}{\rho}} \tag{18}$$

where ρ is the air density and ΔP is the pressure drop. Moreover, Aseat is defined with this equation:

$$A_{seat} = \frac{\pi}{4} D_{seat}^{\ 2} \tag{19}$$

where D is the diameter of the intake valve seat. Closely related to the flow coefficient, discharge coefficient, Cd, is defined as follow:

$$C_d = \frac{Q}{A_v x V_o} \tag{20}$$

where Av is inner curtain area of valve.

3.2 Simulation model

The other goal of this study is to conduct numerical simulation for the in-cylinder flow structures of an internal combustion engine under steady flow conditions. The computation of the in-cylinder engine flow field requires a detailed mathematical description of all significant properties of the process by means of solving number of algebraic equations. Using computational fluid dynamic (CFD) for studying practical engine flow consists of geometry creating, mesh generation, setting-up physical sub-models, solve algebraic equations and post-

processing resulting data. The numerical flow simulations presented in this investigation are obtained by using, as a research tool, a commercial CFD package so-called CONVERGE. The CONVERGE simulation package is a simulation software that can simulate three-dimensional, compressible or incompressible, and chemically reacting transient fluid flows in complex geometries with stationary or moving surfaces. It is an extremely powerful tool for rapidly and accurately simulating all internal combustion engine types. CONVERGE uses a complete structured grid creation technique to create geometry before and during simulation. However, the user can control the size of the grid and the total number of cells through base grid size, fixed embedding and adaptive mesh refinement (AMR) methods. The simulation is generated with the CONVERGE, version 2.3.21[66]. The turbulence model has been applied in the current study, namely, the renormalized group (RNG) k-ε model. The study was used a Windows PC contains 3.60GHz Intel(R) Core (TM) i7-7700 processors; having 16 GB of RAM. The three-dimensional simulation is conducted on the single-cylinder engine head of a pent-roof type for a fixed both valves lifts of (2 mm to 6.46 mm) at two pressure drops of 300 and 600 mmH_2O. This section provides introduction to the numerical model used for this study. In addition, the general descriptions of the computational methods that are employed, the surface preparation in graphical pre-processor, initial value and boundary conditions, the generation of

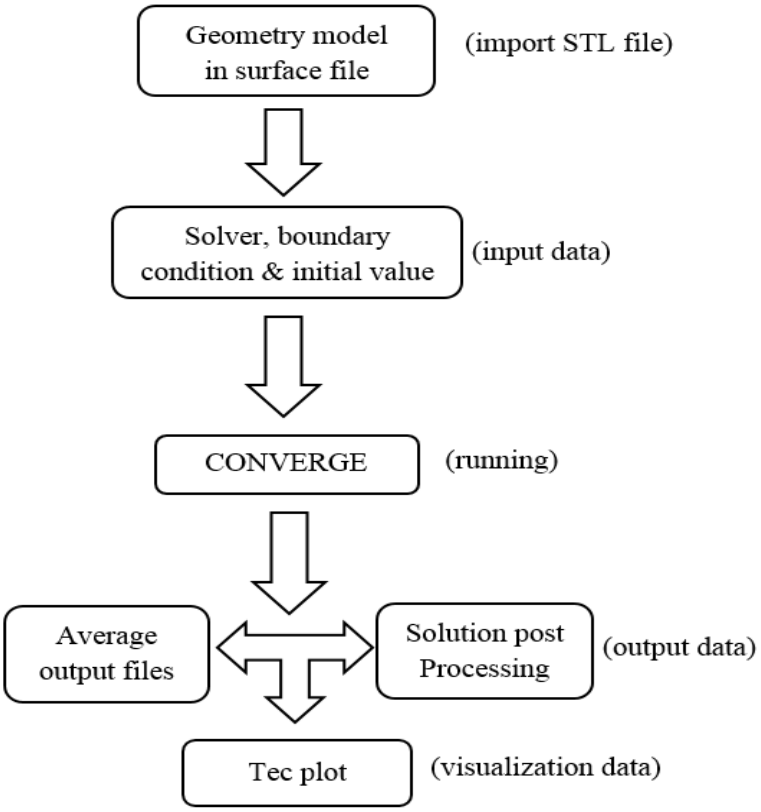

Fig. 3.9. The schematic diagram of the simulation process

the computational mesh calculation, post processing and plot the result in Tecplot are presented and also discussed in this section. Fig 3.9 shows the schematic diagram of the simulation process.

3.2.1. Surface preparation

To run numerical simulations in CONVERGE, efforts must be made to prepare the surface geometry and the input file that controls the simulation. Stereolithography (STL) format files containing surface geometries are needed to import into CONVERGE, which can be easily generated from most CAD packages such as Solidwork. After importing geometry, a pre-processor graphical user interface is used to prepare and export surface definition files, which are one of the input files for the CONVERGE solver. This user interface is called CONVERGE UI, which is shown in Figure 3.10. Surface geometries with unique boundary areas are identified on the surface of the definition file and the volume mesh is created automatically during runtime by the CONVERGE solver. The CONVERGE package uses an innovative boundary approach that eliminates the need for computational grids to coincide with interesting geometries. There are many benefits of generating a grid internally to code at run

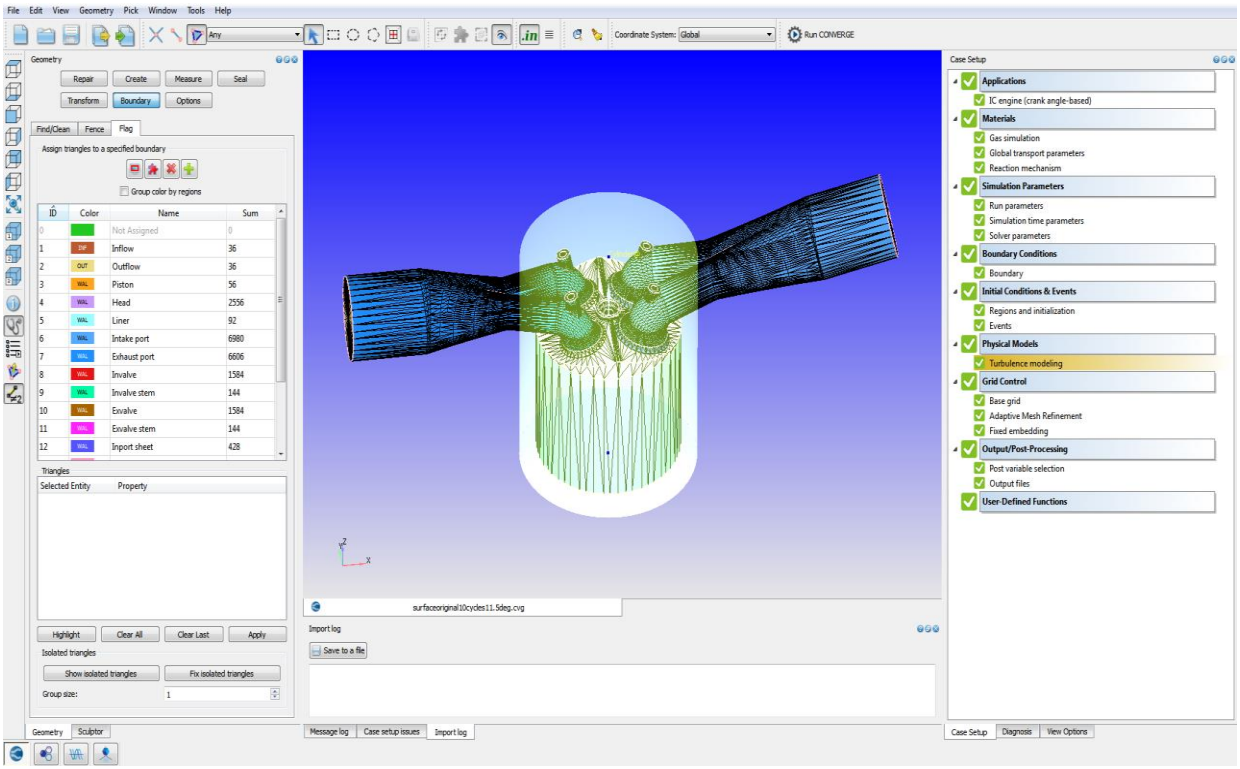

Fig. 3.10. Graphical user interface pre-processor: CONVERGE UI

time. First, this allows the grid to change during simulation. Second, it can handle moving surfaces by re-creating a grid near the moving boundary without having a specified input file. Finally, it offers significant time savings compared to other CFD codes.

3.2.2. Solver, boundary condition and initial value

3.2.2.1. Solver

The CONVERGE software has two solvers namely: transient and steady state solver [66]. Transient solver is used to run this small motorcycle engine model with different engine speeds. In the case of transients, the transport equation used is as follows:

$$\frac{\partial \rho \emptyset}{\partial t} + \frac{\partial \rho u_i \emptyset}{\partial x_i} = \frac{\partial}{\partial x_i}\left(\rho D_f \frac{\partial \emptyset}{\partial x_i}\right) + S \tag{21}$$

where ρ is density, $\emptyset$ is any transported variable, u is velocity, D_f is the diffusion coefficient, S is the source term. The diffusion coefficient is given by:

$$D_f = \frac{V}{Sc} \tag{22}$$

Where V is volume and S_c is Schmidt number.

On the other hand, the experiments carried out in this study were in steady state condition. Therefore, a steady state solver was chosen to run the experimental model. Based on the definition, the steady-state solution doesn't change over time. So, the term derivative, which depends on time, is excluded from the transport equation for steady state. The transportation equation for steady state is given as follow:

$$\frac{\partial \rho u_i \emptyset}{\partial x_i} = \frac{\partial}{\partial x_i}\left(\rho D \frac{\partial \emptyset}{\partial x_i}\right) + S \tag{23}$$

Steady state simulations do not require input in absolute time, and thus time-based inputs that control start time, end time, etc. Given in cycles, not time (seconds). The cycle is the completion of the algorithm shown in Figure 3.11. At the beginning of each cycle, previous values are stored, and explicit sources are calculated for each sub-model. At the beginning of an iteration of calculations, only the momentum, pressure, and velocity are solved. Needed to check for convergence after each iteration. The iteration will continue until convergence is reached. Another iteration, defined as "strict conservation" by CONVERGE, was added after the convergence of computational iterations to improve the results.

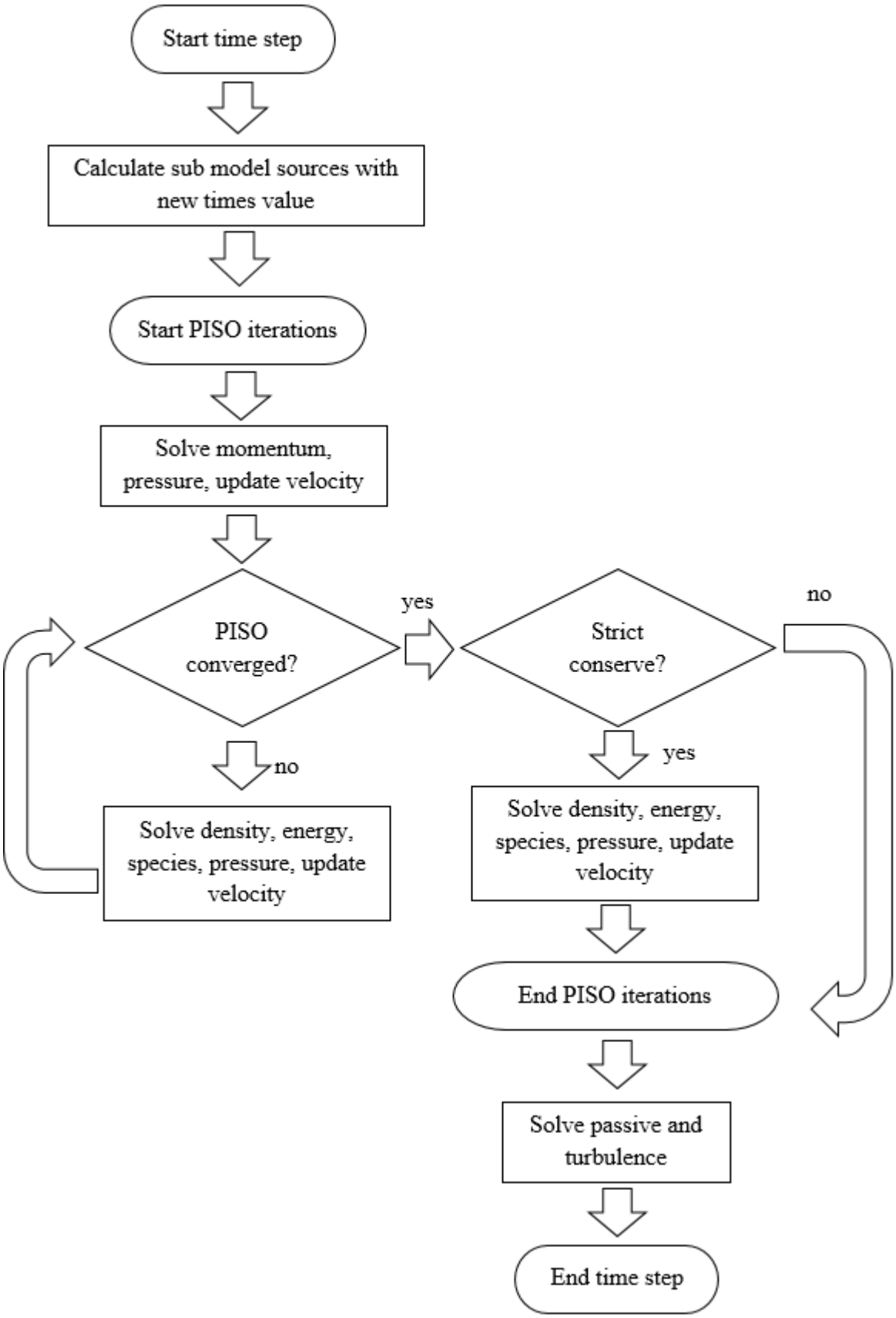

Fig. 3.11. The Flow chart of CONVERGE simulation [68]

3.2.2.2. Boundary condition

In this study the boundary conditions between the transient model and the steady state are similar. The basic difference between the two models is that the steady-state model is equipped with an open-end cylinder while the transient model has a moving piston. Another difference is the position of the initial intake valve and intake valve profile. Figure 3.12 shows the intake valve profile of a motorcycle engine model under transient and steady state conditions. As shown in Figure 3.12, the motorcycle engine model intake valve opens at 247 °CA and closes at 628 °CA during the simulation procedure. To have a better correlation between these two models, the intake valve lift for the steady state model is set to a fixed position based on the valve lift profile of the motorcycle engine model. The average valve lift from a motorcycle engine is around 3.23 mm during the intake process. As an effort to be representative, the steady state model intake valve lift is set at 3 mm in all cases, as shown in Figure 3.13. Fluid for both transient models and steady state models is air. The air temperature was set to be an average of 298 K and the composition of the mixture was defined as 23% oxygen with 77% nitrogen mass. The density of air is calculated by the ideal gas law. There are 17 sets of boundary conditions specified in the transient motorcycle engine model, which are separated into three regions. Region 0 contains the piston, cylinder, cylinder head and bottom of the intake valve and bottom of exhaust valve. Inflow, upper intake valves, intake valves stem, intake port sheet, intake valve angle and intake port are defined as parts in region 1. Region 2 contains outflow, exhaust port, upper exhaust valves, exhaust valves stem, exhaust port sheet and exhaust valve angle. Intake boundary conditions are defined in the inlet area of the intake port. Pressure from the intake limit is set. There are 9 sets of boundary conditions in the steady state model such as inflow, outflow, cylinder head, cylinder, intake port, intake valve, intake port sheet, intake valve angle and intake valve bottom. There are no pistons in this model, and the outflow limit is made to replace the piston. Intake boundary conditions are determined at the intake port inlet and outlet boundary conditions are determined in the cylinder exit field. Steady state air flow calculations are performed with mass input flow rates and a constant pressure condition initially set at the inlet and cylinder. Static pressure is applied at the bottom of the cylinder and the wall is considered a non-slip condition. The velocity distribution in the intake plane is determined as a uniform average speed profile based on a measured or determined flow rate. The specified outlet boundary conditions at the cylinder exit plane are that the flow at all locations in this plane will be directed outward and that continuity is satisfied at the exit.

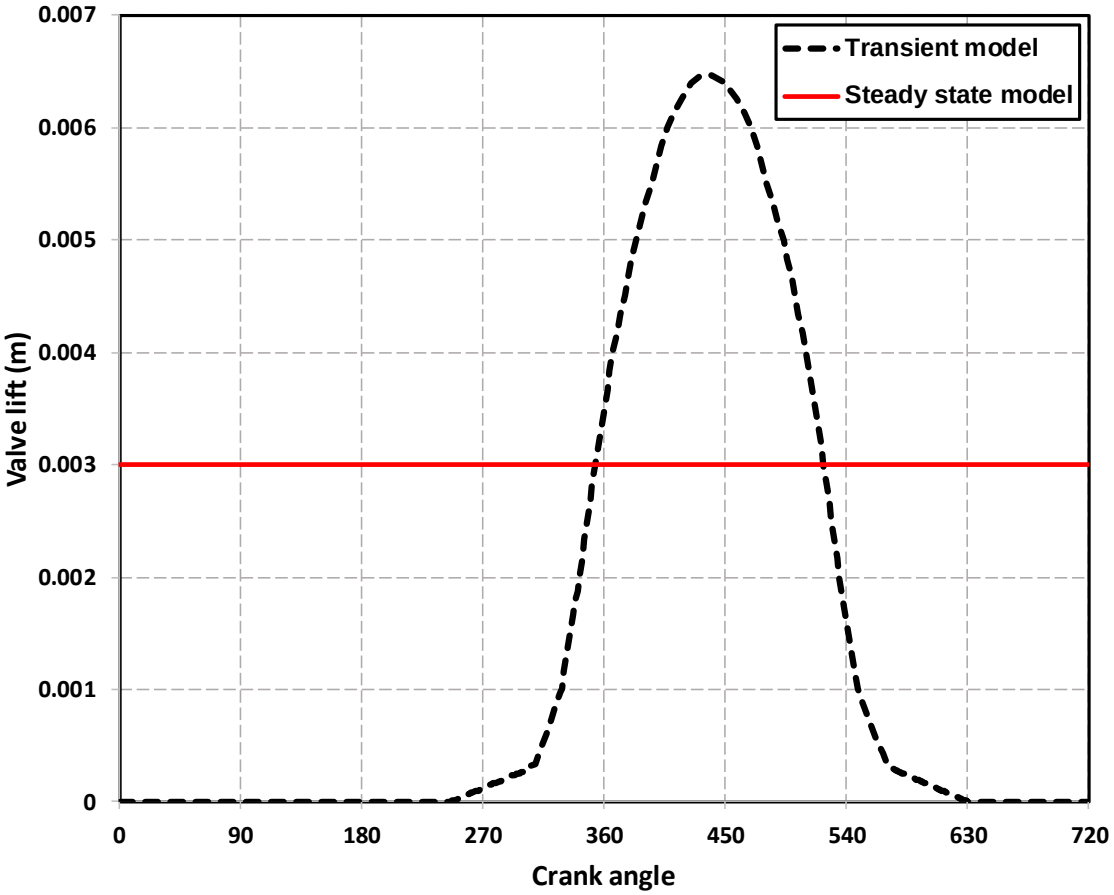

Fig. 3.12. The Valve lift profile of motorcycles engine in transient and steady state model

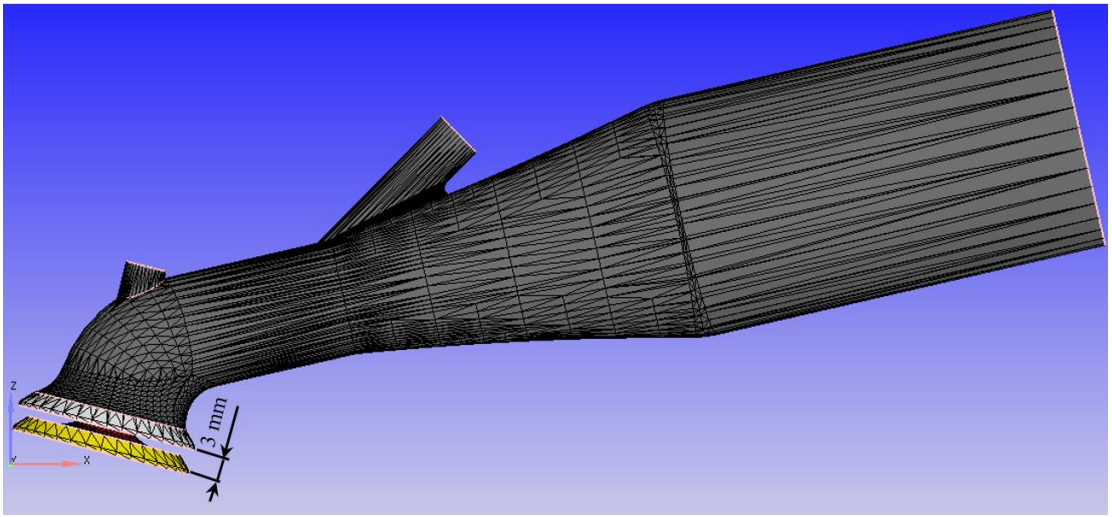

Fig. 3.13. The Intake valve lift position of steady state model

3.2.2.3. Initial condition

Everything related to the simulation conditions is controlled in the input file. The renormalized group (RNG) *k*-*ε* was chosen as a turbulence model to simulate the flow and solid surface to identify the wall law in CONVERGE. As mentioned before, different engine speeds

are simulated using the transient motorcycles engine model and the steady-state model is simulated under similar conditions with mass flow rates, which are correlated to different engine speeds. The engine model simulations with different engine speeds are simulated first and the details of the simulation conditions are provided in Table 2, 3 and 4 for each original engine, modification intake port engine based in flow direction and modification intake port engine based on the inclination model respectively. The average mass flow rate for each condition is calculated from the transient simulation results and these results are used as the initial mass flow rates of the steady-state model simulations. The initial temperature of the engine cylinder is also set at 300 K for all the cases. Since only the intake flow is investigated, the simulation starts at 360°CA and ends at 720°CA. The simulation conditions for the steady-state model are listed in Table 5, 6 and 7. Instead of using the engine speed, the intake mass flow rate correlated to the engine speed is used. The discrete Navier-Stokes equation is solved using the implicit discretization procedure on the Cartesian grid. Mass, momentum, and energy conversion equations are chosen as equations commonly used to construct the flow models in cylinder. While, the velocity-pressure coupling problem is solved by using pressure implicit for the splitting of operator (PISO) algorithm that is applied with the Rhie-Chow scheme [37].

The PISO algorithm as implemented in CONVERGE starts with a predictor step where the momentum equation is solved. After the predictor, a pressure equation is derived and solved, which leads to a correction, which is applied to the momentum equation. This process of correcting the momentum equation and re-solving can be repeated as many times as necessary to achieve the desired accuracy. After the momentum predictor and first corrector step have been completed, the other transport equations are solved in series. The PISO method was chosen for use in CONVERGE for various reasons. With only minor variations, this method can be used for solving either compressible or incompressible flows. In addition, the predictor-corrector concept allows for a semi-implicit treatment of sources and sinks: the sources and sinks can be updated at each corrector step.

All transported quantities in CONVERGE are colocated at the center of the cell. The use of colocated quantities can result in a decoupling of the pressure and velocity. This decoupling can produce fluctuations in the pressure and velocity solution that appear in a checkerboard pattern. In the past, many CFD codes used a staggered grid approach to eliminate the checkerboarding (i.e., velocity located at the cell face and pressure at the cell center). However, the Rhie-Chow interpolation scheme can be used to maintain collocated variables

and eliminate the undesirable checkerboarding. The Rhie-Chow scheme works by approximating the beneficial effects of the staggered grid approach but leaving the variables colocated.

Table 3.2. Simulation conditions for transient model at original engine

Engine speed (rpm)	Intake pressure (bar)	Intake temperature (K)	In-cylinder pressure (bar)
3200	1.02934	300	0.99992
4600	1.05876	300	0.99992

Table 3.3. Simulation conditions for transient model at modification intake port based on the flow direction at 300 mmH_2O

Model intake port	Engine speed (rpm)	Intake pressure (bar)	Intake temperature (K)	In-cylinder pressure (bar)
Helical intake with same direction	750	1.03858	295.4	1.00925
Helical intake with opposite direction (outward)	750	1.04791	293.8	1.01858
Helical intake with opposite rirection (intward)	710	1.04525	296.1	1.01592
Tangential intake	2940	1.04525	294.8	1.01592

Table 3.4. Simulation conditions for transient model at modification inclination of intake port at 300 mmH_2O

Model intake port	Engine speed (rpm)	Intake pressure (bar)	Intake temperature (K)	In-cylinder pressure (bar)
intake -15 degree	2780	1.03725	296.8	1.00792
intake 0 degree	2900	1.03725	294.7	1.00792
intake 11.5 degree	3045	1.02934	298.3	0.99992
intake 15 degree	3120	1.03858	297.0	1.00925
intake 30 degree	3260	1.03725	295.0	1.00792

Table 3.5. Simulation conditions for the steady state model at original engine

Mass flow rate (kg/s)	Intake pressure (bar)	Intake temperature (K)	In-cylinder pressure (bar)
0.02519	1.02934	300	0.99992
0.03638	1.05876	300	0.99992

Table 3.6. Simulation conditions for the steady state model at modification intake port based on the flow direction at 300 mmH_2O

Model intake port	Mass flow rate (kg/s)	Intake pressure (bar)	Intake temperature (K)	In-cylinder pressure (bar)
Helical intake with same direction	0.00567	1.03858	295.4	1.00925
Helical intake with opposite direction (outward)	0.00608	1.04791	293.8	1.01858
Helical intake with opposite rirection (intward)	0.00563	1.04525	296.1	1.01592
Tangential intake	0.02382	1.04525	294.8	1.01592

Table 3.7. Simulation conditions for transient model at modification inclination of intake port at 300 mmH_2O

Model intake port	Mass flow rate (kg/s)	Intake pressure (bar)	Intake temperature (K)	In-cylinder pressure (bar)
intake -15 degree	0.02237	1.03725	296.8	1.00792
intake 0 degree	0.02339	1.03725	294.7	1.00792
intake 11.5 degree	0.02402	1.02934	298.3	0.99992
intake 15 degree	0.02581	1.03858	297.0	1.00925
intake 30 degree	0.02663	1.03725	295.0	1.00792

3.2.3. Governing equation

The dynamics of fluid flow are governed by equations that describe the conservation of mass, momentum, and energy. This section describes the governing equations used in CONVERGE and the associated parameters and input files. Each conservation equation can be solved independently or in combination with the other equations. In addition, we can specify if the fluid (liquid or gas) in the simulation is compressible or incompressible and we can select the phase (gas, liquid, or gas-liquid). The following is some equation that needed in this study. The application of these principles yields a set of partial differential Navier-Stokes equations in terms of time and space. The first principle results in the continuity Equation 24. This equation represents the conservation of mass in a control volume for a compressible flow:

$$\frac{\partial \rho}{\partial t} + \frac{\partial \rho u_i}{\partial x} = S \tag{24}$$

and

$$\frac{\partial \rho u_i}{\partial t} + \frac{\partial \rho u_i u_j}{\partial x_j} = -\frac{\partial P}{\partial x_i} + \frac{\partial \sigma_{ij}}{\partial x_j} + S_i \quad (25)$$

where the viscous stress tensor is given by

$$\sigma_{ij} = \mu\left(\frac{\partial u_i}{\partial x_j} + \frac{\partial u_j}{\partial x_i}\right) + \left(\mu' - \frac{2}{3}\mu\right)\left(\frac{\partial u_k}{\partial x_k}\delta_{ij}\right) \quad (26)$$

where u is velocity, ρ is density, S is the source term, P is pressure, μ is viscosity, μ' is the dilatational viscosity (set to zero), and δij is the Kronecker delta. Note that if a turbulence model (e.g., k-ε) is activated, the viscosity is replaced by the turbulent viscosity, which is given by:

$$\mu_t = \mu + C_\mu \rho \frac{k^2}{\varepsilon} \quad (27)$$

where $C\mu$ is a turbulence model constant, k is the turbulent kinetic energy, and ε is the turbulent dissipation. While, the the energy equation is given by:

$$\frac{\partial \rho e}{\partial t} + \frac{\partial \rho e u_j}{\partial x_j} = P\frac{\partial u_j}{\partial x_j} + \sigma_{ij}\frac{\partial u_i}{\partial x_j} + \frac{\partial}{\partial x_j}\left(K\frac{\partial T}{\partial x_j}\right) + \frac{\partial}{\partial x_j}\left(\rho D_{fm}\sum_m h_m \frac{\partial Y_m}{\partial x_j}\right) + S \quad (28)$$

where ρ is density, Ym is the mass fraction of species m, D_{fm} is the mass diffusion coefficient, S is the source term, P is the pressure, e is the specific internal energy, K is the conductivity, hm is the species enthalpy, σij is the stress tensor, and T is temperature. Note that, if a turbulence model is activated, the conductivity is replaced by the turbulent conductivity, which is given by:

$$K_t = K + C_p \frac{\mu_t}{Pr_t} \quad (29)$$

where Pr_t is the turbulent Prandtl number and μ_t is the turbulent viscosity. In CONVERGE, the formulation for the turbulent Prandtl number is:

$$Pr_t = C_p \frac{\mu_t}{k_t} \quad (30)$$

where Cp is the specific heat, μ_t is the turbulent viscosity, and k_t is the turbulent conductivity.

3.2.4. Turbulence model

Turbulence significantly increases the rate of mixing of momentum, energy, and species. For a wide variety of applications, it is difficult to attain accurate CFD simulation results without including a turbulence model. Turbulence-enhanced mixing is a convective process that results from the presence of turbulent eddies in the flow. These turbulent eddies occur at many length scales. If a CFD solver does not contain a discretized domain (grid) that can resolve the smallest eddy length scales, then the solver cannot entirely account for the enhanced mixing effects of turbulence in the simulation. Currently it is not practical to resolve all of length scales in a typical CFD simulation, and thus turbulence models are used to account for the additional mixing. The following Reynolds-Averaged Navier-Stokes (RANS) turbulence models are available in CONVERGE: Standard *k*-*ε*, RNG (Renormalization Group) *k*-*ε*, Rapid Distortion RNG *k*-*ε* [67], Realizable *k*-*ε*, Standard *k*-*ω* 1998, Standard *k*-*ω* 2006, and *k*-*ω* SST. RNG (Renormalization Group) *k*-*ε* will applied in this study. The modeled Reynolds stress for RNG (Renormalization Group) *k*-*ε* model is given by:

$$\boldsymbol{\tau_{ij} = -\bar{\rho}\widetilde{u'_i u'_j} = 2\mu_t S_{ij} - \frac{2}{3}\delta_{ij}\left(\rho k + \mu_t \frac{\partial \widetilde{u_i}}{\partial x_i}\right)} \quad (31)$$

The RNG *k*-*ε* models require additional transport equations to obtain the turbulent viscosity given by Equation 27. One equation is needed for the turbulent kinetic energy, *k*, and one for the dissipation of turbulent kinetic energy, *ε*. This equation was mentioned in equation 12-15 in chapter two.

3.2.5. Computation mesh generation

In this study, the numerical simulation analysis was carried out using CONVERGE, a commercial CFD package. CONVERGE uses a complete structured grid creation technique to create geometry before and during simulation. However, the user can control the size of the grid and the total number of cells through base grid size, fixed embedding and adaptive mesh refinement (AMR) methods [34]. The base grid size is determined before simulation. Fixed embedding refines the grid at specified locations and times. AMR automatically changes the grid, based on fluctuating conditions such as temperature and velocity. AMR is valuable when using a highly refined grid to simulate complex phenomena, (such as high-velocity flow), without unnecessarily slowing the simulation with a globally refined grid. The AMR algorithm will add higher grid resolution where the flow field is most under-resolved, or where the sub-

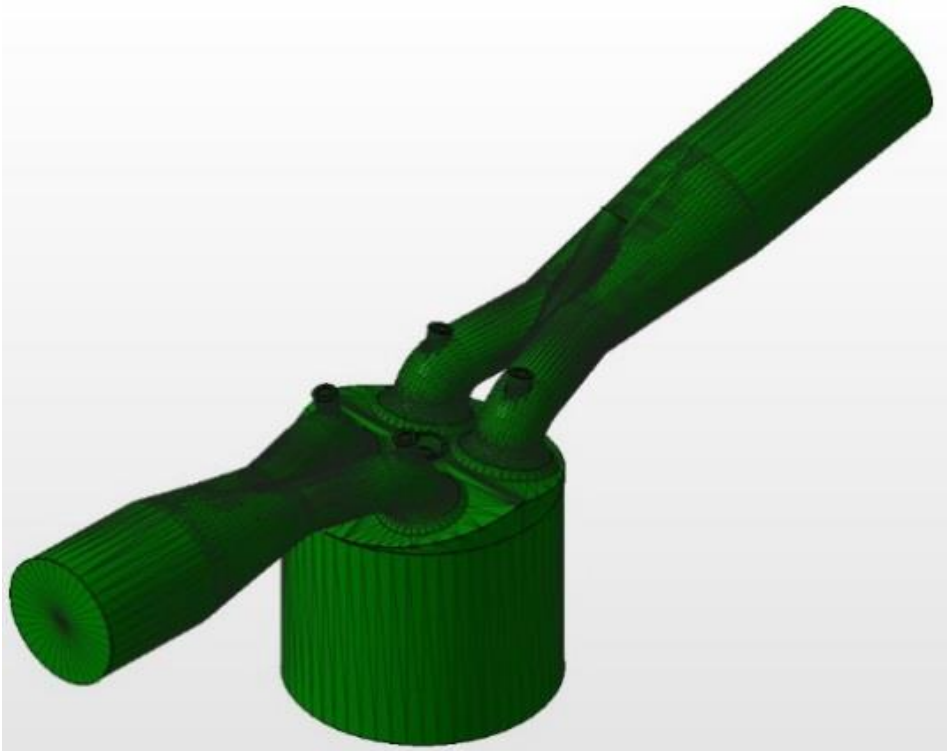

(a). Isometric view of the small motorcycle engine

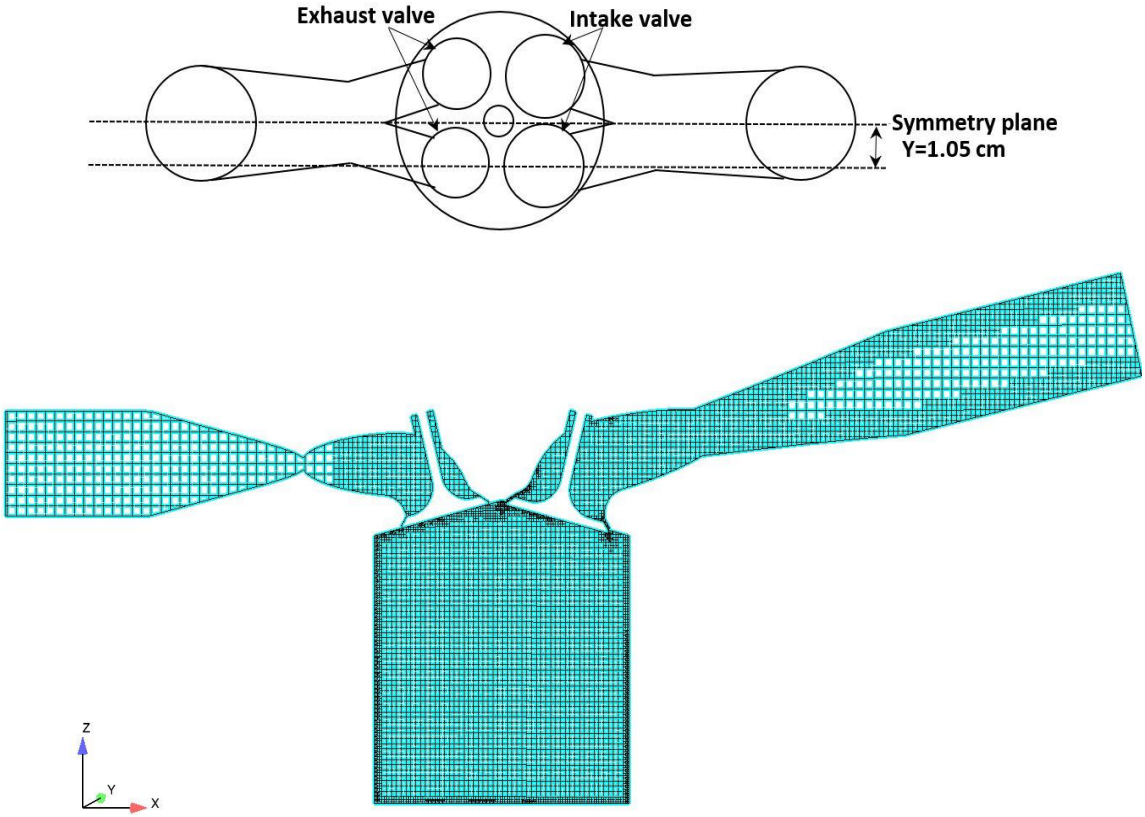

(b). The plane in which the flow motion is analyzed

Figure 3.14. Discretized domain of the small motorcycle engine

grid field is the largest. The AMR method in CONVERGE estimates the magnitude of the sub-grid field to determine where CONVERGE will add embedding. In this study, 2 mm was chosen as the base grid size. In the valve and engine cylinder regions, the grid was permanently changed to 1 mm. Furthermore, using the fixed embedding method, the grid was refined in the regions near the valve surface during the corresponding events to a size that changes around 0.25 mm. The overall size of the grid varied between 0.25 to 2 mm in the entire computational domain at any given simulation time. The regions of in-cylinder, exhaust, and intake flow were initialized using atmospheric conditions. Figure 3.14 shows the discretized domain of the engine.

3.2.6. Calculation and post-processing

There are two types of output files that are generated from simulations in CONVERGE: spatial average data and cell-by-cell data [66]. Each row of data in a cell, the average output file, represents the values of one particular cycle or time step. In cell-by-cell files, calculated results for each individual cell in the domain are provided - one file for each time step at a user-specified frequency. The CONVERGE package has no way to visualize output directly. Instead, it has a converter to allow output to be converted to formats for visualization such as Tecplot, EnSight or Matlab code. The converter can also create cell-by-cell output files in column format for the selected variable. In this work, the output file is converted to cell-by-cell output in column format and Tecplot is used as a tool to visualize the simulation results.

3.3 Summary

This chapter has explained the detailed step of the research work. Experimental setup, detail of instrumentation, measurement method, simulation model, boundary condition and initial value have been outlined. The first step in conducting this research was the numerical simulation and experimental investigations on an original small motorcycles engine to know the flow characteristics in-cylinder engine during intake and compression stroke. The second step was numerically and experimentally analyzed the results of the in-cylinder flow of small motorcycle engines using steady flow benches for various intake port modifications based on the flow direction. The intake port modifications are the helical intake port with the same direction, helical intake port with the opposite direction (inward), helical intake port with the opposite direction (outward), and the tangential intake port. This study also investigates the intake port velocity distribution using all models of the intake port around the valve curtain of

the two intake valves for varied valve lifts. In addition, this study also analyzed variations of the inflow motion of the in-cylinder engine in both the horizontal and vertical planes on all intake port models. Moreover, this study also investigates the cycle-to-cycle behavior of the tumble ratio and turbulent kinetic energy development of all intake port models under motoring conditions to assess the stability at the beginning of the developing stage. The third step was numerically and experimentally the results of the in-cylinder flow of small motorcycle engines using steady flow benches based on the variation of the intake port inclination. The variation of intake port inclination is -15º, 0º, 11.5º(original), 15º and 30º. In addition, this study also investigates variations inflow motion in-cylinder engine in both horizontal and vertical planes on all variations of the intake port inclination. Moreover, this study also aimed to investigate the effect of the variation of the intake port inclination on the characteristics of the in-cylinder airflow which is carried out in small motorcycle engines under motoring conditions. The sequential of experimental and simulation works, to improve the mixing of fuel-air and finally it can ultimately improve the engine efficiency, were briefly outlined. Based on the experimental and simulation works explained in this chapter, the results will be presented and discussed in Chapter 4, 5 and 6.

4. EFFECT OF PRESSURE DROP ON IN-CYLINDER FLOW OF SMALL MOTORCYCLE ENGINE USING EXPERIMENTAL STUDY AND NUMERICAL SIMULATION

This study investigated the experimental and numerical simulation on the in-cylinder flow of small motorcycle engine under steady state conditions. The experiment has been carried out on the engine head for the number of fixed valve lifts at two pressure drops, 300 and 600 mmH_2O that correlate with engine speeds of 3200 and 4600 rpm respectively. This study illustrates the evolution of the small motorcycle engine in-cylinder flow motion using CFD methods. Moreover, this study also analyzed some of the characteristics of air flow in cylinder flow that was performed for small motorcycle engine under motoring condition. The results show there was a good level of agreement was reached between the experiment result in steady-state flow benches and simulation result of the flow coefficient, air flow rate and coefficient of discharge at 300 and 600 mmH_2O pressure drop. In the horizontal plane, it was observed that the symmetrical four counter-rotating vortices seem in all images for high valve lift. In the vertical plane, it was observed that the wider the valve lift is opened the more vortex is formed. The biggest vortex occurs in the center of the cylinder. Related to the effect of the increase in pressure drop both in horizontal and vertical plane, the structure of flow remains of similar direction. However, the velocity magnitude of these flow is increased. In the horizontal and vertical plane, the vorticity was dominated in the right area of the cylinder where the intake valve is located. The strength of vorticity increases with the increase in valve lift and the magnitude of the vorticity also will increase at a higher pressure drop even though the vortices formed to maintain their shape. Increasing the pressure drop at the beginning of the valve lift opening has no effect on the swirl ratio until the valve lift reaches 5 mm. After that point, it has the effect to reduce the swirl ratio up to 75% when the valve lift reaches 6.25 mm. Increasing in pressure drop on the small motorcycle engine at the beginning of the intake stroke doesn't have a significant effect on the tumble ratio and the accumulated air mass. However, there is an increase in accumulated air mass around 3.77 % in compression strokes. Increasing in pressure drop on the small motorcycle engine gives a significant effect on TKE and reached the highest value of around 200 % at 470 °CA. This may be caused a significant increase in the inlet air velocity in the cylinder engine when the pressure drops increased. Related to the effect of the increasing of pressure drop, turbulent length scale and turbulent kinematic viscosity have similarities where the biggest increase occurred at around 590 °CA where the intake valve was

almost closed. The increase in turbulence made the air-fuel mixing in-cylinder more homogeneous. In addition, the increase in turbulence directly increased the rate of fire propagation. Further study is expected to be carried out by changing the intake port angle or intake port flow direction on the engine cylinder head so that the characteristics of air flow on the small motorcycle engine can be increased. Finally, this study is expected to help decrease the number of experiments necessary to obtain optimized systems in small motorcycle engines.

4.1 Comparison experiment and simulation result of air flow rate

The comparison of the air flow rate as a valve lift function based on the experimental result in steady-state flow benches and simulation result at 300 and 600 mmH_2O pressure drop is illustrated in Fig. 4.1. Figure 4.1 shows that air flow rate increase when the valve lift increases especially until 4.5 mm. From 4.5 mm to maximum valve lift 6.46 mm, the air flow rate almost constant. The increasing of pressure drop also makes the increasing of the air flow rate. The air flow rate is increased around 42.86 % at 600 mmH_2O than that of 300 mmH_2O. There was a good agreement between experiment and simulation in all pressure drop. The biggest deviation is only 17.76% occurs at 2.176 mm pressure drop 300 mmH_2O.

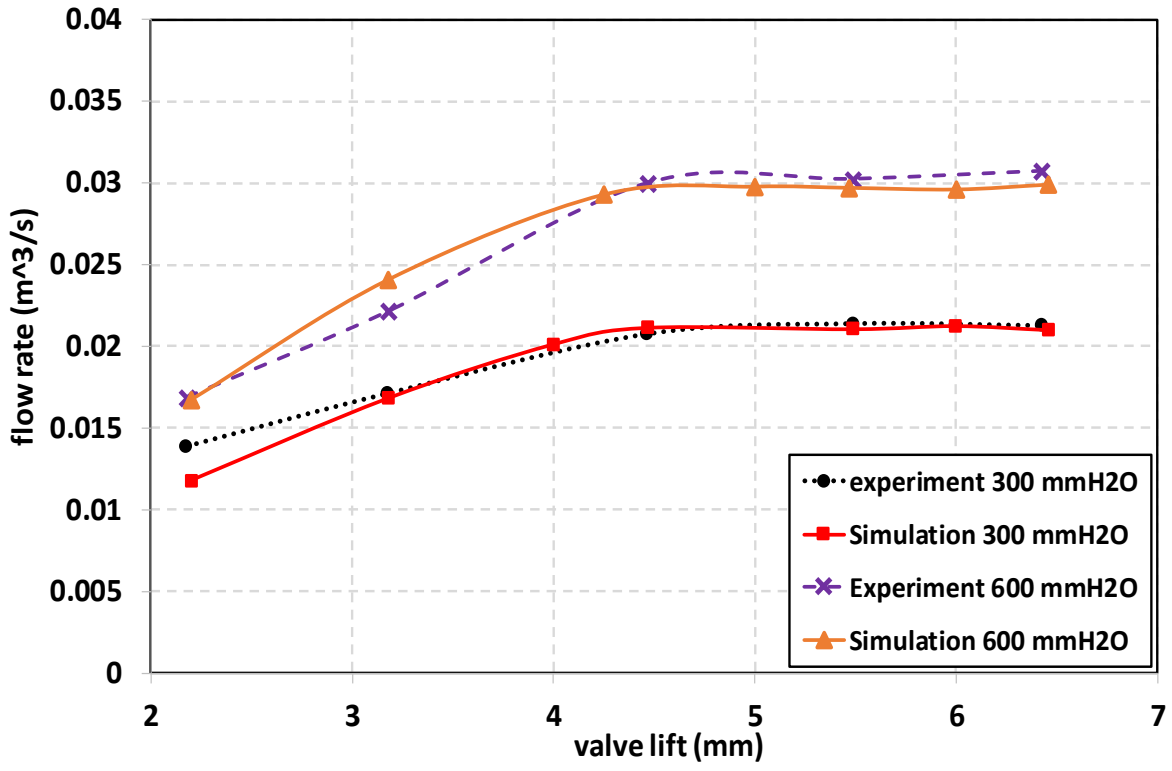

Fig. 4.1 Air flow rate in steady state flow bench experiment and simulation

4.2 Comparison experiment and simulation result of flow coefficient

The comparison of the flow coefficient measured based on the experimental result using steady state flow benches and the simulation result at different valve lifts and different pressure drop was shown in Fig. 4.2. The coefficient of flow increases proportionally with valve lift as the flow of effective region thru the valve also increases until 4.5 mm valve lift. From 4.5 mm to the maximum valve lift, 6.46 mm, the flow coefficient almost to be constant. The effect of the flow coefficient is very significant on the engine's breathing capacity when a lot of air enters the cylinder on a higher valve lift. But in lower valve lifts, the effect of coefficient of flow on engine breathing capacity is very small. It can be seen clearly from the figure 4.2 that the increase of pressure drop doesn't make effect significantly to the flow coefficient. There was a good agreement between experiment and simulation. The biggest deviation is only 15.87% occurs at 2.176 mm and pressure drop 300 mmH_2O.

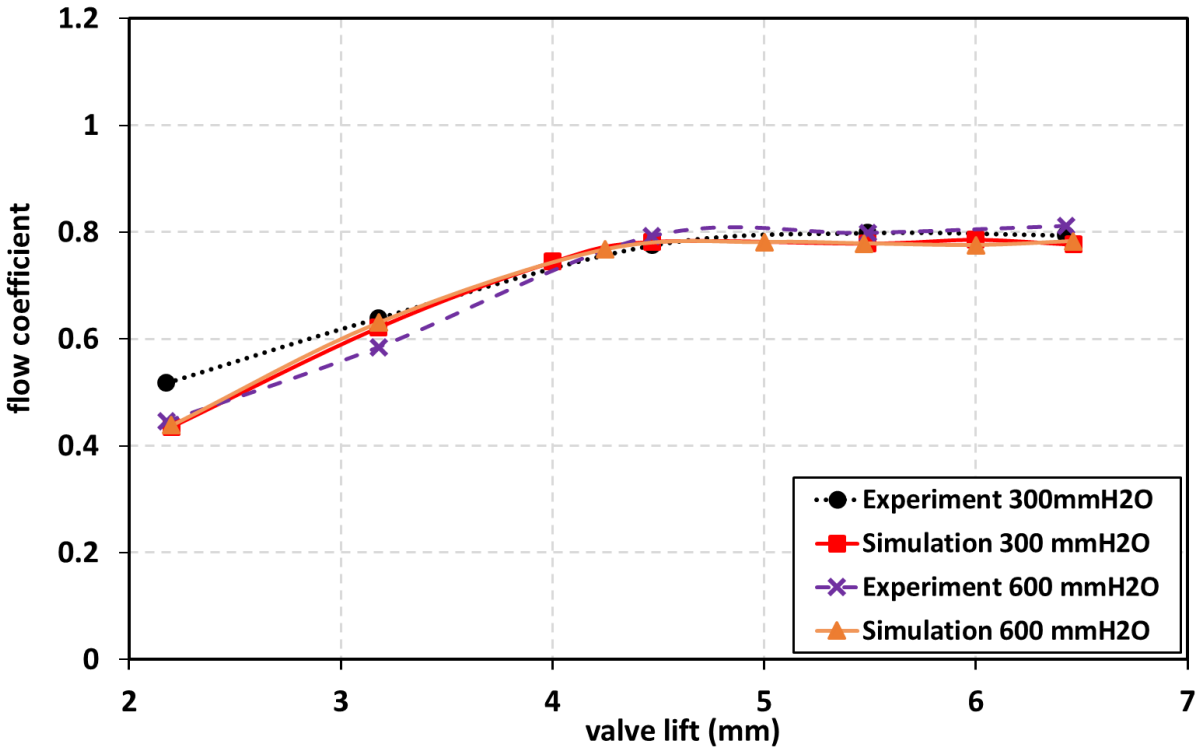

Fig. 4.2 Flow coefficient in steady state flow bench experiment and simulation

4.3 Comparison experiment and simulation result of discharge coefficient

The comparison of discharge coefficient that measured using the steady state flow benches and simulation at different valve lift at 300 and 600 mmH_2O pressure drop is illustrated in Fig. 4.3. Figure 4.3 shows that there is a dependence on the discharge coefficient that identifies the limitation of flow by the seat lips and valve on the valve lift. Initially, when the valve lift at a low level, air added to the engine cylinder passes through both the seat lip and valve so that a viscous shear effect occurs. Since air entering the cylinder increases because the valve lift is getting higher, the discharge coefficient slightly decreases with the increase in the Reynolds number. This is because of the viscous shear effect decreases. When the valve lifts at a high level, the fluid inertia prevents the flow from rotating along with the valve seat, so that the flow broke away and forms a free jet. On the other hand, an increase in pressure drop did not significantly influence the decrease in the discharge coefficient. However, there is a slight drop coefficient of discharge at 3.179 mm and pressure drop 600 mmH_2O which may indicate the flow segregation from the valve. There was a good agreement between experiment and simulation. The biggest deviation is only 11.51% occurs at 2.176 mm and pressure drop 300 mmH_2O

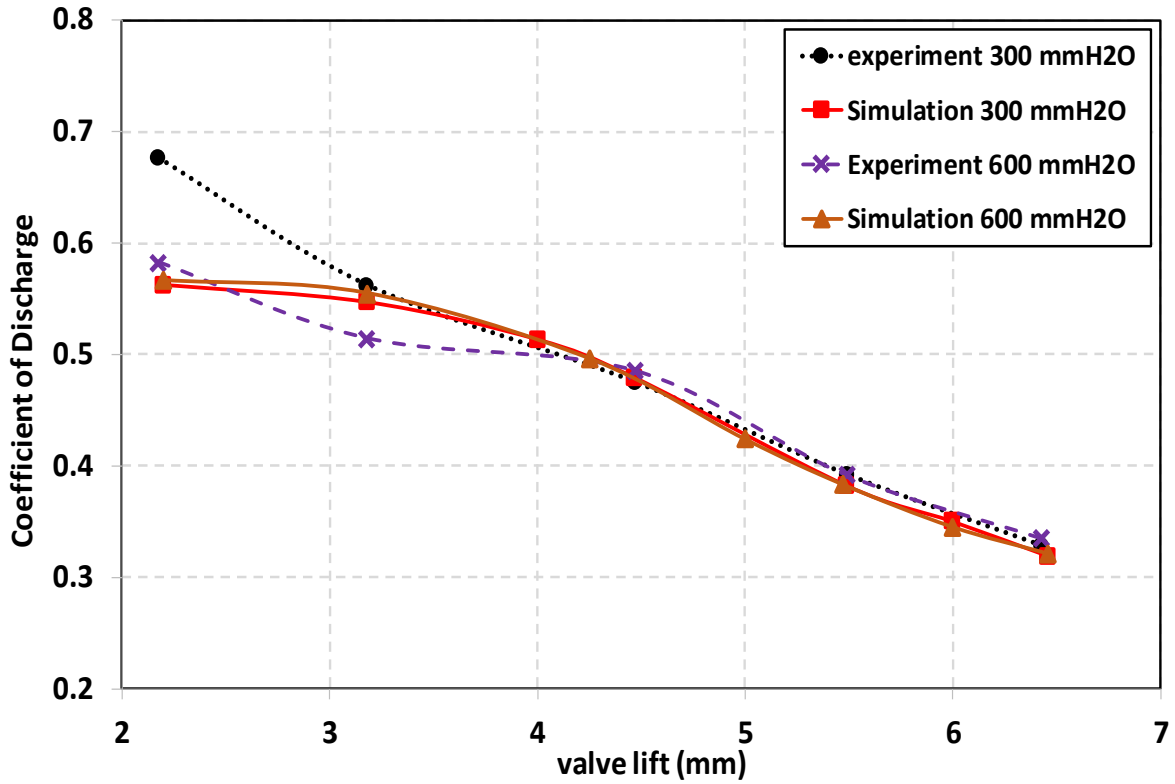

Fig. 4.3 Coefficient of discharge in steady state flow bench experiment and simulation

4.4 Velocity vectors for in-cylinder flow field

4.4.1. Horizontal Swirl Plane

4.4.1.1. Effect of Valve Lift

The comparison of the in-cylinder flow field velocity vectors with different valve lift, along a sectional x-y plane (z=-4 mm) passing through the intake valve and in-cylinder small motorcycle engine, for two pressure drops (300 and 600 mmH_2O) under motoring conditions is illustrated in figures 4.4. It can be seen the variation of swirl flow patterns caused by variations of valve lifts in 300 mmH_2O pressure drop (Figure 4.4a) and in 600 mmH_2O pressure drop (Figure 4.4b). It can be seen from the figure that the velocity of flow is increased when the valve lift increased up to the maximum valve lift (in this study the maximum valve lift is 6.46mm). This situation opposed to 6.1mm and 5.7mm where the velocity of flow is smaller than 6.46 mm. The general pattern that appears in the flow motion is a lot of variation with an increase in valve lift. Symmetrical counter-rotating vortices also appear in all images for high valve lift. This process occurs both in 300 and 600 mmH_2O pressure drop. In the case of the valve lift opened 6.1 mm and 6.46 mm, the velocities of flow near the edge of the cylinder are more seen clearly. However, the highest velocity occurs in the center of the cylinder. The higher the valve lift, the greater the velocity in the center of the cylinder. This is because of the high level of turbulence in these areas. The increase in turbulence made the air-fuel mixing in-cylinder more homogeneous. In addition, the increase in turbulence directly increased the rate of fire propagation.

4.4.1.2. Effect of Pressure Drop

The variation in flow motion caused by increasing pressure drop from 300 to 600 mmH2O is also illustrated in figure 4.4. Figure 4.4 shows that in the same valve lift and increasing pressure drop, the vortices established to maintain their shape in all images. The only change in all cases is only the change in the strength of the vortex where the greatest velocity is in the maximum valve lift 6.46 mm and 600 mmH_2O pressure drop around 67% larger than 300 mmH_2O pressure drop. This is in accordance with Bernoulli's calculation where the maximum inlet speed for cases of pressure drops of 300 and 600 mmH_2O are 60 m/sec and 100 m/sec respectively.

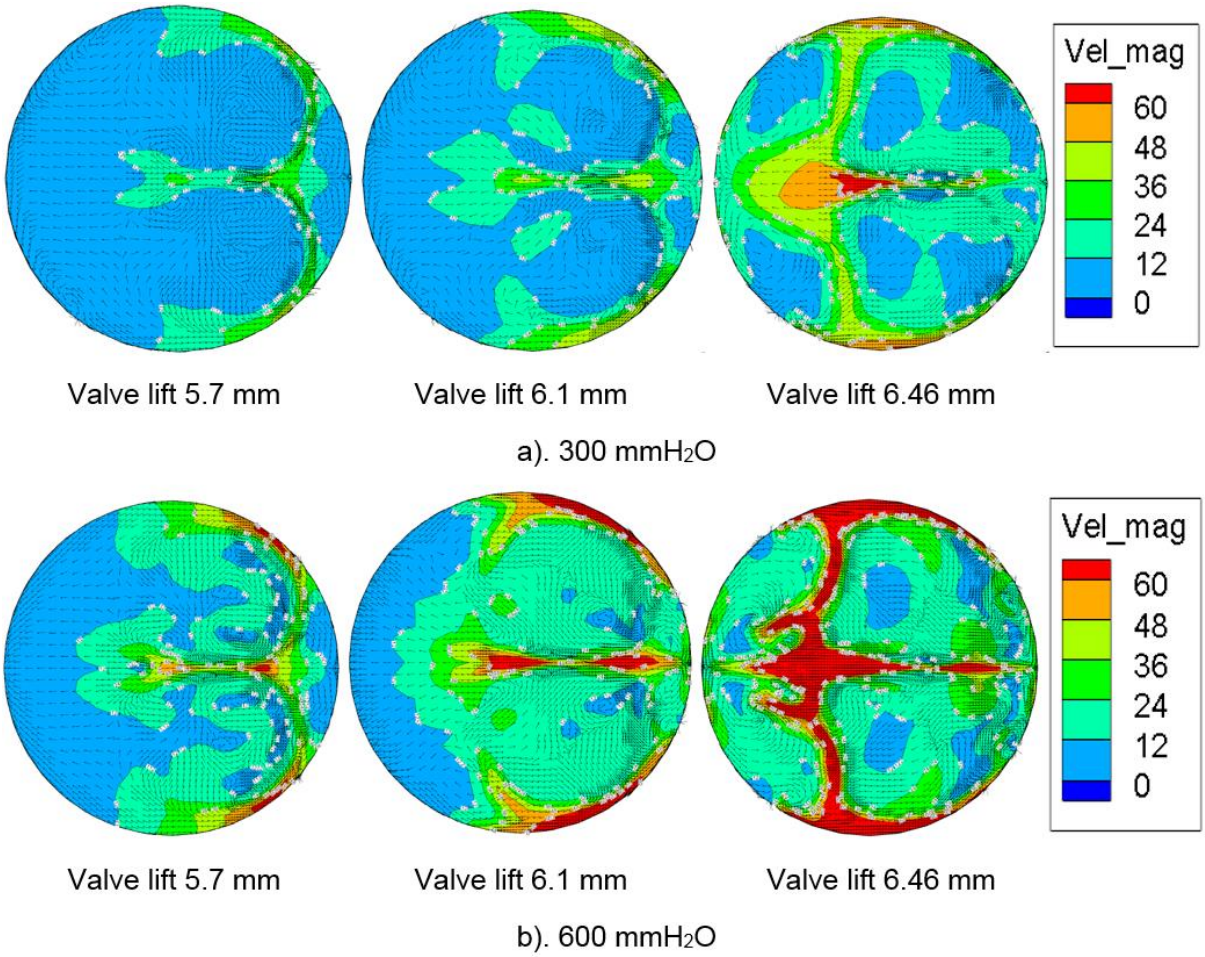

Fig. 4.4 Velocity vector with variation valve lift and pressure drop at x-y plane (z= -4 mm)

4.4.2. Vertical Tumble Plane

4.4.2.1. Effect of Valve Lift

The comparison of the in-cylinder flow field velocity vectors with different valve lift, along a sectional x-z plane (y=11.47 mm) passing through the intake valve and in-cylinder small motorcycle engine, for two pressure drops (300 and 600 mmH_2O) under motoring conditions is illustrated in figures 4.5. Figure 4.5 shows the variation in tumble flow patterns caused by various valve lifts both in 300 and 600 mmH_2O pressure drop. As expected, the flow pattern remains similar, but the velocity of flow in this pattern increases with increasing valves lift both at a pressure drop of 300 mm and 600 mmH_2O. At valve lift 5.7 mm, a small vortex began to form with a clockwise direction close to the intake valve. This is clearer in 600 mmH_2O pressure drop. In this step, air enters the engine cylinder through the side of seat lips and valve on the exhaust side interacted with air entering near the side of the cylinder wall. This interaction created a small vortex close to the intake valve. At 6.1 mm, more air entered

the to the engine cylinder. In this stage, many vortices were formed such as a vortex close to the intake valve and another vortex close to the exhaust valve. At 6.46 mm, there is one big vortex in the center of the cylinder. The maximum flow velocity shown for the 6.46 mm valve lift is illustrated to be quite higher than at the 6.1 mm and 5.7 mm valve lift. This is in accordance to the calculated maximum flow velocities that were achieved by the measured volumetric flow rate. The maximum flow velocity for the 6.46 mm valve lift is 100.56 m/s, for the 6.1 mm valve lift is 100.51 m/s and for the 5.7 mm valve lift is 100.48 m/s.

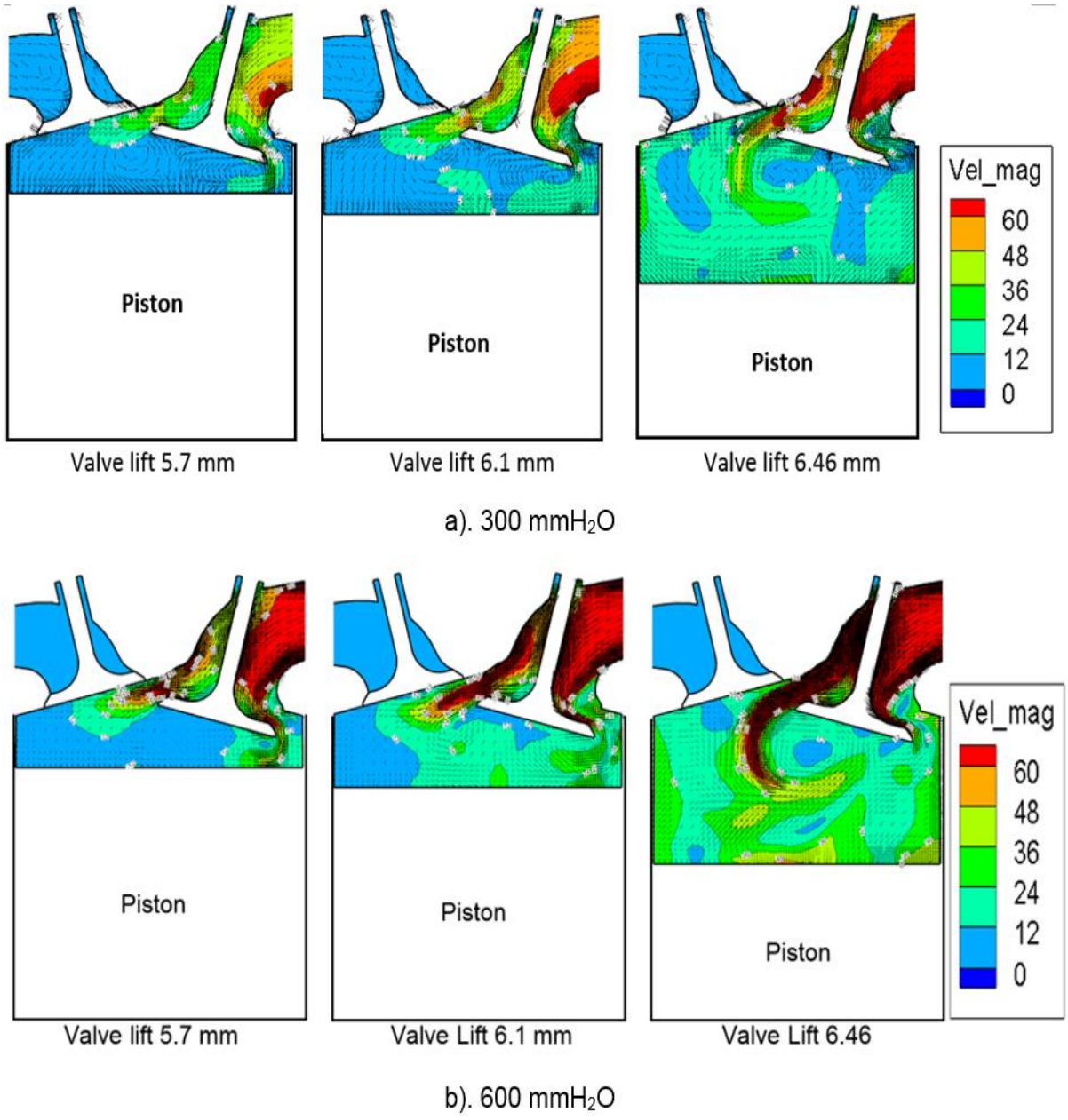

Fig. 4.5 Velocity vector with variation valve lift and pressure drop at x-z plane (y=11.47 mm)

4.4.2.2. Effect of Pressure Drop

The variation in the tumble flow motion caused by increasing pressure drop from 300 to 600 mmH_2O is also illustrated in figure 4.5. As expected, the flow pattern remains with the same orientation. However, the velocity magnitude in this flow pattern increases. It can be concluded related to the flow pattern that there is a similarity between the increase in pressure drop and the increase in valve lift, i.e. reduces the area from which the vector field can be generated. This is caused by a higher flow rate inside the cylinder, which causes an increase in the velocity of spread across the cylinder. This occurs in all valve lifts such as 5.7 mm, 6.1 mm and 6.46 mm.

4.5 Vorticity magnitude for in-cylinder flow field

4.5.1. Horizontal Swirl Plane

4.5.1.1.Effect of Valve Lift

Vorticity is the velocity field curl thus it is a measure of the local rotation of the fluid. Moreover, vorticity is the quantity used to express the initiation, transformation and extinction of vortices. The comparison of the in-cylinder flow field vorticity magnitude with different valve lift, along a sectional x-y plane (z=-4 mm) passing through the intake valve and in-cylinder small motorcycle engine, for two pressure drops (300 and 600 mmH_2O) under motoring conditions is illustrated in figures 4.6. Vorticity of 5.7 mm valve lift with 300 mmH_2O pressure drop is dominated in the right area of the cylinder where the intake valve is located. While on the left side of the cylinder around the exhaust valve, the vorticity magnitude is very small. When the valve lift increases to 6.1 mm, the dominance of the vorticity is still on the right side of the cylinder and reaches its peak in the center of the cylinder. At a 6.46 mm valve lift, the vorticity magnitude gets bigger on the left side of the cylinder even though the biggest vorticity is still in the center of the cylinder. vorticity change process at 300 mmH_2O pressure drop is also similar to 600 mmH_2O pressure drop. It can be concluded that the strength of vorticity increases with the increase in valve lift.

4.5.1.2.Effect of Pressure Drop

Figure 4.6 also shows the variation vorticity magnitude for in-cylinder flow pattern generated by increasing in the pressure drop across the cylinder head from 300 mmH_2O to 600 mmH_2O in the same valve lift. Based on figure 9, it is shown that the increasing pressure drop from 300 to 600 mmH_2O in the same valve lift made the vorticity pattern remains in similar

orientation, but the vorticity magnitude is increased. It can be understood that in areas that have large vorticity such as the central area of the cylinder and along the edge of the cylinder that is close to the intake valve showing high local rotation in the area. This occurs in all valve lifts (5.7 mm, 6.1 mm and 6.46 mm).

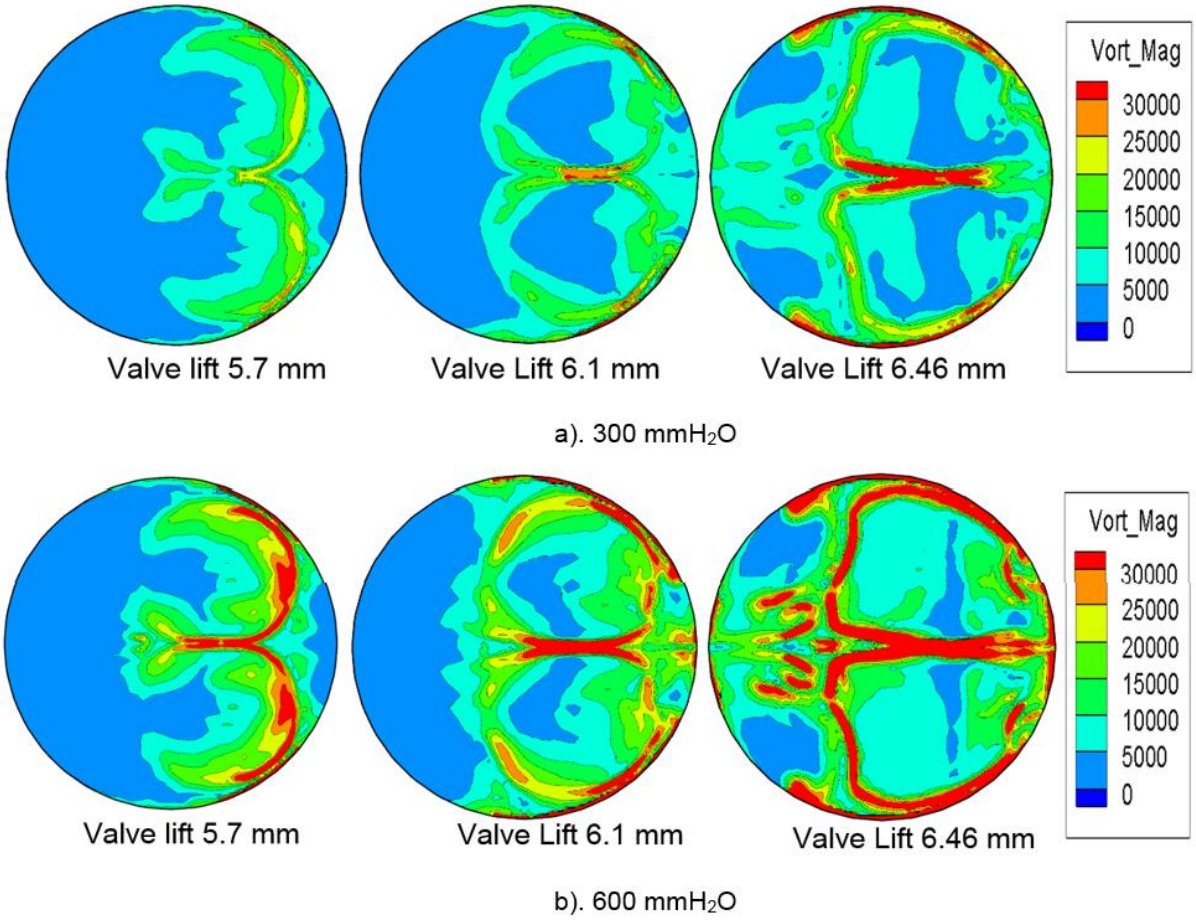

Fig. 4.6 Vorticity magnitude with variation valve lift and pressure drop at x-y plane (z= -4 mm)

4.5.2. Vertical Tumble Plane

4.5.2.1. Effect of Valve Lift

The comparison of the in-cylinder flow field vorticity magnitude with different valve lift along a sectional x-z plane (y=11.47 mm) passing through the intake valve and in-cylinder small motorcycle engine, for two pressure drops (300 and 600 mmH_2O) under motoring conditions is illustrated in figures 4.7. It is shown that the variation vorticity magnitude for in-cylinder flow structures produced by increasing valve lift in 300 mmH_2O pressure drop (Figure 4.7a) and in 600 mmH_2O pressure drop (Figure 4.7a) across the cylinder head. The vorticity of 5.7 mm valve lift with 300 mmH_2O pressure drop starts to form on the side of the intake valve

and reaches maximum conditions at both intake valve valves due to collisions of air flow at the end of the intake valve side with the cylinder wall when the intake valve starts to open. Vorticity starts to expand in the same position when the intake valve is opened larger to 6.1 mm. When the intake valve reached its maximum point, 6.46 mm, vorticity began to spread in several places. Although the maximum vorticity is still around the end of the intake valve. This process is similar with what happened at a 600 mmH_2O pressure drop both on the elevator valve 5.7 mm, 6.1 mm and 6.46 mm. This can be explained that the increase in intake valve both at 300 and 600 mmH_2O pressure drop resulted in an increase in vorticity magnitude and the largest vorticity magnitude occurred around the end of both sides of the intake valve.

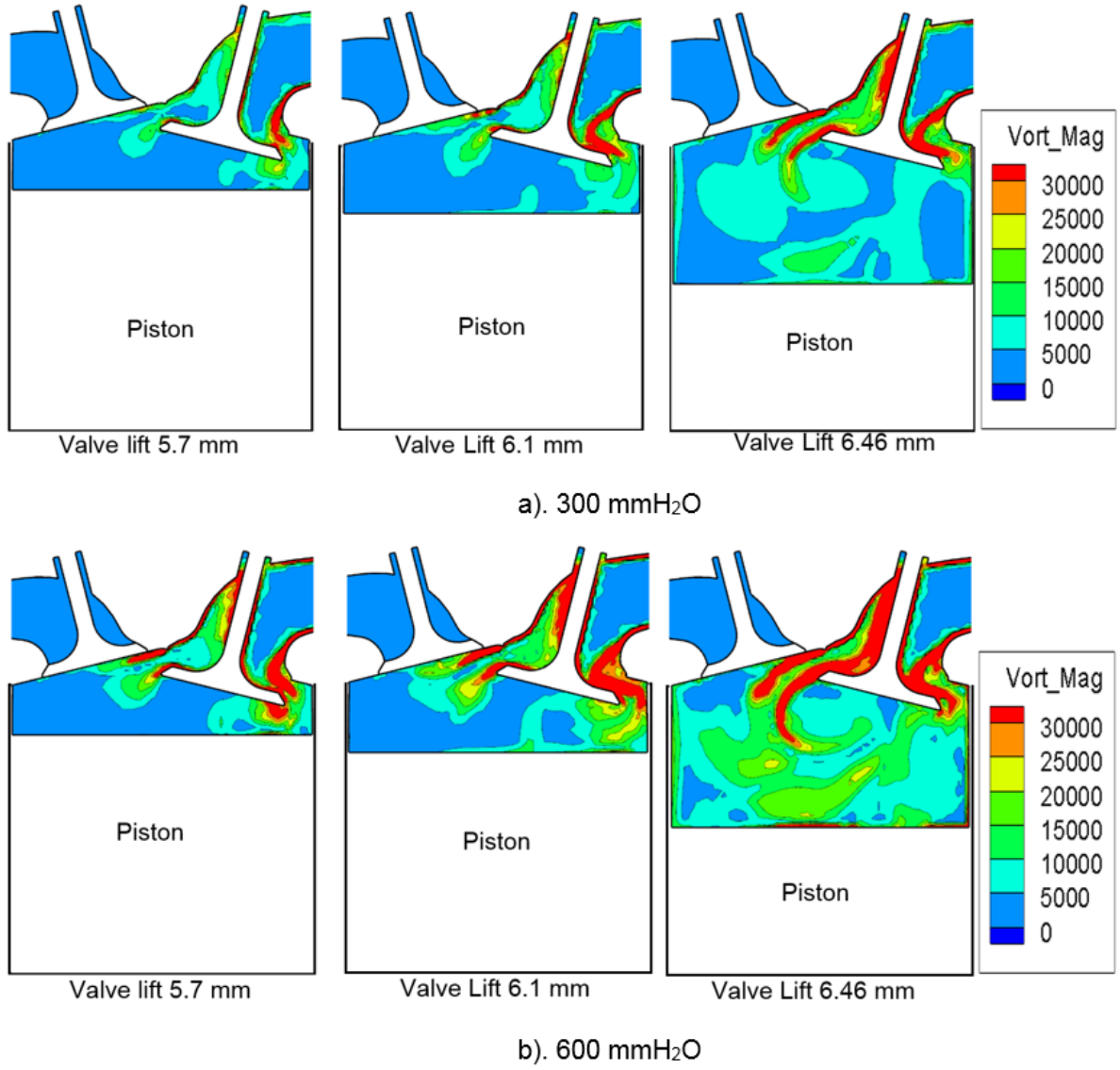

Fig. 4.7 Vorticity magnitude with variation valve lift and pressure drop at x-z plane (y=11.47 mm)

4.5.2.2. Effect of Pressure Drop

The variation of vorticity magnitude caused by increasing pressure drop from 300 to 600 mmH_2O and in the same valve lift is also illustrated in figure 4.7. As expected, the vorticity pattern remains with the same shape. However, the vorticity magnitude in this flow pattern increases where there was an increase in vorticity magnitude of 57% greater in the valve lift 6.46 mm and 600 mmH_2O (91000 1/s) than in valve lift 6.46 mm and 300 mmH_2O pressure drop (58000 1/s)

4.6 Characteristic of in-cylinder flow

In this section, some parameters as the characteristic of the in-cylinder flow of small motorcycle engines such as swirl ratio, tumble ratio, angular momentum, TKE, turbulent length scale, in-cylinder air mass, and turbulent velocity during the intake and compression strokes, under motoring conditions, are presented and discussed. In the results presented and discussed in this section, some values have been normalized. Normalization is the process of grouping data attributes that form entities that are simple, nonredundant, flexible, and adaptable, so that it can be ensured that the database created is of good quality. The purpose of Database Normalization is to eliminate and reduce data redundancy and the second goal is to ensure data dependencies. In this study, several graphs, especially those related to data with engine speed variations, have been normalized. The swirl and tumble ratios were normalized using the following equation:

$$\boldsymbol{x'} = \frac{\boldsymbol{x - mean(x)}}{\mathbf{max}(\boldsymbol{x}) - \mathbf{min}(\boldsymbol{x})} \tag{32}$$

where x is an original value of the swirl or tumble ratio, x' is the normalized value of the swirl or tumble ratio, *mean(x)* is the mean value from all original value, *max(x)* is the maximum value from all original value and *min(x)* is the minimum value from all original value. The angular momentum was normalized by $V\rho Bu_p$ where V is the displacement (125cm^3), ρ is air density (1.225 kg/m^3), B is bore (57 mm) and u_p is the mean piston speed (3.25 m/s for 2000 rpm, 4.88 m/s for 3000 rpm, and 6.51 m/s for 4000 rpm). TKE was normalized by $0.5u_p^2$. The turbulent length scale was normalized by the bore B. The in-cylinder air mass was normalized by $V\rho$, and turbulent velocity was normalized by u_p [73].

4.6.1. Swirl Ratio

The formation of swirl flow starts with the flow from the intake port into the engine cylinder with the initial angular momentum and the interaction between the cylinder wall, intake port and piston surface. Figure 4.8 shows the comparison of the swirl ratio with two different pressure drops (300 and 600 mmH_2O) during the intake and compression strokes. Rotating flow is formed first in the initial phase of the process of induction. This flow was up and down until achieved the maximum position in the negative axis around 500 °CA and after this point became almost stable until around 600 °CA. This is possible because the angular momentum disappears into the wall and turbulent dissipation in the flow. Then, the swirl ratio increased during the last stages of the compression stroke. This was evident at all pressure drops except at crank angle 700 °CA at 300 mmH_2O pressure drop. This occurs because of the tangential velocity of the swirl flow, which increased because of the interaction between the piston and the cylinder wall. Moreover, figure 4.9 shows the effect of the pressure drop to the swirl flow in the variation of valve lift. Increasing the pressure drop on the small motorcycle engine at the beginning of the intake stroke, especially at the beginning of the valve lift opening, has no effect on the swirl ratio. This happens until the valve lift reaches 5 mm. However, after an open valve lift exceeds 5 mm pressure drop, it has the effect of reducing the swirl ratio to 75% when the valve lift reaches 6.25 mm. This is probably caused by the poor strength of the intake flow in the engine, even though the pressure drop was increased to the point that only swirling vortices were generated. When the valve lift increases from 6.39 mm to the maximum valve lift, (6.46 mm) at the pressure drop of 300 mmH_2O, the swirl ratio decreases again. This is probably due to the angular momentum lost to the wall and turbulent dissipation in the flow.

For more comprehenshive, this swirl flow also was analyzed under motoring conditions at three different speeds. The comparison of the normalized swirl ratios according to the crank angle at three engine speeds (2000, 3000, and 4000 rpm) during the intake and compression strokes is shown in Fig. 4.10. The increments of engine speed in the small motorcycle engine caused the swirl ratio to have an irregular shape. This phenomenon began to appear at the beginning of the intake stroke at 400 °CA, and from this point up to 495 °CA, the swirl ratio became more irregular as engine speed increased. The swirl ratio tended to be stable and almost constant in the beginning of the compression stroke, until 630 °CA, and to be unstable at the end of compression stroke. This may be attributed to the poor strength of the intake flow in the engine, even though the engine speed was increased to the point that only

swirling vortices were generated, and these were not sustained during the stabilization and spin up phase.

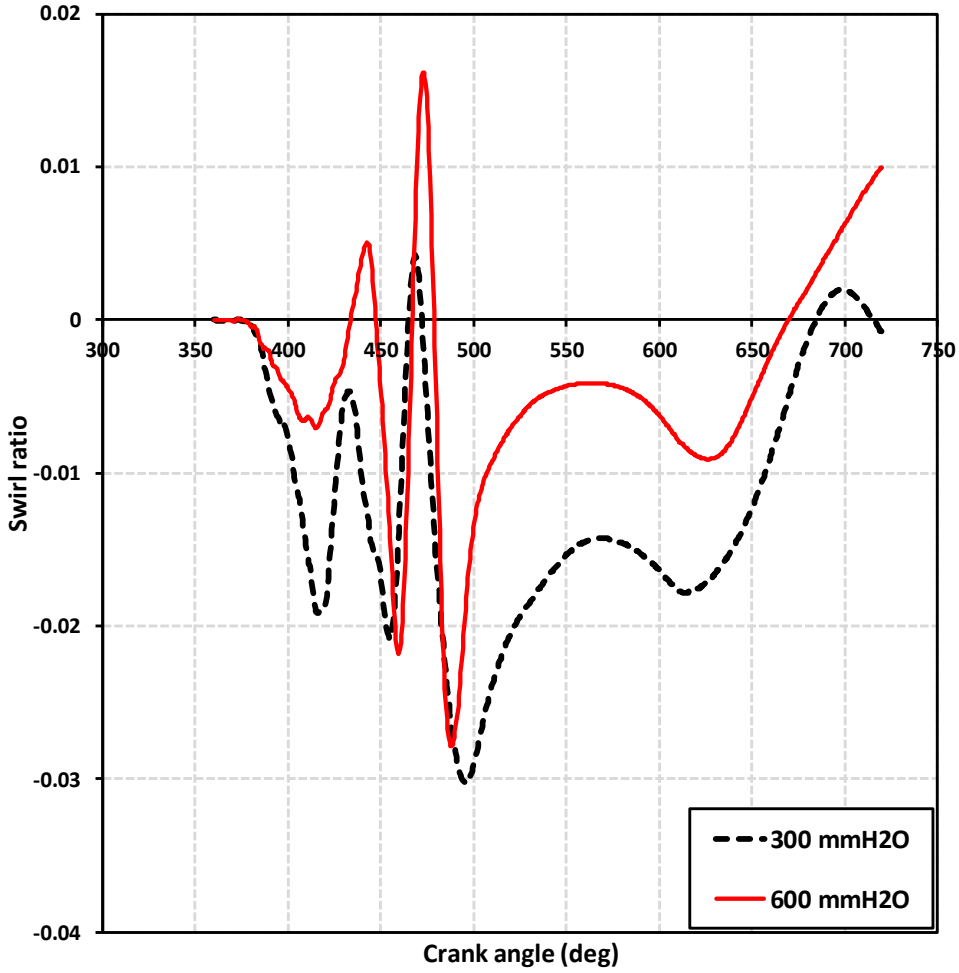

Fig. 4.8 The In-cylinder swirl ratio at different pressure drop

This phenomenon is very different from what generally occurs in large engines. An increase in engine speed in large engines has an impact on the increasing of swirl ratio such as the study carried out by Ramesh and James [105]. Ramesh and James conducted a study on a large engine (86 mm x 86 mm) with pent roof combustion chamber and engine speeds of 1000, 2000, and 3000 rpm. Their research showed that the swirl ratio at 1000 rpm generated and reached the maximum value at 390 °CA and go down to be zero at 430 °CA and achieved maximum value at 480 °CA in negative axis and to be stable until the end of the compression stroke. This tendency also occurred at engine speeds of 2000 rpm and 3000 rpm. However, the swirl ratio at 2000 rpm was five times the swirl ratio at 1000 rpm, and the swirl ratio at 3000 rpm was two times the swirl ratio at 2000 rpm.

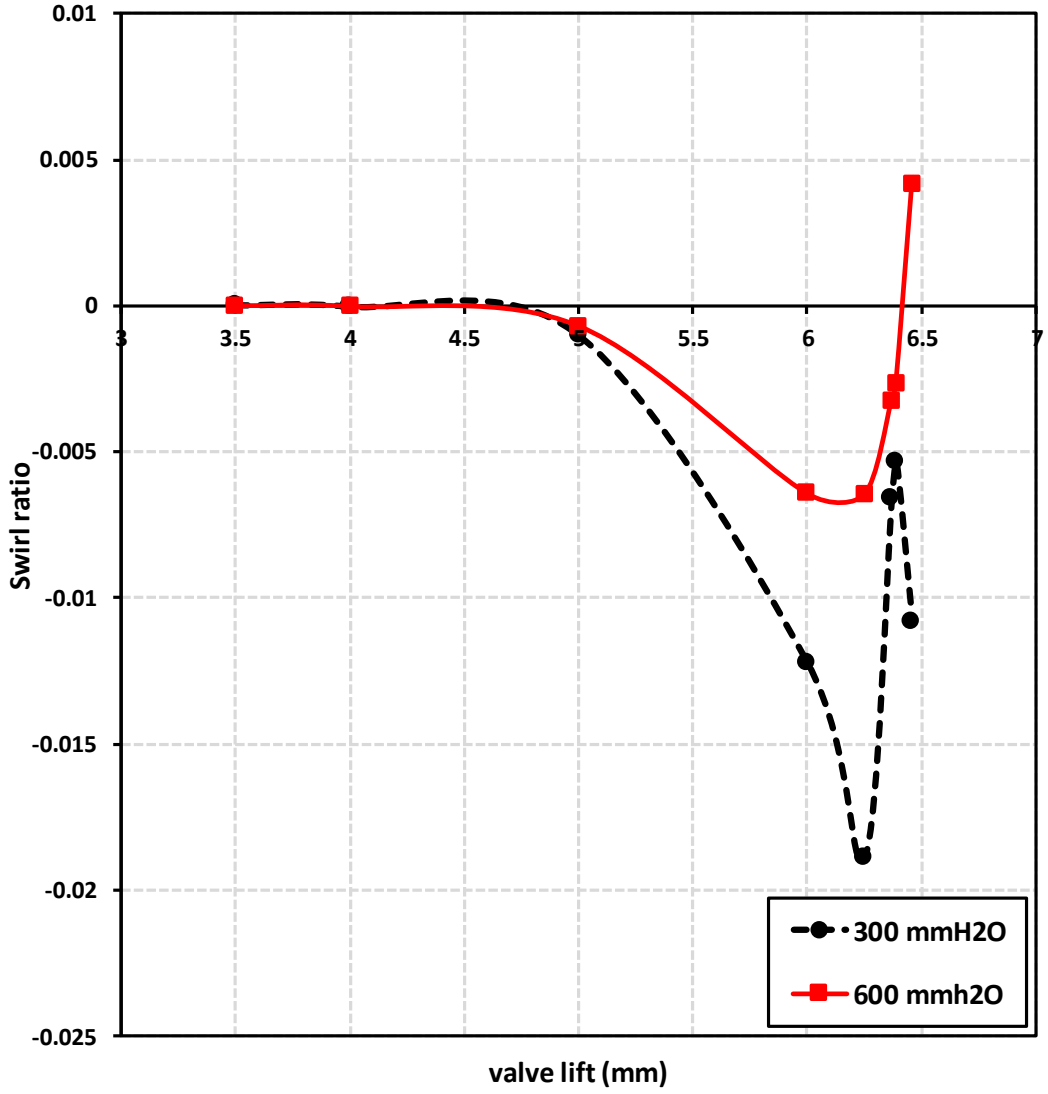

Fig. 4.9 The variation of swirl ratio at different valve lift

From this comparison, it can be concluded that increasing the engine speed of the small motorcycle engine caused the swirl ratio to be of irregular shape, especially during the intake stroke up to 495 °CA, but increasing the engine speed in large engines increases the swirl ratio at all the crank angle degrees (CADs). This may be because large engines provide an opportunity for the air flow entering the cylinder to be more flexible, and create more interaction at the intake port, the cylinder wall, and the piston face. However, it does not guarantee that the increase in the swirl ratio will improve the performance of the engine. There are many parameters that determine the performance of an engine. Therefore, in the next study, the design of the intake port will be maximized to improve the engine performance, even though the swirl ratio is not too high.

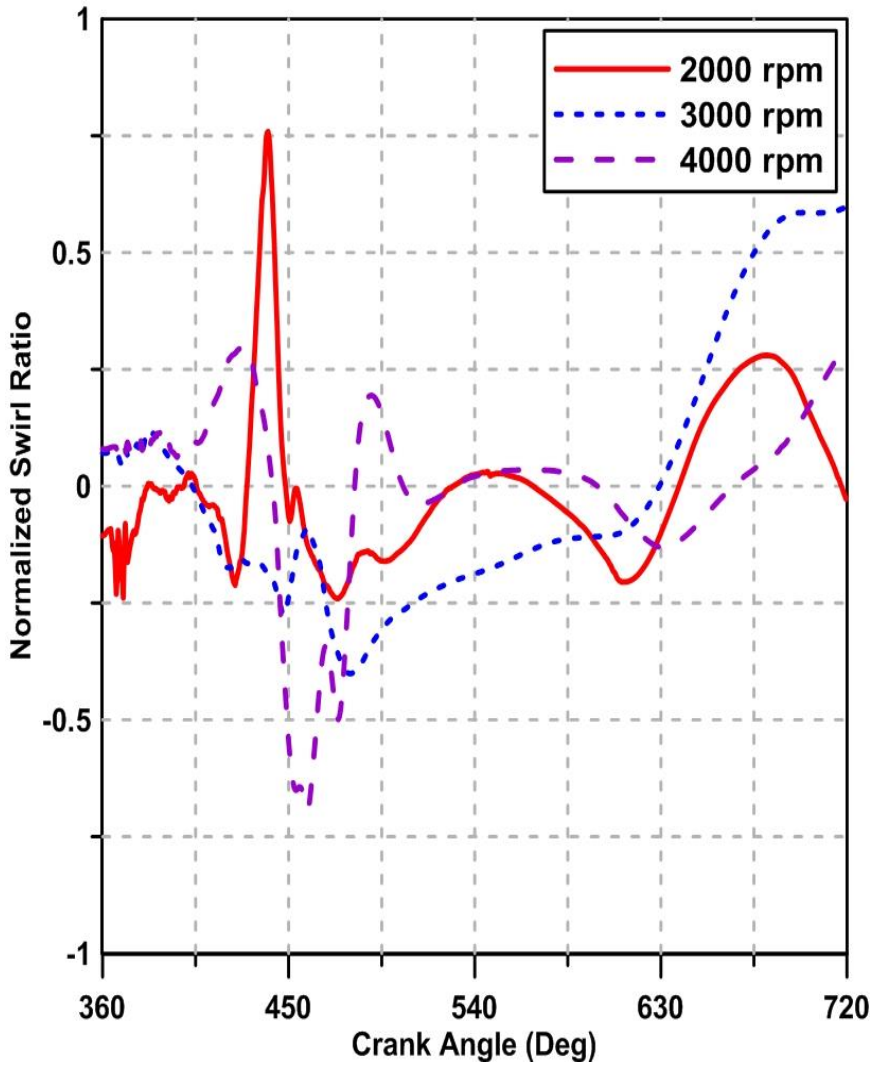

Fig. 4.10 The In-cylinder Normalized swirl ratio at different engine speeds

4.6.2. Tumble Ratio

The tumble ratio usually had to be approximated to offer a significant effect on the in-cylinder tumble flow. Figure 4.11 illustrates the comparison of the tumble ratio for two different pressure drops (300 and 600 mmH_2O) under motoring conditions. Cross tumble (TRx) and normal tumble (TRy) are two important tumble vortices rotation in flows motion. Tumble Ratio (TR) is total from these two tumbles. There are three phases of tumble ratio i.e. production, stabilization and destruction. In this case, the production phase occurred in the early intake process up to 380 °CA and then decrease until zero at 400 °CA. Then, the phase of stabilization began and reached the highest level at 490 °CA and dropped dramatically until 560 °CA, because of the incoming momentum of flow to the cylinder engine through the valves decreased and the cylinder volume increased to BDC.

From this point, the tumble flows upward again until 630 °CA, due to the conservation of angular momentum. The last phase is the destruction phase that happened at the last of the compression stroke until 720 °CA. There is a dramatic decrease due to the dissipation effect. Regarding the effect of pressure drop, it can be observed that the increments of the tumble ratio in the small motorcycle engine between 300 to 600 mmH_2O only marginal. The biggest increase of tumble ratio occurs at 490 °CA for only 2.99%. This might be due to the poor strength of intake flow in a small motorcycle engine, even though the pressure drop was increased to the point that it only generated tumbling vortices, which was not sustainable during the stabilization phase. This shows that an increase in pressure drop on a small motorcycle engine doesn't have a significant effect on increasing the tumble ratio. Moreover, figure 4.12 shows the effect of the pressure drop to the tumble flow in the variation of valve lift. It can be seen detailly that increasing the pressure drop on the small motorcycle engine at the beginning of the intake stroke until the end of compression stroke doesn't have effect on the tumble ratio.

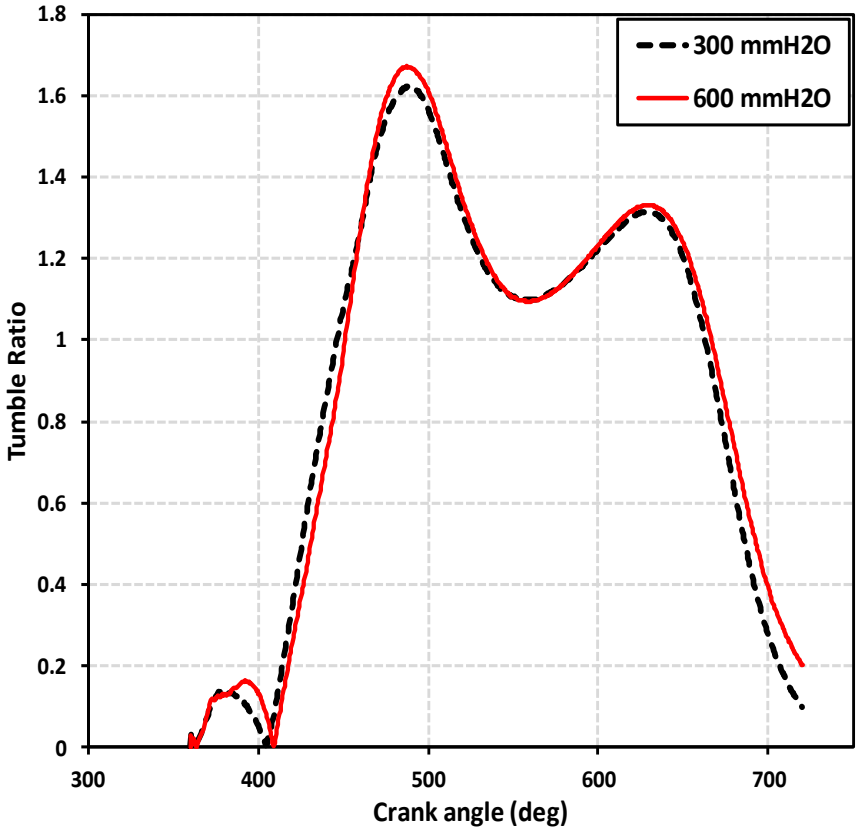

Fig. 4.11 The In-cylinder tumble at different pressure drop

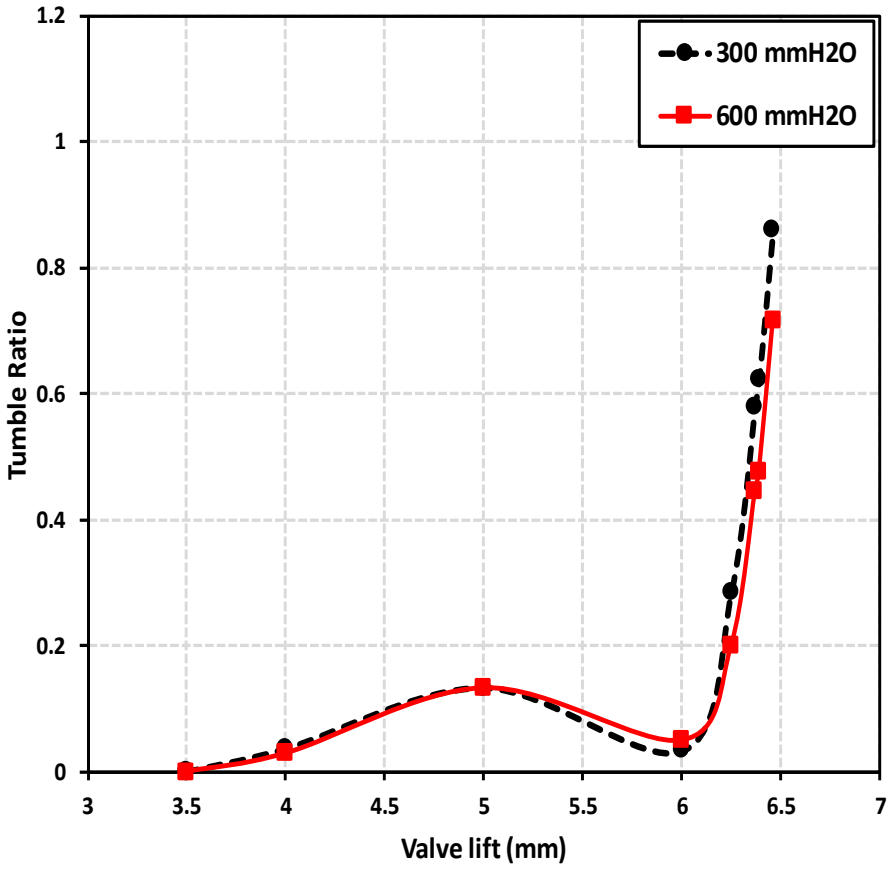

Fig. 4.12 The variation of tumble ratio at different valve lift

For more comprehenshive, this tumble flow also was analyzed under motoring conditions at three different speeds. The comparison of the normalized tumble ratios according to the crank angle at three engine speeds (2000, 3000, and 4000 rpm) during the intake and compression strokes is shown in Fig. 4.13. However, in the following study, only *TRy* is considered as the tumble flow considering variations of engine speed, since the geometry of the engine is symmetrical and the value of *TRx* is very small then the model of total of *TR* and *TRy* is similar. Regarding the effect of the engine speed, it can be observed that the increments of tumble ratio in the small motorcycle engine between 2000 to 3000 rpm and between 3000 to 4000 rpm were negligible during the intake stroke, until the beginning of compression stroke, around 630 °CA. However, the increase of tumble ratio in the range of 2000 to 3000 rpm and in the range of 3000 to 4000 rpm, from this point until the end of the compression stroke, was only marginal. This may be attributed to the poor strength of the intake flow in small motorcycle engines, even though the engine speed was increased to the point that it only generated tumbling vortices, which were not sustained during the stabilization and spin up phase. This indicates that the increasing of engine speed in small motorcycle engines has no

significant effect on the increase in the tumble ratio. Based on Fig. 4.13, it also is clear that at the three engine speeds, the flow distribution is similar, from the early intake stroke until the end of the compression stroke.

In comparing this study to the study conducted by Ramesh and James [105] using a large engine (86 mm x 86 mm), it was found that a phenomenon appeared in the characteristics of tumble flow in the small motorcycle engine that did not appear in the large engine. This phenomenon is the initial formation of tumble flow, at the beginning of the intake stroke until the crank angle reaches 400 °CA. This initial formation did not occur for a long time and reached a maximum value of only 0.25, then decreased again to zero, then increased again to reach the peak point at a crank angle of approximately 460 °CA. This may be due to the bifurcation zones and low pressure that occurs in the beginning of the intake stroke in a small motorcycle engine. On the other hand, the large engine starts to produce the tumble flow from 400 °CA and immediately increases significantly until reaches the peak point at 460 °CA. Starting from this point until the end of the compression stroke, the trend of tumble ratio in the large engine has the same tendency to the small motorcycle engine. This trend occurs both at engine speeds of 2000 and 3000 rpm.

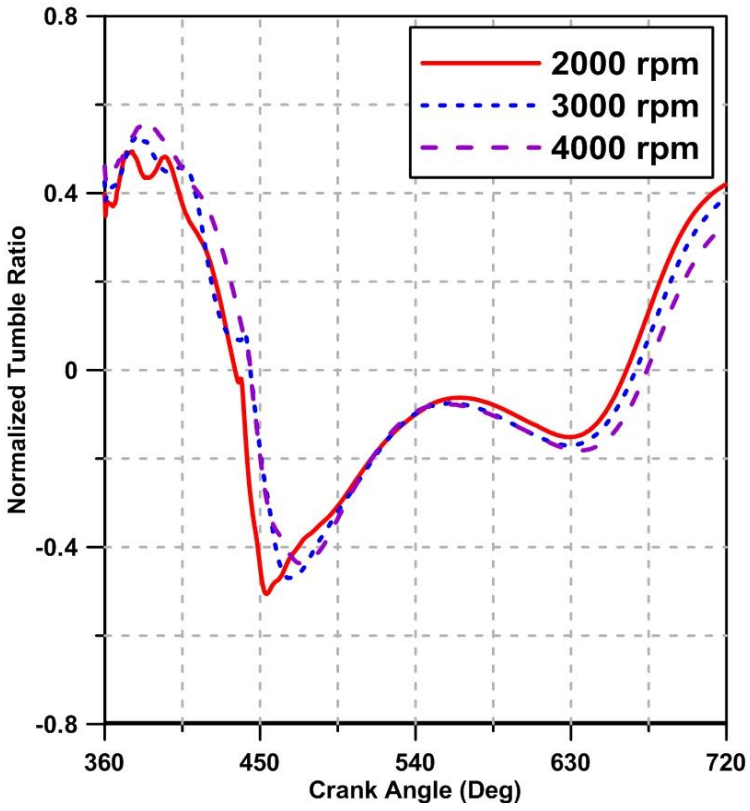

Fig. 4.13 The variation of tumble ratio at different engine speeds

4.6.3. Turbulent Kinetic Energy (TKE)

In the turbulent flow, TKE is the mean of kinetic energy per unit mass that is indicated by the root-mean-square (RMS) measure from the velocity fluctuation. One of the important parameters to estimate the turbulent viscosity is TKE. The comparison of TKE with the crank angle for two pressure drops (300 and 600 mmH_2O) under motoring conditions during intake and compression strokes is shown in Figure 4.14. There were two peaks in the TKE. The first peak occurs in the middle of the intake stroke around 460 ° CA and is the highest peak. The first peak occurs because of the turbulence produced when air flows through the intake valve curtain area. The second peak occurs after the first peak and is lower than the first peak. The second peak occurs in the last stage of the compression stroke. The second peak occurs probably because when the piston moves further up in the cylinder, it falls into a smaller space.

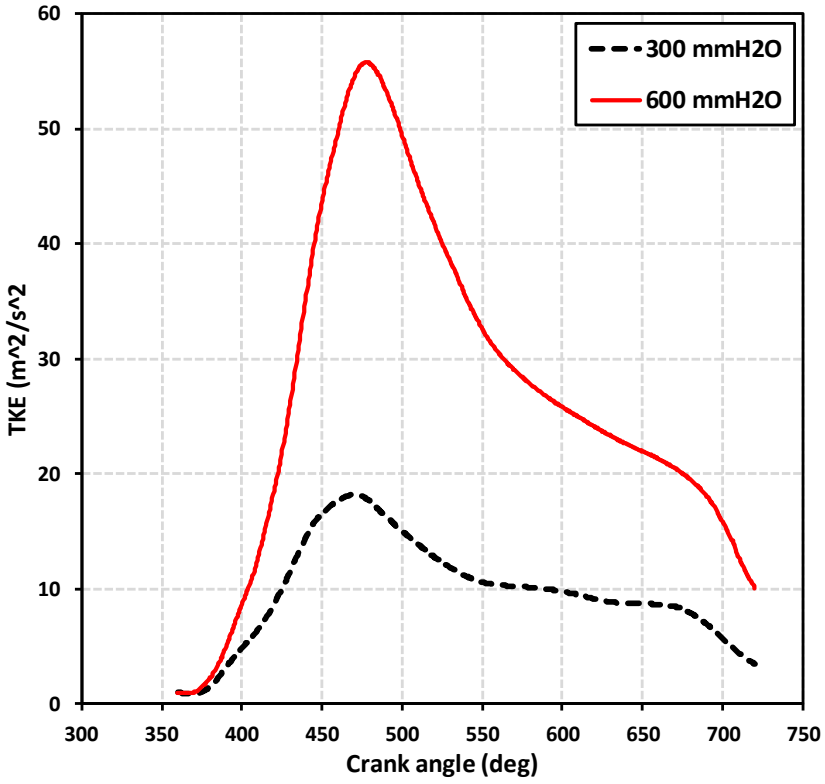

Fig. 4.14 The In-cylinder TKE at different pressure drop

Regarding the effect of pressure drops, it can be observed that the increments of TKE in the small motorcycle engine between 300 to 600 mmH_2O from the early intake stroke until the end of the compression stroke, reached the highest value of around 200 % at 470 °CA. This may be because when the pressure drops increased from 300 to 600 mmH_2O, it caused a significant increase in the inlet air velocity, especially when occurs the transition dynamics of

intake valve which starts closing from full opening position. Increasing the incoming air velocity indicates a collapse of tumbling vortices. The destruction of tumbling vortices increases turbulence, resulting in a higher TKE. This is confirmed by Figure 4.15 when the valve lift starts to open until the valve lift reaches 5 mm, where the value of TKE does not change significantly with the increase in pressure drop from 300 to 600 mmH_2O. However, after the valve lift is open more than 5 mm, there is a significant increase in the value of TKE with an increase in pressure drop.

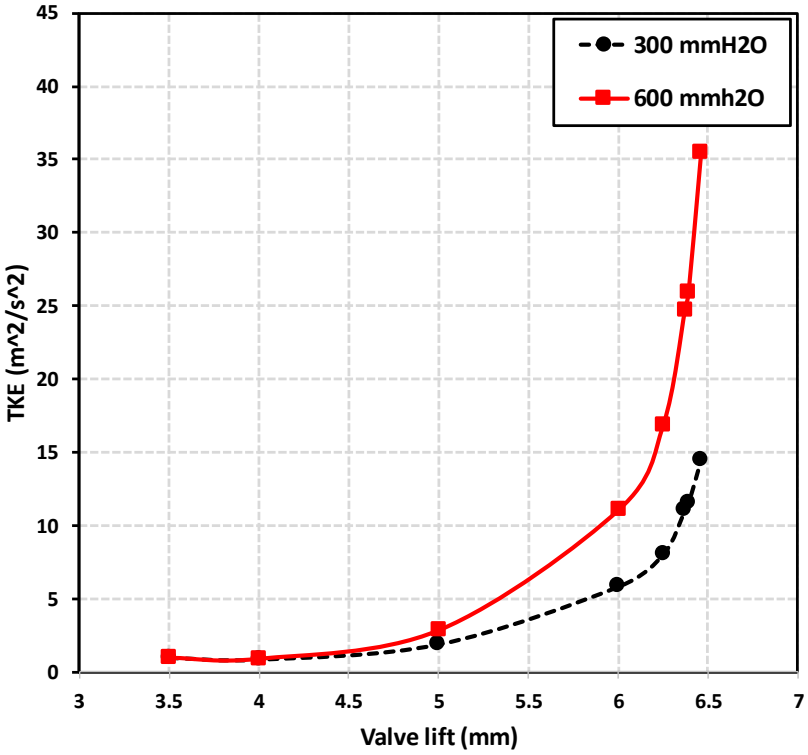

Fig. 4.15 The variation of TKE at different valve lift

For more comprehenshive, this TKE also was analyzed under motoring conditions at three different speeds. The comparison of the normalized TKE according to the crank angle at three engine speeds (2000, 3000, and 4000 rpm) during the intake and compression strokes is shown in Fig. 4.16. Regarding the effect of speed, it can be observed that the increments of TKE in the small motorcycle engine between 2000 to 3000 rpm and 3000 to 4000 rpm were negligible from the early intake stroke until the middle of the intake stroke at 450 °CA. On the other hand, the increase of TKE between 2000 to 3000 rpm, from this point until the end of compression stroke, was only marginal, where the biggest increase of TKE is around 8 % at 460 °CA. However, the increase in TKE between 3000 to 4000 rpm, from this point until the end of compression stroke, reached the highest value of around 50 % at 460 °CA. This may be

because when the engine speed increased from 3000 to 4000 rpm, it caused a significant increase in the inlet air velocity, especially when occurs the transition dynamics of intake valve which starts closing from full opening position. The increasing of inlet air velocity indicates the destruction of tumbling vortices. The destruction of tumbling vortices increases turbulence, resulting in a higher TKE.

The small motorcycle engine had an additional unique phenomenon that is not possessed by large engines. This phenomenon is the process of up and down from TKE at the beginning of the intake stroke until the crank angle reaches around 440 °CA. This process doesn't occur for long time. Starting from this point, the TKE increased significantly until it reached the first peak in the middle of the intake stroke, around 460 °CA. This was evident at all engine speeds (2000, 3000, and 4000 rpm). It was probably due to the bifurcation areas and low pressure occurring in the beginning of the intake stroke. This is different from the results of a study conducted by Addepalli and Mallikarjuna [106]. Addepalli and Mallikarjuna conducted research on a large engine with 87.5 mm x 110 mm and engine speeds of 2000, 3000, and 4000 rpm. In all three engine speeds, the TKE in the large engine increased significantly from the beginning of intake stroke until it reached a peak point around 460 °CA. Starting from this point until the end of the compression stroke, the trend of TKE in the large engine has the same tendency to the small motorcycle engine.

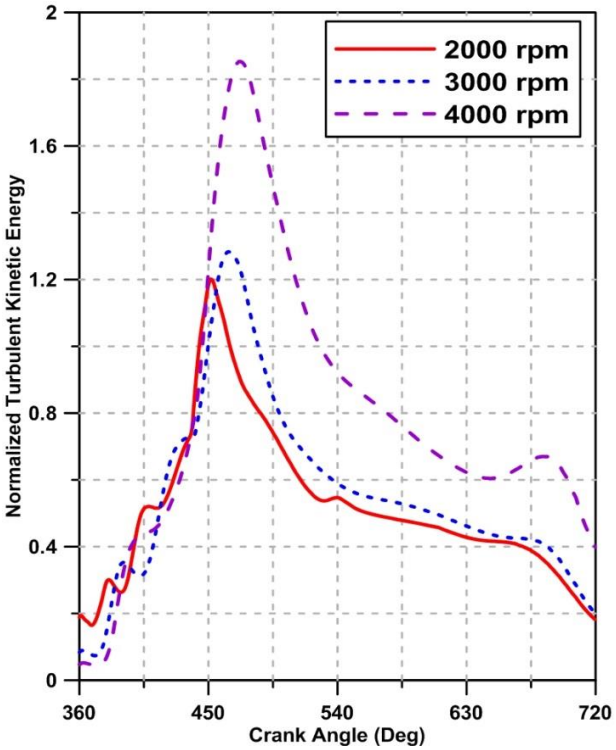

Fig. 4.16 The In-cylinder normalized TKE at different engine speeds

4.6.4. Air Mass

Gasoline engine speed is regulated by quality rather than quantity. Speed adjustments set by throttle can be eliminated by quality settings. Figure 4.17 shows the comparison of in-cylinder air mass versus CAD at two different pressure drops (300 and 600 mmH_2O) under motoring conditions during intake and compression strokes. The accumulated air mass enters the cylinder engine from the early of the intake stroke when the valve lift starts to open, then continues to increase until the end of the intake stroke at 540 ° CA. Then the air mass became stable until the end stages of the compression stroke. Regarding the effect of increasing the pressure drop from 300 to 600 mmH_2O, there was no significant effect on the air mass accumulating in the small motorcycle engine along the intake stroke. This can be seen in more detail in figure 4.18 which compares air mass with variations in valve lift where there is no significant effect on the air mass entering the cylinder engine even though the pressure drop has been increased. However, during compression stroke, there is the increasing of air mass around 3.77% because of increasing pressure drop from 300 to 600 mmH_2O. This is probably due to the inertia of the air entering more than the inertia of the air mass moving upward near the piston.

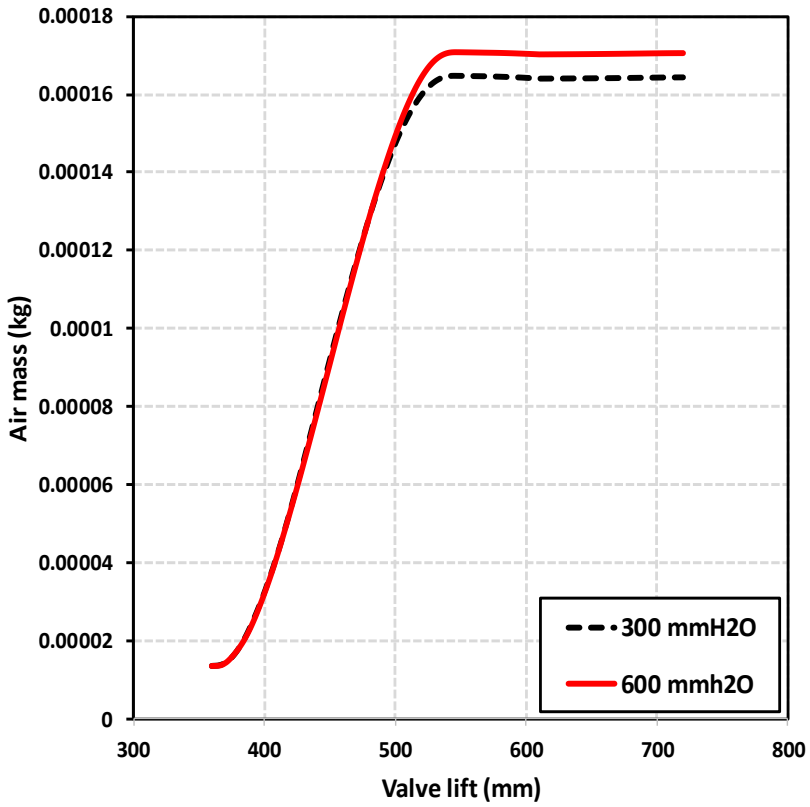

Fig. 4.17 The In-cylinder air mass at different pressure drop

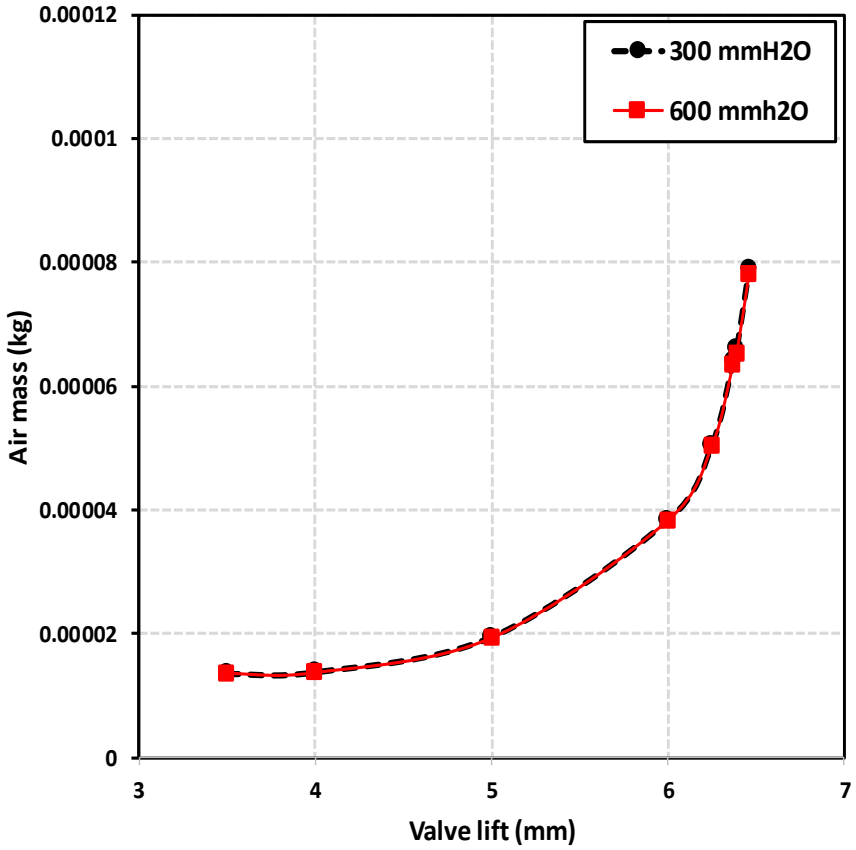

Fig. 4.18 The variation of air mass at different valve lift

Figure 4.19 shows the comparison of normalized in-cylinder air mass for the filling process with CAD at three engine speeds (2000, 3000, and 4000 rpm) during intake and compression strokes under motoring conditions. Regarding the effect of varying engine speeds, there was no significant effect on the accumulated air mass in the small motorcycle engine, although there were several small fluctuations from the beginning of the intake stroke until the end of intake stroke. From that point, engine speed 4000 rpm case had the lowest value of air mass when compared with the 2000 and 3000 rpm cases. However, the maximum decrease in air mass for speeds in the ranges of 4000 rpm to 2000 rpm and 4000 rpm to 3000 rpm, was very small (around 7.6 % and 3.5 %, respectively). This may be because the inertia of the incoming air was less than the inertia of the air mass moving upward near the piston.

Yet another unique phenomenon occurred regarding the accumulated air mass in the small motorcycle engine when the engine speed was increased. The phenomenon was a reduction of the accumulated air mass when the engine speed increased from 2000 rpm to 3000 rpm and from 3000 rpm to 4000 rpm, at the beginning of the compression stroke (at 540 °CA) until the end of the compression stroke. This is the opposite of what occurred in the study of a

large engine conducted by Ramesh and James [105]. This is probably due to the effect of the intake valve ramp profile on the small motorcycle engine that is not too steep compared to a large engine. Moreover, the intake valve closing time in the small motorcycle engine was faster than in the large engine, which may have affected the change in the accumulated air mass in the small motorcycle engine.

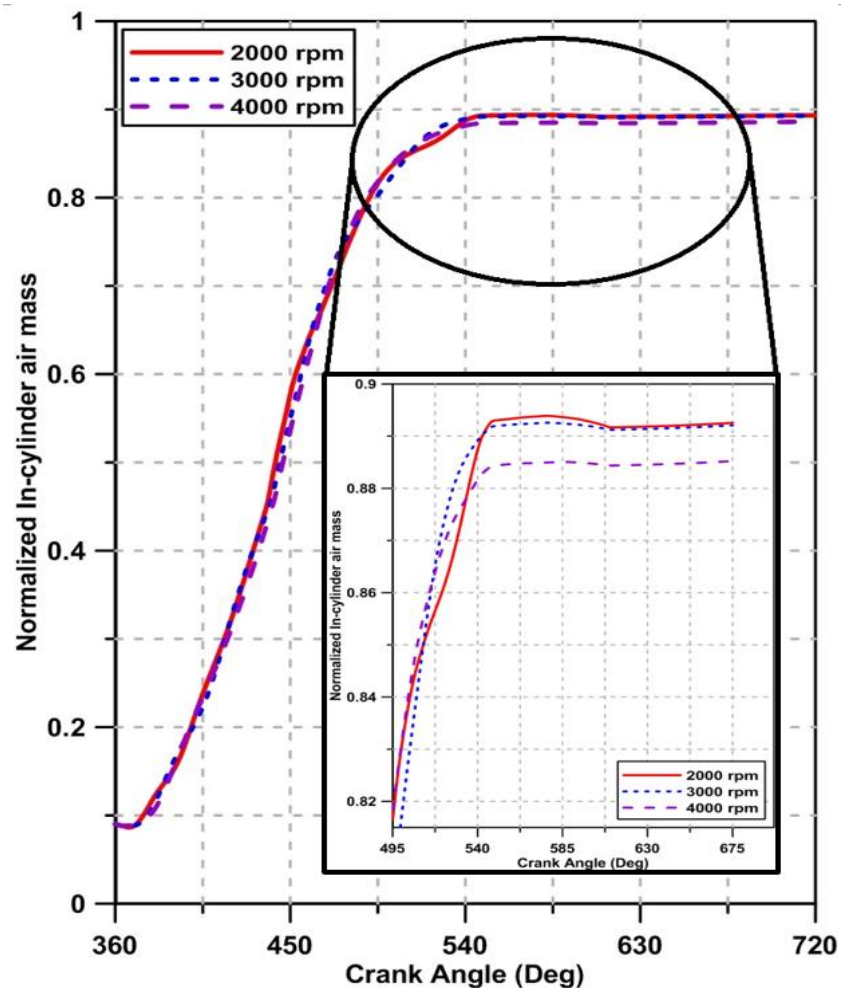

Fig. 4.19 The variation of air mass at different engine speeds

4.6.5. Turbulent length scale

The turbulence length scale is a measure to approximate the inlet turbulence characteristics during a CFD simulation. This is a measurement of the physical quantity of large eddies that is loaded with energy in a turbulent flow. Each eddy scale appropriates to a specific turbulence length scale. One type of the eddy scale that has been standardized is integral length scales. In this case, the integral length scale is used to estimate the turbulent length scale. The comparison of the turbulent length scale versus CAD for two different

pressure drops (300 and 600 mmH_2O) under motoring conditions during intake and compression strokes is shown in figure 4.20. Figure 4.20 shows that at the beginning of intake stroke until 450 °CA, the turbulent length scale is almost constant. Then, it increased rapidly and achieved the highest peak when the intake valve was almost closed, around 590 °CA.

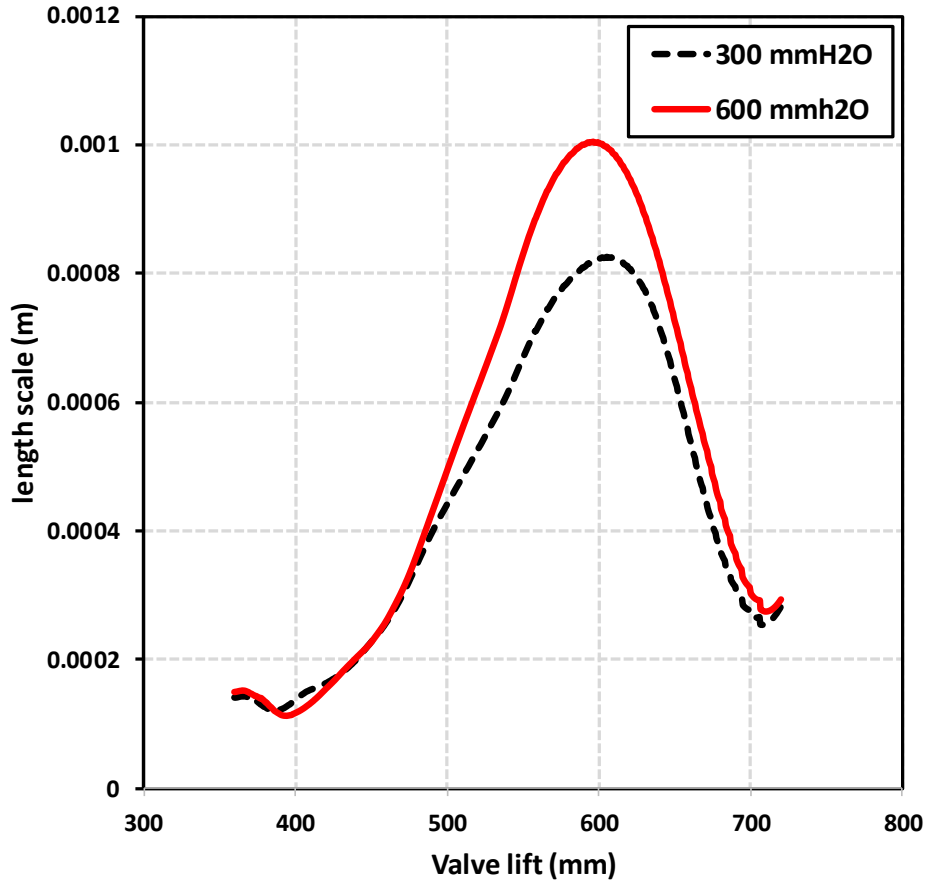

Fig. 4.20 The In-cylinder length scale at different pressure drop

Finally, it dropped dramatically until the last stage of the compression stroke. This tendency was present at all pressure drops. One factor that influences the turbulent length scale is the level of dissipation [107]. If the turbulent length scale has a small size, it represents a big dissipation rate. A big dissipation rate occurs due to the increased in-flow work carried out against the action of the viscous stresses. Increased flow work performed on the action of viscous stresses can increase the rate of dissipation.

Regarding the effect of pressure drop, turbulent length scales in the small motorcycle engine appeared insensitive to increasing pressure drop, especially in the intake stroke up to 490 °CA. From this point, the turbulent length scale increased as pressure drop increased. The

highest value of increasing length scale occurred at 595 °CA around 44.5 %, where the intake valve was almost closed. This is maybe because when the intake valve was closed and the pressure drop was increased, the dissipation rate had the tendency to reduce, due to the reduced in-flow work carried out against the action of the viscous stresses. When the dissipation rate decreased, the turbulent length scale will be increased.

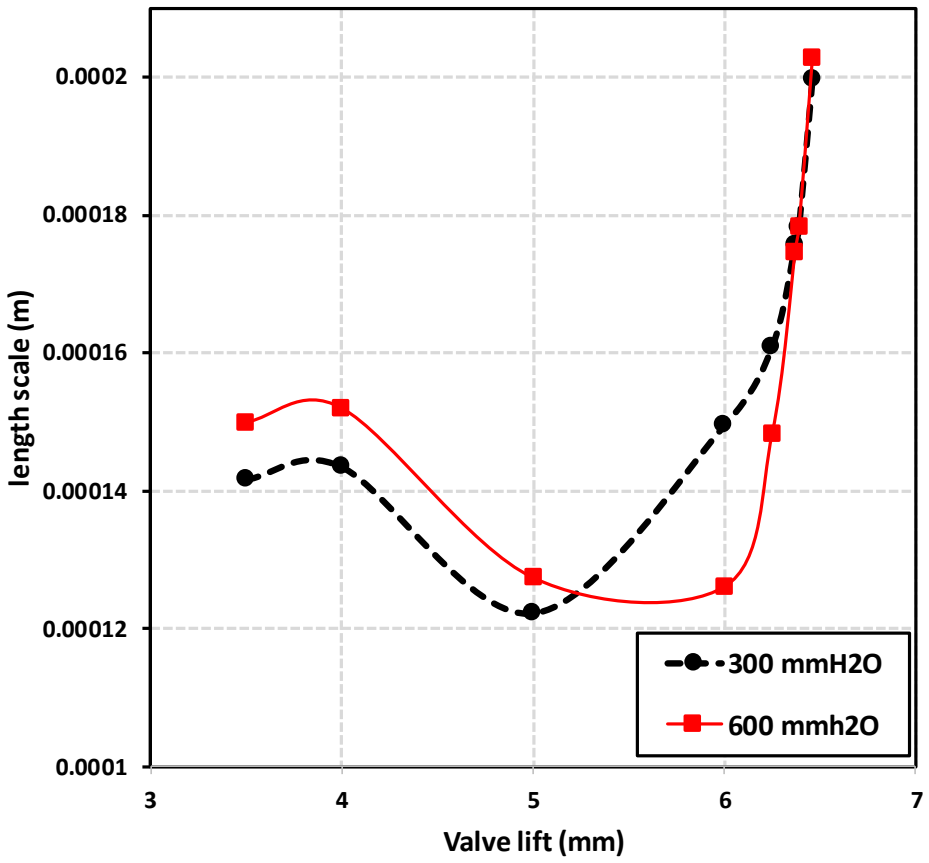

Fig. 4.21 The variation of length scale at different valve lift

Moreover, it can be seen in more detail in figure 4.21 which compares length scale with variations in valve lift and increased pressure drop. Figure 4.21 shows that when the valve lift is opened 3.5 to 5 mm, there is an increase in length scale because the pressure drop is increased from 300 to 600 mmH_2O. However, when the elevator valve is opened larger than 6.25 mm, the length scale decreases even though the pressure drop has been increased from 300 to 600 mmH_2O. Then, it went up again after the valve lift reached its maximum condition, 6.46 mm. This shows fluctuations in length scale at the beginning of stroke intake. This is probably due to the shape of the intake port on the air entrance near the valve lift. Although this fluctuation is not too big, it needs to be considered because the turbulent length scale is an

important parameter in determining turbulence. To improve this condition, it may help by changing the shape of the intake port on the engine cylinder head.

Figure 4.22 shows the comparison of the normalized turbulent length scale with CAD for three engine speeds (2000, 3000, and 4000 rpm), under motoring conditions during intake and compression strokes. Regarding the effect of engine speed, turbulent length scales in the small motorcycle engine appeared insensitive to increasing engine speed, especially in the intake stroke up to 490 °CA. This result is similar to the results obtained by [108]. From this point, the turbulent length scale increased as engine speed increased. The biggest increase in turbulent length scale occurred around 590 °CA, where the intake valve was almost closed. The biggest increase is similar for two specific ranges (2000 to 3000 rpm and 3000 to 4000 rpm) of 20 %. This is possible because when the intake valve was closed and the engine speed was increased, the dissipation rate had the tendency to decrease, due to the decreased in-flow work carried out against the action of the viscous stresses. When the dissipation rate decreased (based on Equation 16), the integral length scale increased.

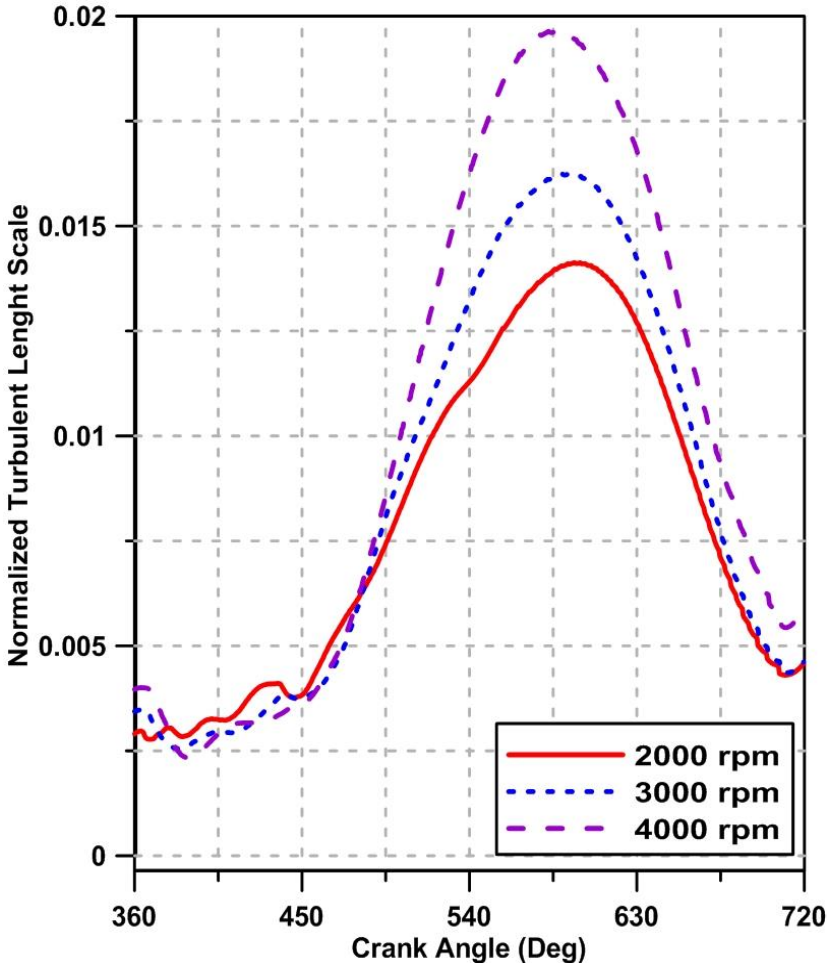

Fig. 4.22 The In-cylinder length scale at different engine speeds

When compared to the study conducted by Micklow and Gong [109] that used a large engine (137.6 mm x 165.1 mm), it was found another instance of a phenomenon that appeared in the characteristics of the small motorcycle engine but did not appear in a study on a large engine. This phenomenon was the turbulent length scale moving almost constantly, starting from the beginning of the intake stroke until the middle of the intake stroke, around 450 °CA. This was evident at all engine speeds (2000, 3000, and 4000 rpm). On the other hand, the turbulent length scale of Micklow and Gong's large engine increased significantly from the beginning of the intake stroke until it reached its peak at 590 °CA. This phenomenon needs to be considered, because the turbulent length scale is an important parameter in determining turbulence. To improve this condition, it may help to change the angle of the intake port to the cylinder head of engine.

4.6.6. Turbulent Kinematic Viscosity

Turbulent kinematic viscosity (or also call eddy viscosity) is a measure of the relative magnitudes of fluid viscosity and inertia. Turbulent kinematic viscosity is a parameterization for eddy momentum flux that works well when there is a small vortex in the flow. But it works poorly when there is a large vortex. Figure 4.23 shows the comparison of the turbulent kinematic viscosity with CAD for two pressure drops (300 and 600 mmH_2O) under motoring conditions during intake and compression strokes. Figure 4.18 shows that at the beginning of the intake stroke there is a decrease in turbulent kinematic viscosity of up to 400 °CA. From this point, the turbulent kinematic viscosity again rises sharply until it reaches its peak at around 590 °CA and again drops dramatically until the stroke compression ends. This tendency was present at all pressure drops.

Regarding the effect of pressure drop, turbulent kinematic viscosity in small motorcycle engine at the start of stroke intakes to 400 °CA decreased when the pressure drop was increased from 300 to 600 mmH_2O. This decrease may be caused by the shape of the intake port at the air entrance near the valve lift. However, this process does not occur for a long time because after 400 °CA turbulent kinematic viscosity has increased sharply due to an increase in pressure drop. With the opening of the valve lift and the effect of the movement of the piston making more and more small eddies inside the cylinder. The increasing number of small eddies causes turbulent kinematic viscosity to increase.

This can be seen in more detail in Figure 4.24 which compares the turbulent kinematic viscosity with variations in valve lift and increased pressure drop. Figure 4.24 shows when the valve lift is opened 3.5 to 5 mm, there is a decrease in turbulent kinematic viscosity because the pressure drop is increased from 300 to 600 mmH_2O. However, when the valve lift is opened larger until reaches the maximum condition, 6.46 mm, there is an increase in turbulent kinematic viscosity when the pressure drop is increased from 300 to 600 mmH_2O. This shows that turbulent kinematic viscosity fluctuations occur at the beginning of the intake stroke. This is probably due to the shape of the intake port on the air entrance near the valve lift. Although this fluctuation is not too big, it needs to be considered because turbulent kinematic viscosity is one of the important parameters in determining turbulence. To improve this condition, it may help by changing the shape of the intake port on the engine cylinder head.

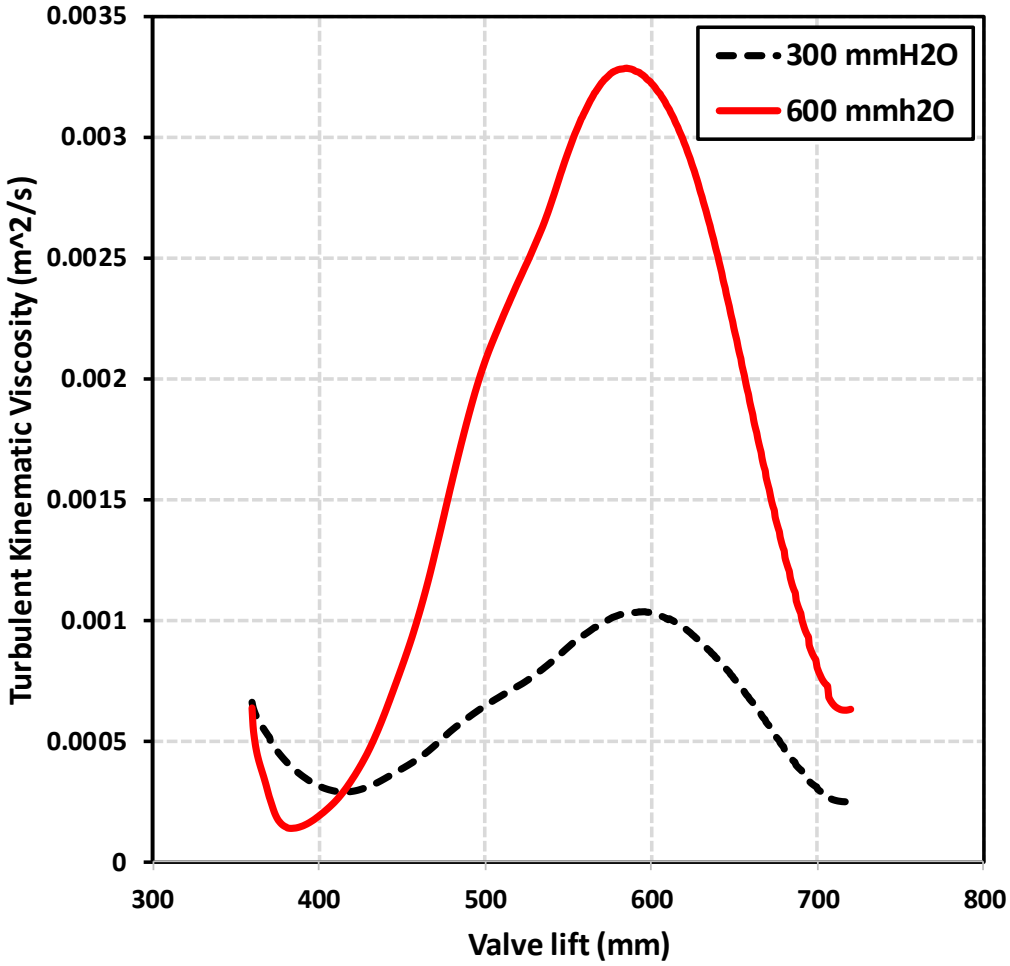

Fig. 4.23 The In-cylinder of turbulent kinematic viscosity at different pressure drop

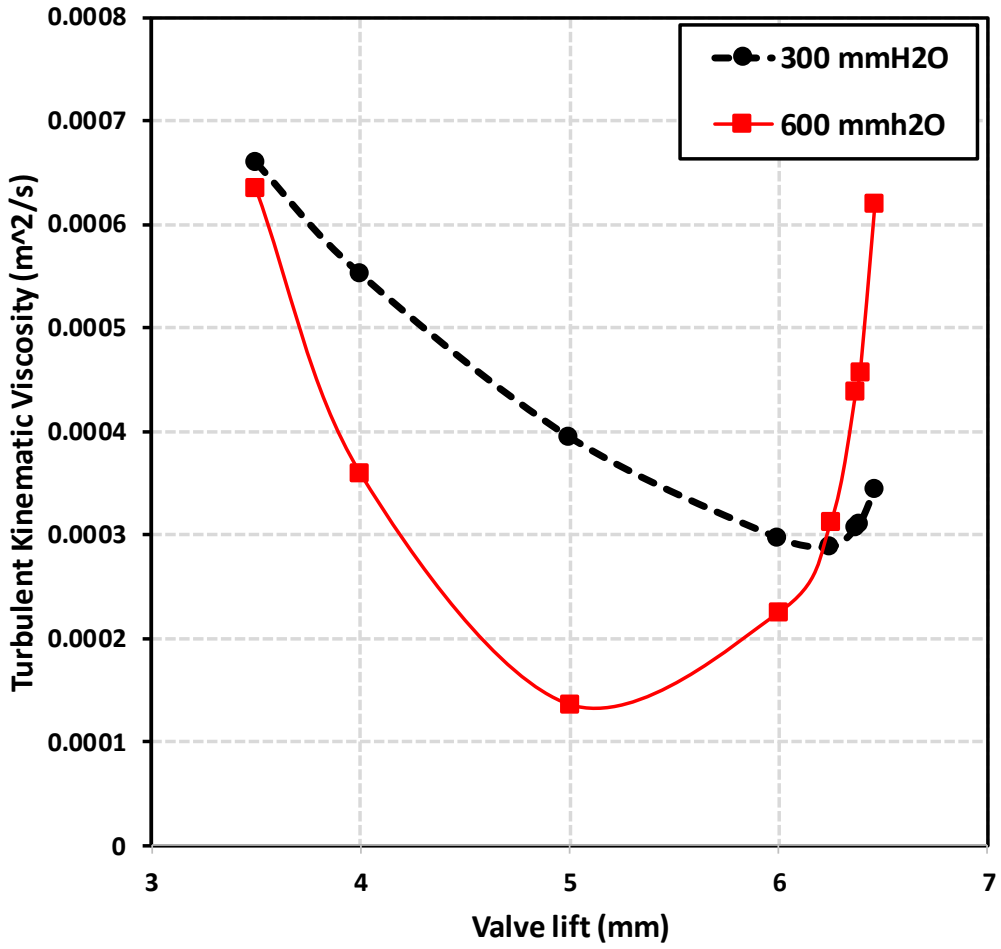

Fig. 4.24 The variation of turbulent kinematic viscosity at different valve lift

4.6.7. Angular momentum

To measure the behavior of the engine system, the in-cylinder angular momentum in the engine cylinder need to be evaluated. The variation of the normalized angular momentum over the engine cycle is shown in Fig. 4.25. Figure 4.25 shows the comparison of normalized angular momentum with CAD for engine speeds of 2000, 3000, and 4000 rpm under motoring conditions during intake and compression strokes. Fig 4.25 reveals that the angular momentum had a tendency to increase until the late phase of the intake process (around 495 °CA), due to the effect of the tangential velocity component used to blow the fresh air into the cylinder engine. This increase in angular momentum also occurred due to the increase of the tumble flow radius when the piston was moving down the cylinder. On the other hand, the piston's inward motion caused a decrease in the gas port's flow area and an upsurge of in-cylinder pressure, which resulted in a decrease of the intake mass flow speed. This produced an unanticipated decrease in angular momentum that happened just prior to the closure of the

intake valve. However, the angular momentum rapidly decreased during the compression stroke and faded almost completely at the end of compression stroke. This drop may have happened because of the decreasing velocity in the intake mass flow due to the increased in-cylinder engine pressure and the decrease in the air flow area from the inward flow of the piston.

Regarding the effect of the speed, it can be observed that the increments of angular momentum in the small motorcycle engine for engine speeds 2000 and 3000 rpm was only marginal. When the engine speed was increased from 3000 to 4000 rpm, the biggest increase in angular momentum was 10 %, at 495 °CA and the increment was only 5 % at 720 °CA. This considerable increase is likely due to the increase in the fluctuation of the tangential velocity component, due to the engine speed increase from 3000 rpm to 4000 rpm. This fluctuation increase occurred primarily during the valve opening period, and continuously decreased in the middle of the stroke compression. This fluctuation indicates the destruction of tumbling vortices, which increased the turbulence, resulting in a higher angular momentum.

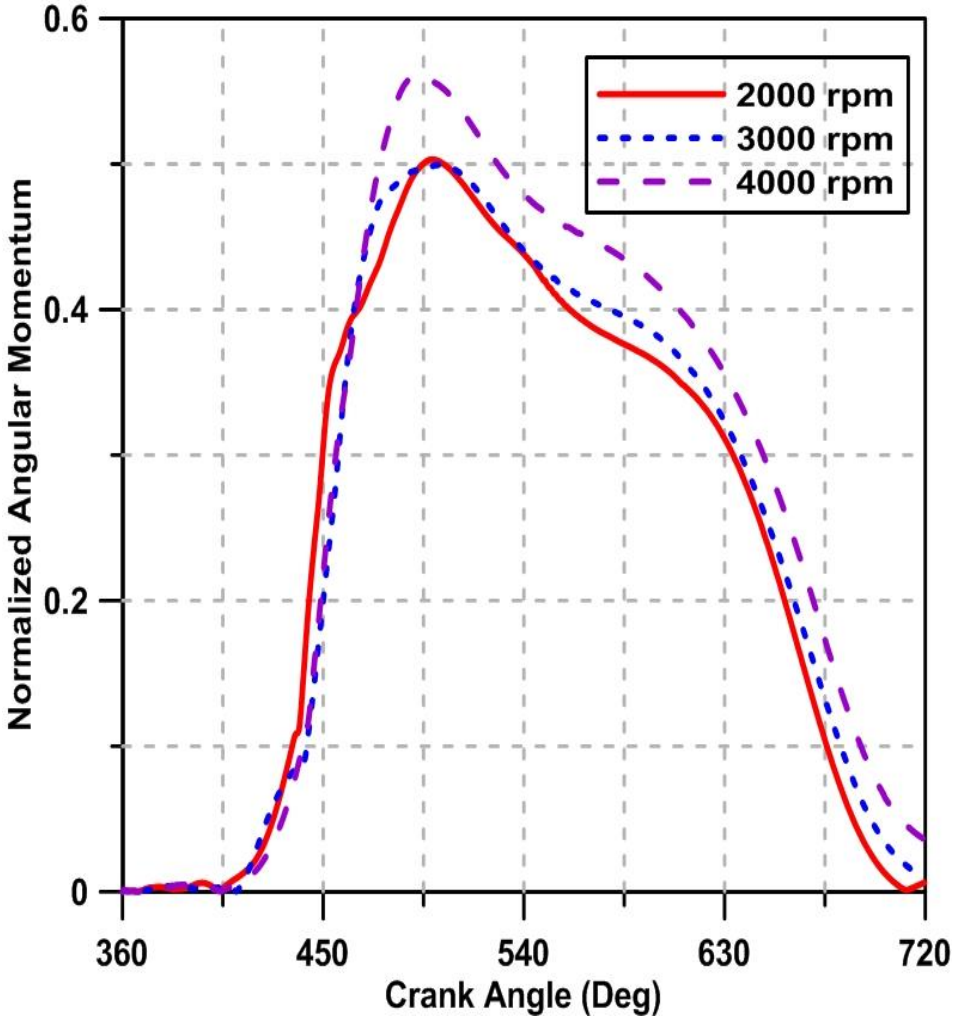

Figure 4.25. The In-cylinder of angular momentum at different engine speeds

When compared to the large engine research performed by Micklow and Gong [109], the small motorcycle engine had a unique behavior pattern that did not appear in the large engine. This pattern was evident at all three engine speeds. It was the gradual decrease in angular momentum, from the peak point at around 495 °CA until the end of the compression stroke. Even at the beginning of compression stroke, the angular momentum was still quite high. This phenomenon is not found in large engines. In large engines, angular momentum decreases rapidly from the peak point to the end of the intake stroke and is constant at the beginning of compression stroke until the end of the compression stroke. This phenomenon is probably due to the fact that the small motorcycle engine, from peak point until the closing phase of the valve lift, had a process of increasing tumble generation. This process was caused by two things: the substantial change in flow distribution at high valve lift, and the reduction in the mass flow rate that entered across negative curtain.

4.7 Summary

The aim of this study is to experimentally study in-cylinder flow of a small motorcycle engine using steady state flow bench and comparing to the simulation result based on the variation of pressure drop. This study also illustrates the evolution of the small motorcycle engine in-cylinder flow motion using CFD methods. Moreover, this study also analyzed some of the characteristics of air flow in cylinder flow that was performed for a four-stroke small motorcycle engine under motoring condition at two different pressure drops (300 and 600 mmH_2O). This characteristic included swirl ratio, TKE, turbulent length scale, tumble ratio, turbulent kinematic viscosity and in-cylinder air mass in both intake and compression strokes. From the results, the following conclusions were:

1. There was a good agreement achieved between the experiment result in steady-state flow benches and simulation result of the air flow rate, flow coefficient and coefficient of discharge at 300 and 600 mmH_2O pressure drop. The biggest deviation is only 17.76% for air flow rate, 15.87% for flow coefficient and 11.51% for the coefficient of discharge that all occur at 2.176 mm and pressure drop 300 mmH_2O.

2. In the horizontal plane, the vortices were noticed that the general patterns seen within the bulk flow motions show quite a lot of variations with an increase in valve lift. It can be seen the symmetrical four counter-rotating vortices appeared in all images for high valve lift. Similar occurrences were present with an increase in pressure drop. The

difference between the 300 mmH2O and 600 mmH_2O cases is in terms of the vortex strength where the velocity will increase at a higher pressure drop.

3. In the vertical plane, it was observed that the flow structures remain similar, but the velocities within these structures increase with increasing valve lift both in 300 and 600 mmH_2O pressure drop. Vortex is formed by the interaction of the outer side of the intake valve and cylinder wall. The wider the valve lift is opened the more vortex is formed. The biggest vortex occurs in the center of the cylinder. Similar occurrences were present with an increase in pressure drop. The flow structures remain of similar orientation, however, the magnitude of the velocities within these flow structures is increased.

4. In the horizontal plane, the vorticity was dominated in the right area of the cylinder where the intake valve is located. When the valve lift increases, the dominance of the vorticity is still on the right side of the cylinder and reaches its peak in the center of the cylinder. The strength of vorticity increases with the increase in valve lift. The difference between the 300 mmH_2O and 600 mmH_2O cases is in terms of the magnitude of the vorticity where the vorticity will increase at a higher pressure drop. This explanation is strengthened in the vertical plane where the wider the valve lift, the greater the vorticity magnitude on the side of the intake valve. When pressure drop is increased, the vortices formed to maintain their shape. But the vorticity magnitude will increase.

5. Increasing the pressure drop at the beginning of the valve lift opening has no effect on the swirl ratio until the valve lift reaches 5 mm. After that point, it has the effect to reduce the swirl ratio up to 75% when the valve lift reaches 6.25 mm. The increase of the engine speed in small motorcycle engine caused the swirl flow to be irregular in shape during the intake stroke, until 495 °CA. However, the swirl flow had a trend of being stable and almost constant in the beginning of the compression stroke and increasing in the end of the compression stroke. This is different from large engines, which exhibit increasing swirl ratios as engine speed increases, in all crank angles.

6. The increasing of pressure drop on the small motorcycle engine at the beginning of the intake stroke until the end of compression stroke has no significant effect on the tumble ratio. the same thing happened to the accumulated air mass at the beginning of the intake

stroke. However, there is an increase of 3.77% because of the effect of increasing pressure drop in compression strokes.

7. The increasing of pressure drop on the small motorcycle engine gives a significant effect on TKE and reached the highest value of around 200 % at 470 °CA. This may be because when the pressure drops increased from 300 to 600 mmH_2O, it caused a significant increase in the inlet air velocity in the cylinder engine.

8. The biggest increase in angular momentum in small motorcycle engine occurred when the engine speed was increased from 3000 to 4000 rpm, due to the effect of increasing tangential speed fluctuations at 495 °CA. There was a phenomenon of gradually decreasing angular momentum in small motorcycle engine, from the peak point around 495 °CA, until the end of the compression stroke. This is a contrast to large engines, in which the angular momentum drops dramatically from the peak point to the end of the intake stroke.

9. The increasing of pressure drops gives a significant effect on turbulent length scale and turbulent kinematic viscosity and these two parameters have similarity trend where the biggest increase occurred at around 590 CA where the intake valve was almost closed. It may be because at that position the piston moves to TDC so that more vortices are formed and result in length scale and eddy viscosity increases significantly. There was an occasion in which the turbulent length scale of small motorcycle engine moved almost constantly, starting from the beginning of the intake stroke until the middle of intake stroke, around 450 °CA, at all engine speeds. However, this behavior does not appear in large engines.

10. The increase in turbulence made the air-fuel mixing in-cylinder more homogeneous. In addition, the increase in turbulence directly increased the rate of fire propagation.

11. Further research is recommended with the use of a new design of several types of intake ports as well as combinations of different intake ports, so that the effects on air flow characteristics can be studied and improved.

5. EFFECT OF INTAKE PORT MODIFICATION BASED ON THE FLOW DIRECTION ON SMALL MOTORCYCLE ENGINE

This study aimed to numerically and experimentally analyze the results of the in-cylinder flow of small motorcycle engines using steady flow benches for various intake port modifications based on the flow direction. The intake port modifications are the helical intake port with the same direction, helical intake port with the opposite direction (inward), helical intake port with the opposite direction (outward), and the tangential intake port. This study also investigates the intake port velocity distribution using all models of the intake port around the valve curtain of the two intake valves for varied valve lifts. In addition, this study also analyzed variations of the inflow motion of the in-cylinder engine in both the horizontal and vertical planes on all intake port models. Moreover, this study also investigates the cycle-to-cycle behavior of the tumble ratio and turbulent kinetic energy development of all intake port models under motoring conditions to assess the stability at the beginning of the developing stage. The results show that there was a good agreement between the experimental results of the steady flow bench and the simulation results of the flow coefficients for various intake port modifications based on the flow direction. The velocity distribution with the tangential intake port model around the valve curtain of the two intake valves generally spreads in all directions and mostly towards the center of the cylinder, with a maximum flow velocity nearly doubling compared to the other three models. In the horizontal and vertical planes. The flow patterns of all intake port models are similar where the valve lift is greater, along with a greater flow velocity and a more varied flow pattern. However, the tangential intake port model has the greatest flow velocity compared to the other intake port models. The changes in the intake port model have a significant effect on the change in the tumble ratio. However, the tumble helical intake port with the same direction has the highest tumble peak of more than double those of the other models at a 460° crank angle (CA). The changes in the intake port model do not have a significant effect on the formation of the turbulent kinetic energy (TKE). However, an important effect is that the maximum value of the first peak of the TKE is highest for the intake port with the tangential model relative to the other models. However, cyclic scattering of the TKE occurs in the intake port tangential model where the first cycle is quite large and the second to tenth cycles are quite stable. This is a concern because TKE conversions arise from various flow structures with different intensities, which can be a potential problem for

combustion stability. Finally, this study is expected to decrease the number of experiments required for investigating the optimized engine parameters, especially for small motorcycle engines.

5.1 Comparison experiment and simulation result of flow coefficient

Fig. 5.1 represents the flow coefficient with valve lifts using various models of helical intake port modifications based on the flow direction, which is compared with the tangential intake port using experimental and simulation methods. The comparison of the flow coefficient based on the experimental and simulation results, with the helical intake port in the same direction, is shown in Fig. 5.1a. The flow coefficient seems to increase gradually from the start of the 0.5 mm valve lift to the 1.5 mm valve lift. This is probably caused by an increase in the effective flow area through the valve. However, from a 1.5 mm valve lift to a valve lift reaching a maximum value of 6.46 mm, the flow coefficient tends to be constant. The flow coefficient affects the engine's breathing capacity because more air enters the cylinder at the higher valve lifts. However, in the lower valve lift regime, this effect is quite small. There is good agreement between the results of the experiments and simulations.

The flow coefficient with the helical intake port in the opposite direction (inward) tends to increase at the onset of the valve lift, as shown in Figure 5.1b. The trend of the flow coefficient in the experimental and simulation results is similar for this intake port model where the flow coefficient is enlarged with a valve lift of up to 1.5 mm and from this point to 6.46 mm, the flow coefficient becomes constant. There is good agreement between the results of experiments on a stable flow bench and the numerical results. The maximum difference is 19.95% for the 0.5 mm lift valve.

Similar to Fig. 5.1a and 5.1b, Fig. 5.1c shows the flow coefficient with the helical intake port in the opposite direction (outward). The experimental and modeled trend of the flow coefficient are similar in the respect that the flow coefficient increases rapidly from the beginning of the valve lift 0.5 mm until the valve lift increase reaches 1.5 mm. However, the flow coefficient becomes constant from the valve lift 1.5 mm to 6.46 mm. The flow coefficient for the helical intake port in the same direction and opposite direction (inward) shows a similar trend. This is because the cross-sectional areas of the intake flow passages at lift valves lower than 1.5 mm are relatively small. Another important factor is the dominance of the valve lifting effect when the valve lift is lower than 1.5 mm. There is a good agreement between the results of experiments and simulations. However, the maximum difference is 40.45% for a 0.5 mm lifting valve. The maximum difference in 0.5 mm is large due to the difficulty of determining the position of the valve at the beginning of the opening valve lift. However, overall, the trends produced from the experiments and simulations are similar.

Figure 5.1d shows the flow coefficient with a tangential intake port. Flow coefficients with tangential intake ports tend to increase gradually at the beginning of the valve lift of 0.5

mm to 4 mm but from this point to 6.46 mm the coefficients tend to be constant. This is quite a striking difference when compared to the flow coefficient with the helical intake port on all models, in which the increase of the flow coefficient of the tangential model is quite sharp to the 4 mm valve lift. This is probably because the cross-sectional area of the intake flow passages in the tangential model is greater than that in the helical model. Because of its shape, the helical model tends to have a small flow coefficient. This is increasingly evidenced by seeing a four-times greater increase in the flow coefficient at the intake port with tangential models relative to the helical model.

The above-mentioned results show that the change in the flow direction of the helical model intake port does not greatly affect the change in the flow coefficient. It is true that changes between the helical and tangential intake port model sufficiently influence a change in the flow coefficient. However, this does not guarantee that the tangential model is the best model. It must be noted that although the intake port model has a high flow coefficient, it does not guarantee that this model is the best model that can be applied for use in engines. There are several other factors that affect the intake port model when chosen as a reference, especially for improving the engine performance. Some of these factors will be discussed in the next section.

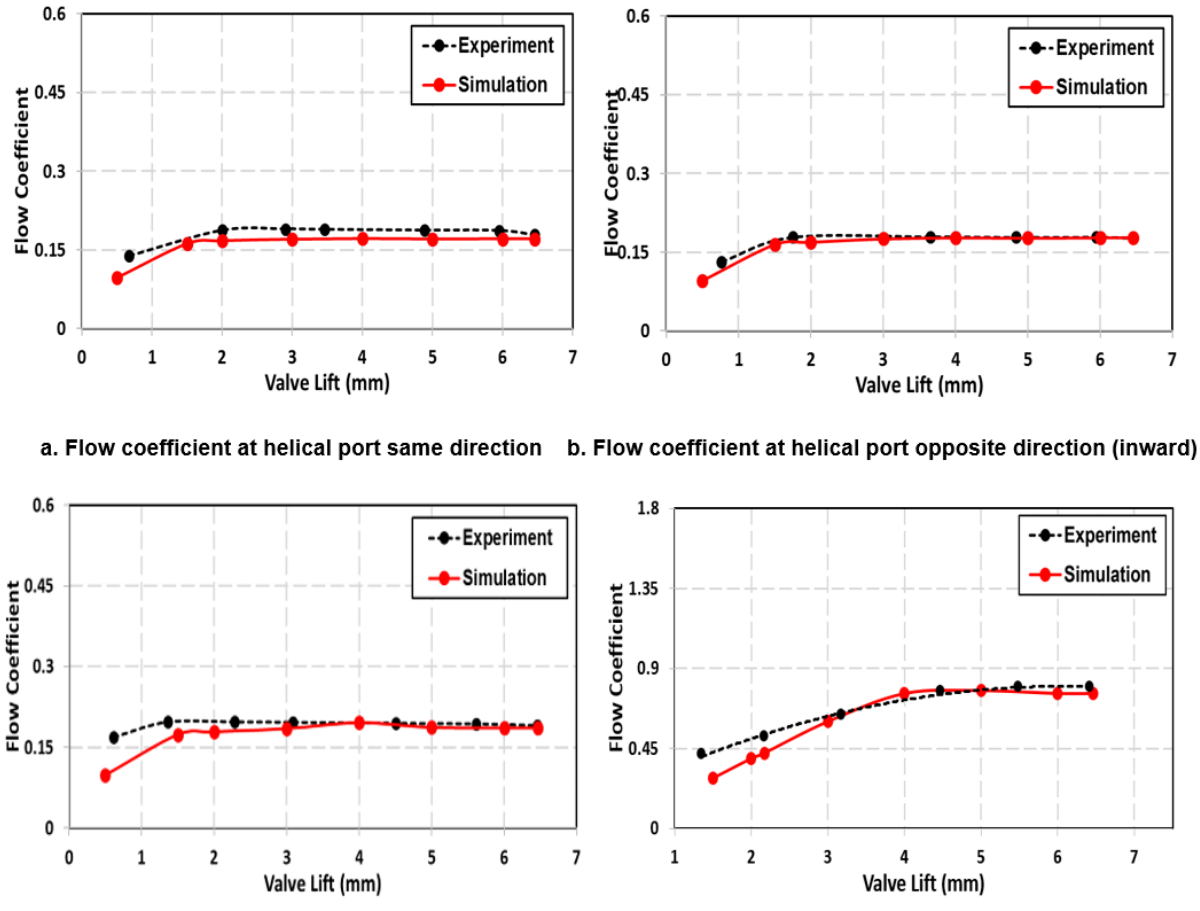

a. Flow coefficient at helical port same direction

b. Flow coefficient at helical port opposite direction (inward)

c. Flow coefficient at helical port opposite direction (outward)

d. Flow coefficient at tangential port

Fig. 5.1 Flow coefficient in the steady-state flow bench experiment with simulations

5.2 Intake Port Velocity Distribution

The intake port velocity distribution for varied valve lifts at the x-y plane (z = 5 mm) is shown in Fig. 5.2 for many models of the intake port. Fig. 6a shows the intake port velocity distribution at the x-y plane (z = 5 mm) with the helical intake port in the same direction around the valve curtain of the two valves for varied valve lifts. Based on Figure 5.2a, in medium valve lifts, such as 5.7 mm, most of the inflow into the cylinder follows a spiral model, in which the direction of flow is towards the cylinder wall for the left valve and towards the middle of the cylinder for the right valve. This is clearly seen in Fig. 5.2a, in which the flow direction is towards directions 1, 3, and 11 for the left and right intake valves. However, with the increase in valve lifts, as in the valve lifts of 6.1 mm and 6.46 mm, the flow distribution is slightly towards the center of the cylinder. This can be seen in directions 2 and 4.

The intake port velocity distribution at the x-y plane (z= 5 mm) with a helical intake port in the opposite direction (inward) around the valve curtain of two valves for varied valve lifts is shown in Fig. 5.2b. In medium valve lifts, such as 5.7 mm, Figure 5.2b shows that most of the flow distribution goes into the center of the cylinder on both the left valve and right valve. This is clearly seen in Fig. 5.2a, where the flow direction is in the direction of 6, 7, 8, and 9 for the left intake valve and 2, 1, 12, and 11 for the right intake valve. This phenomenon will be increasingly apparent with an increase in the valve lift for both the 6.1 mm and 6.46 mm valve lifts. This can be seen in direction 5 on the left valve and 3 on the right valve.

Fig. 5.2c shows the intake port velocity distribution at the x-y plane (z = 5 mm) with the helical intake port in the opposite direction (outward) around the valve curtain of the two valves for varied valve lifts. As noted for medium valve lifts, such as 5.7 mm, most of the inflow into the cylinder follows a spiral model, in which the direction of flow is towards the cylinder wall. This can be seen in Fig. 5.2c where the flow direction is towards directions 1 and 2 for the left intake valve and 6 and 7 for the right intake valve. This is emphasized for the 6.1 mm and 6.46 mm valve lifts, where the flow distribution is progressively oriented towards the cylinder wall.

Fig. 5.2d shows the intake port velocity distribution in the x-y plane (z= 5 mm) with the tangential intake port around the valve curtain of two valves for varied valve lifts.

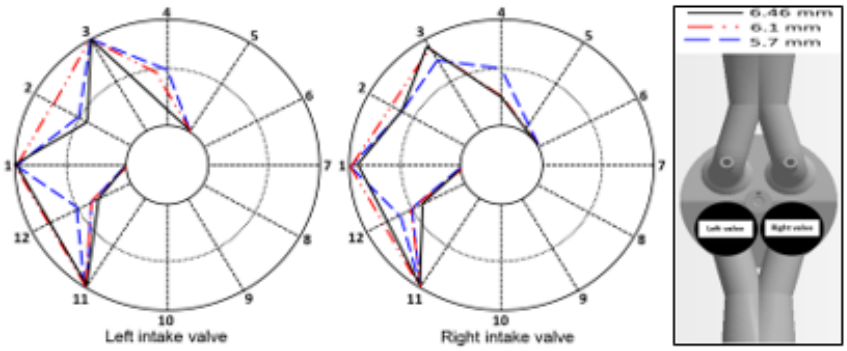

a. Intake port Velocity distribution with helical intake port same direction

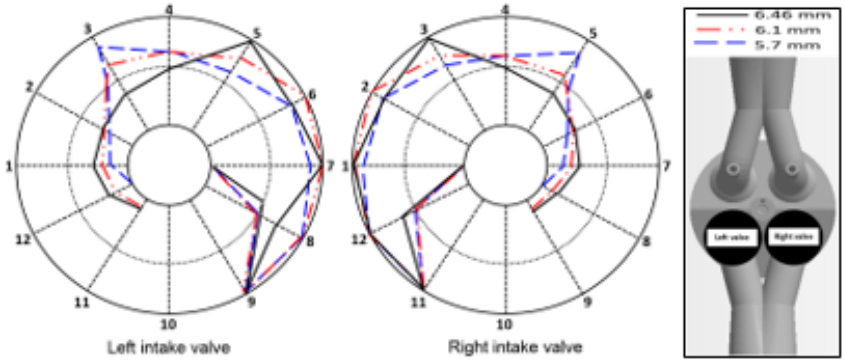

b. Intake port Velocity distribution with Helical intake port opposite direction (inward)

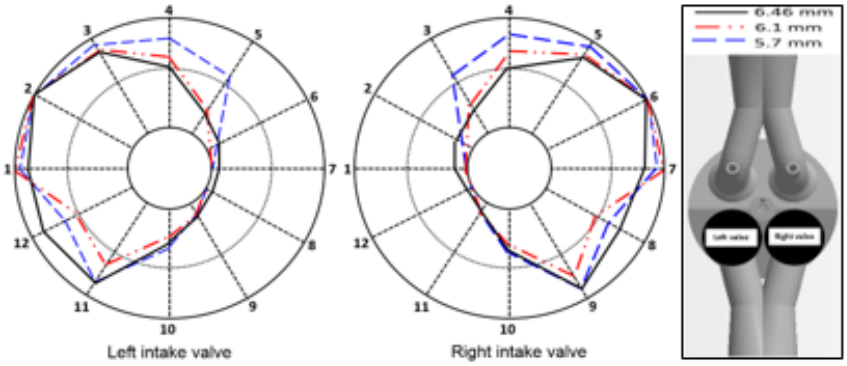

c. Intake port velocity distribution with helical intake port opposite direction (outward)

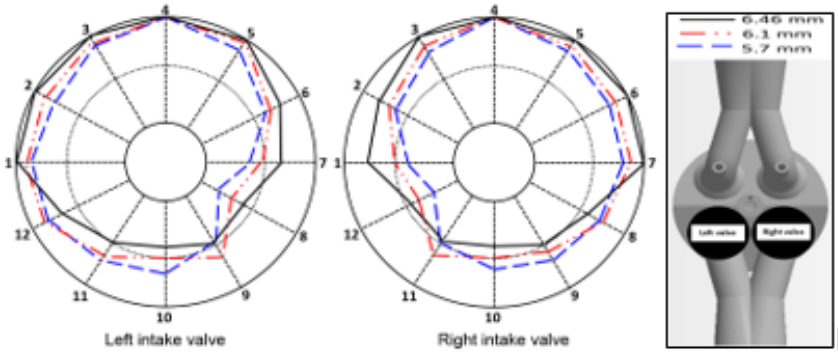

d. Intake port Velocity distribution with tangential intake port

Fig. 5.2 Intake port velocity distributions for varied valve lifts in the x-y plane (z= 5 mm) with selected intake port models

Compared to the three previous models, the flow distribution with the tangential intake port for medium valve lifts like 5.7 mm and spreads in all directions, predominately towards the center of the cylinder, as shown in Figure 5.2d, where the flow directions go to 4 and 5 for the left and right valves, respectively. This condition continues for valve lifts of 6.1 and 6.46 mm where direction 10, 11, and 12 become smaller and directions 5, 6, and 7 become larger for both valves. The maximum flow velocity that occurs with the tangential intake port model is almost double compared to the previous three models at 35 m/s.

5.3 In-Cylinder Velocity Vectors

5.3.1. Horizontal Plane

A comparison of the in-cylinder velocity vector under the variation of valve lifts with various intake port models under the motoring condition, along the x-y plane (z = -4 mm) that passes the intake valves and cylinder in small motorcycle engines, is shown in Fig. 5.3. Fig. 5.3a. shows the in-cylinder velocity vector along the x-y plane (z = -4 mm) by using the helical intake port in the same direction. The flow patterns in Fig. 5.3a obviously vary, which is caused by an increase in the valve lift. In addition, the flow velocity increases when the valve lift increases until the valve lift reaches a maximum value (6.46mm), especially near the middle of the cylinder and on the left edge of the cylinder. When the valve lift reaches 5.7 mm, some vortices are formed around the intake valve seat and this is clearly visible on the left edge of the cylinder. When the valve lift increases to 6.1 mm and 6.46 mm, the flow velocity near the edge of the cylinder and the center of the cylinder becomes clearer. However, the highest flow velocity occurs at the edge of the cylinder at 18.5 m/s. This is caused by the shape of the intake port in the form of a spiral, where the flow at both ends of the intake valves point to the left edge of the cylinder, where there is a higher local turbulence. Figures 5.3b-5.3d show the same overall result as Figure 5.3a, where the flow pattern and flow velocity increase with an increase in the valve lift. However, Figure 5.3b, which is the velocity vector in the cylinder using the helical intake port in the opposite direction (inward), shows a symmetrically distributed flow pattern for each valve lift. It appears that vortices are beginning to form around the intake valve holder and in the middle of the cylinder. The largest flow velocity is dominated in the middle area of the cylinder and near the intake valve. The greater the valve lift, the more concentrated the vortices formed in the middle of the cylinder. However, the maximum velocity is not much different from the previous model of 18.5 m/s. The only difference is where the maximum velocity in this model occurs in the middle of the cylinder.

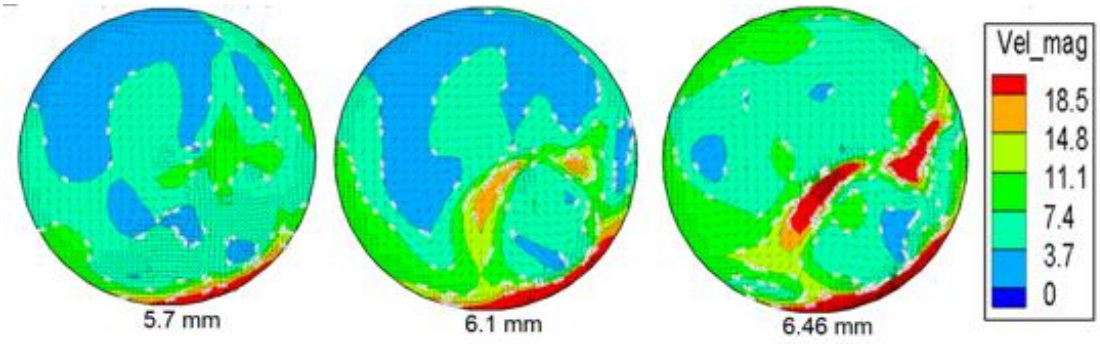

a. Velocity vector at x-y plane (z= -4 mm) with helical intake port same direction

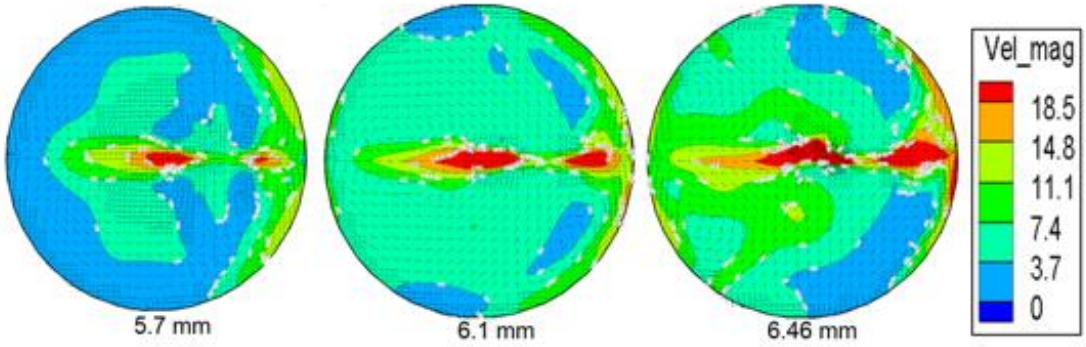

b. Velocity vector at x-y plane (z= -4 mm) with helical intake port opposite direction (inward)

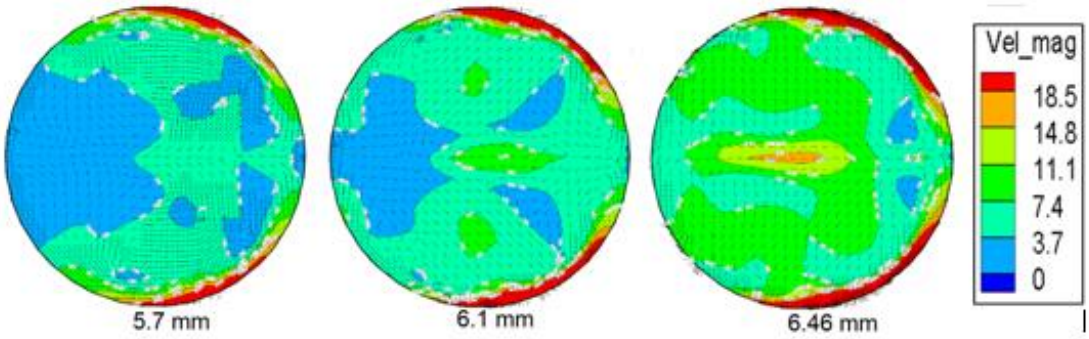

c. Velocity vector at x-y plane (z= -4 mm) with helical intake port opposite direction (outward)

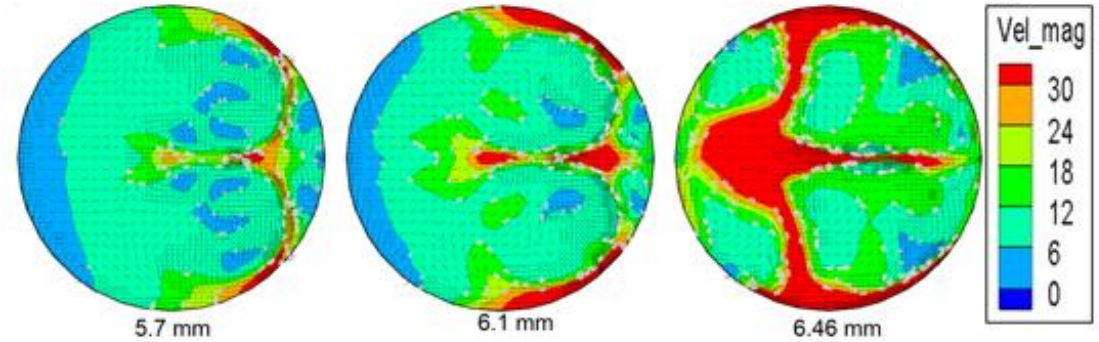

d. Velocity vector at x-y plane (z= -4 mm) with tangential intake port

Fig. 5.3 Velocity vectors for varied valve lifts in the x-y plane (z = -4 mm) for selected intake port models

A very striking difference occurs in Figure 5.3c, which is the velocity vector in the cylinder using the helical intake port in the opposite direction (outward), when compared to Figure 5.3b. Although the flow pattern is also distributed symmetrically, the flow velocity of the intake port model in Figure 5.3c is dominated by the edge of the cylinder. This is very easy to understand because the spiral model that leads to the exit that results in the formation of many vortices on both the left and right edge of the cylinder. However, with an increasing valve lift the maximum flow velocity begins to increase in the middle of the cylinder. Nevertheless, the maximum velocity occurs at the edge of the cylinder at 18.5 m/s.

In Figure. 5.3d, which shows the velocity vectors in the cylinder using tangential intake ports, the flow pattern is evenly distributed in all areas and is clearer at the maximum valve lift of 6.46 mm. Likewise, the flow velocity is greater when compared to the previous three models. At the tangential intake port, the largest flow velocity occurs in the middle of the cylinder at 35 m/s, which increases almost twice as fast as the flow velocity at the intake helical port. From Figure 5.3a-5.3d, it can be concluded that the flow patterns of all intake port models are similar where the valve lift is greater and that the flow pattern will be more varies and the flow velocity will also be greater. However, what is quite striking is the position and values at which the maximum velocity occurs. The tangential intake ports have the greatest flow velocity compared to other intake port models and are in the middle of the cylinder. The greater the flow velocity in an area shows increased turbulence in this area. Increased turbulence results in a more homogeneous mixing of air fuel in cylinders. Therefore, increasing turbulence directly increases the rate of fire propagation.

5.3.2. Vertical Plane

A comparison of the in-cylinder velocity vectors under the variation of valve lifts for various intake port models under the motoring condition, along the x-z plane (y = 0 mm) that passes the in-cylinder of a small motorcycle engine, is shown in Fig. 5.4. Figure 5.4a. shows the velocity vector in the cylinder along the x-z plane (y = 0 mm) using the helical intake port in the same direction. The greater the valve opening, the more intense the flow pattern and the higher flow velocity. At the beginning of the intake stroke, air passes through the side of the seat lip. In this process, a small vortex begins to form clockwise near the intake valve at the 5.7 mm valve lift. The greater the valve lift, the more air enters the cylinder, as seen for the valve lifts of 6.1 and 6.46 mm. This results in more vortices forming in some areas of the cylinder.

The flow velocity at the 6.46 mm valve lift is also greater than the 5.7 mm and 6.1 mm valve lifts that occur under the intake valve. The maximum flow velocity occurs at the 6.46 mm valve lift of 18.5 m/s on the upper side of the cylinder near the intake port.

The same phenomenon is observed in Fig. 5.4b-5.4d where the flow pattern and flow velocity increase with increasing valve lift. The difference is in the position and distribution of the flow velocity in the cylinder. The measure of the flow velocity is indicated by a color index. The red index shows the highest flow velocity. In Figure 5.4b, which shows the velocity vector in the cylinder along the x-z plane (y = 0 mm) using the helical intake port in the opposite direction (inside), there is a centralized flow distribution near the top of the seat lip. This results in the formation of vortices centered on the upper side of the seat lip. The increased valve lift results in greater flow velocity in the area that spreads down the intake port towards the cylinder wall and cylinder center. The greatest velocity occurs for a 6.46 mm valve lift at 18.5 m/s on the upper side of the seat lip. In Figure 8c, there is a quite striking difference when compared to the two previous images related to flow distribution.

Figure 5.4c, which shows the velocity vectors in the cylinder along the x-z plane (y = 0 mm) using the helical intake port in the opposite direction (exit) at a low valve lift of 5.7 mm, has a sufficient flow distribution and vortices have not yet formed. The greater the valve lift, the more vortices appear in some areas in the cylinder, as seen in the 6.1 mm valve lift. The flow velocity increase and the biggest increase occurs for the 6.46 mm valve lift, which occurs in the middle of the cylinder with a large velocity of 18.5 m/s.

In Figure 5.4d, which is the velocity vector in the cylinder along the x-z plane (y = 0 mm) using the tangential intake port, has similarities with Figure 5.4b. However, the difference is that the vortices not only occur on the upper side of the seat lip but also appear in several areas in the cylinder, like the middle of the cylinder and the edge of the cylinder. Moreover, the greatest velocity (35 m/s) of this model is almost double that of the previous three models, which occur under the intake valve. From Figures 5.4a-5.4d, it can be concluded that the greater the flow velocity of a volume sensibly corresponds to increased turbulence in this volume. Increased turbulence results in a more homogeneous mixing of air fuel in cylinders. Logically, increasing the turbulence directly increases the rate of fire propagation.

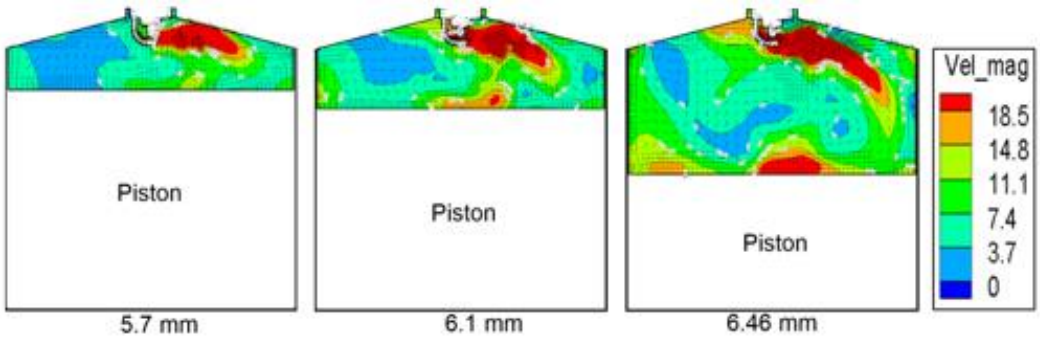

a. Velocity vector at x-z plane (y= 0 mm) with Helical intake port same direction

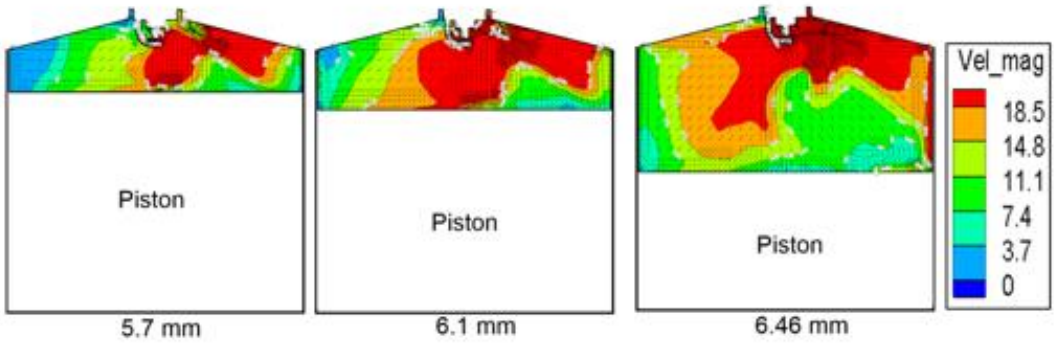

b. Velocity vector at x-z plane (y= 0 mm) with helical intake port opposite direction (inward)

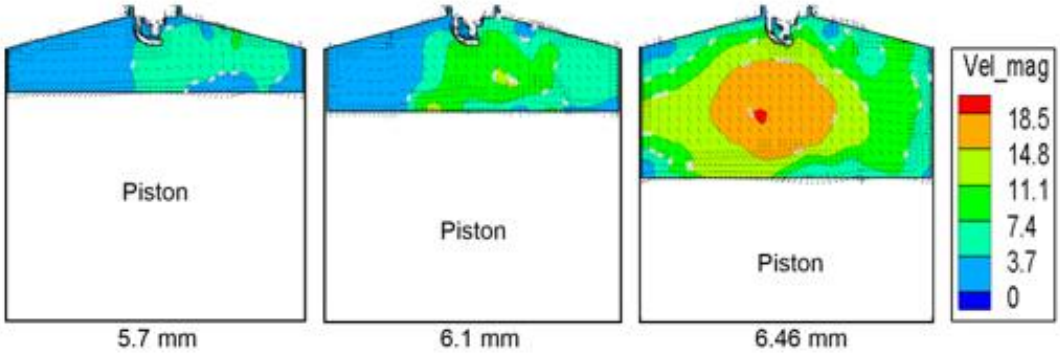

c. Velocity vector at x-z plane (y= 0 mm) with helical intake port opposite direction (outward)

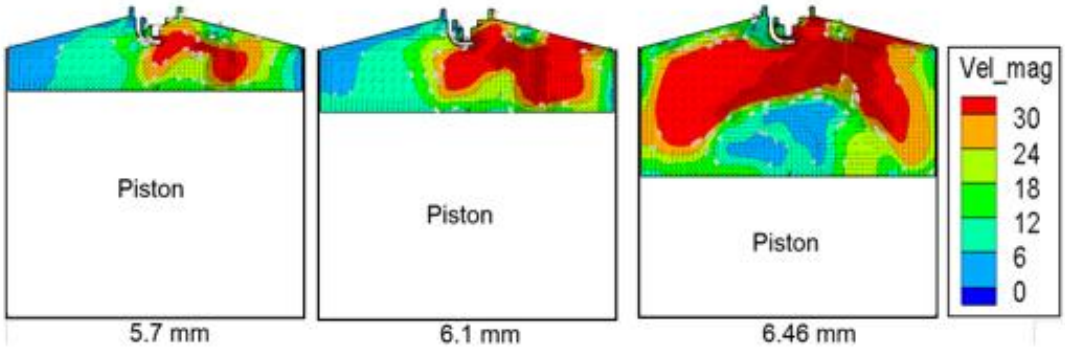

d. Velocity vector at x-z plane (y= 0 mm) with tangential intake port

Fig. 5.4 Velocity vectors for varied valve lifts in the x-z plane (y= 0 mm) with selected intake port models

5.4 Cycle to cycle of tumble ratio

Significant effects of the in-cylinder tumble flow are typically approximated using the tumble ratio. The illustration of the cycle-to-cycle behavior of the tumble ratio development under selected intake port models and under motoring conditions is shown in Fig. 5.5. The effect of the change of the intake port model can be explained by considering that the change of the intake port model has a significant effect on the change in the tumble ratio. The tumble ratio with the helical intake port in the same direction has the same tendency as tumble ratio for the tangential intake port where at the beginning of the intake process during the opening period of the intake valve there is a production phase where the tangential intake port is slightly longer than a 50 °CA. The tumbling ratio peak in the same direction of the helical intake port occurs at a 460 °CA, while the tangential port occurs 25 °CA slower than the same direction of the helical intake port, which is caused by a slowing of the production process. However, the tangential intake port has the advantage that it does not decrease drastically and rise again in the stabilization process compared to the helical intake port in the same direction at the end of the compression step. This can be seen from Figures 5.5a and 5.5d, where the second peak of the tumble ratio at the tangential intake port is 0.75° CA from the first peak while at the helical intake port in the same direction it is 0.4° CA from the first peak. This is due to the decrease in the momentum of the inflow into the engine cylinder through the valve and the increase in the volume of the cylinder to the BDC at the tangential intake port is much better than the helical intake port in the same direction.

While the tumble ratio with the helical intake port in the opposite direction (inward) has the same tendency with the tumble ratio with the helical intake port in the opposite direction (outward), there are several tumble ratio’s peaks at the beginning of the compression stroke. The difference is found in the earliest tumble increase during the opening period of the intake valve with high reproducibility in the initial phase up to 50 °CA at the helical intake port in the opposite direction (exit) where the highest peak occurs at the intake stroke at 410 °CA. There are similarities within these four models, namely the existence of two peak tumble ratios that occur in the middle of the intake process and the middle of the compression process around 630 °CA and the destruction process that occurs at the end of the compression step up to 720 °CA, where there is a dramatic decrease due to the dissipation effect.

Regarding the cycle-to-cycle variation of the tumble ratio for each intake port model, the first 10 cycles are depicted in Figure 5.5. The tumble helical intake port model in the same

direction has the highest tumble peak compared to other models at a 460 °CA. Furthermore, the cyclic scattering of the tumble ratios is proportional to all configurations except in the helical intake port in the opposite direction (inward), where a large range of the distribution can be observed in Figure 5.5b. This happens especially in the compression process at high crank angles. In the final compression configuration, the helical intake port in the same direction shows less cyclic scatter than the other models, which begin the tumble decay at the same value of 630 °CA.

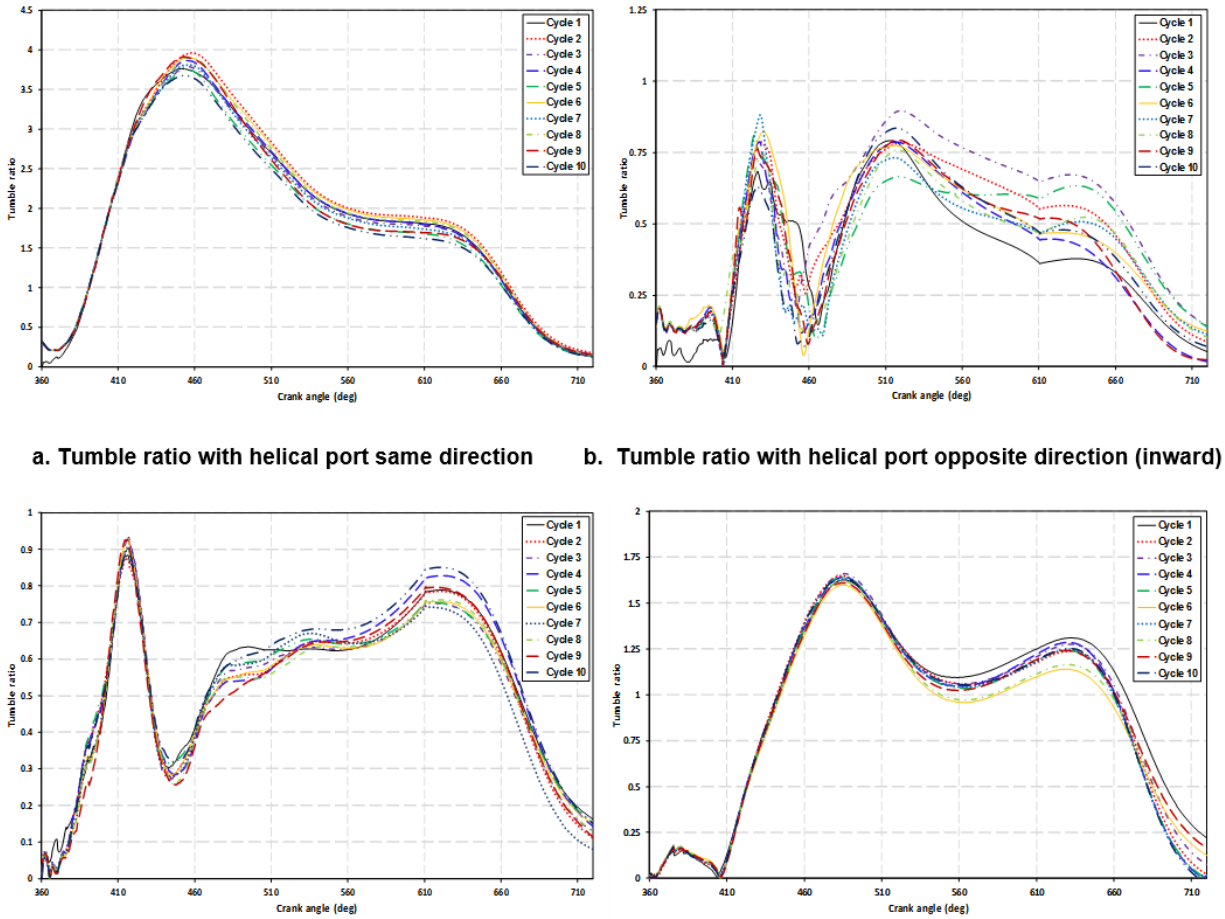

a. Tumble ratio with helical port same direction **b. Tumble ratio with helical port opposite direction (inward)**

c. Tumble ratio with helical port opposite direction (outward) **d. Tumble ratio with tangential port**

Fig. 5.5 In-cylinder cyclic tumble ratio with 10 cycles for selected intake port models

5.5 Cycle to cycle of turbulent kinetic energy

The turbulent kinetic energy (TKE) is the average kinetic energy per unit mass, which is shown by the fluctuation measure of the root mean square velocity (RMS). The TKE is an important parameter to estimate the turbulent viscosity and to quantify the conversion of energy

from the large scale to small scale. The illustration of the cycle-to-cycle behavior of the TKE development with some intake port models under motoring conditions is shown in Fig. 5.6.

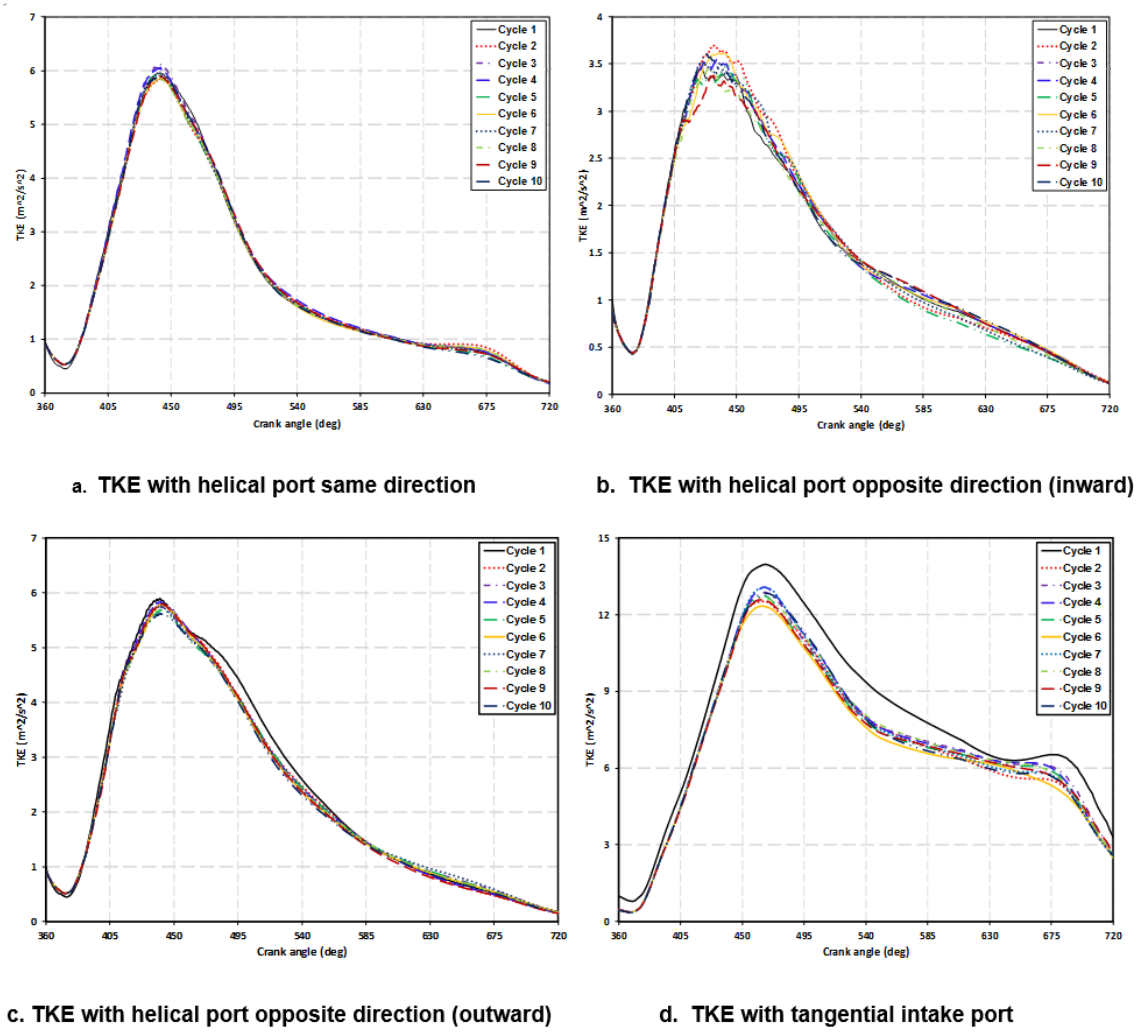

a. **TKE with helical port same direction**

b. **TKE with helical port opposite direction (inward)**

c. **TKE with helical port opposite direction (outward)**

d. **TKE with tangential intake port**

Fig. 5.6 In-cylinder TKE with 10 cycles for selected intake port models

Generally, there are two peaks of the TKE. The first TKE peak occurs around 450 °CA, which is likely to occur due to turbulence generated when air flows by means of the curtain area of the intake valve. The second TKE peak occurs at the compression stroke around 680 °CA, which occurs due to the movement of the piston in the cylinder and displays more narrow area. Associated changes in the intake port model show that changes in the intake port model do not have a significant effect on the process of the formation of TKE from the beginning of the intake stroke until the compression stroke ends. However, the change that occurs is the maximum value of the first peak of the TKE and the formation of the second peak of the TKE, which has a lower value than the first peak. The intake port with the tangential model gives the highest maximum TKE value compared to the other models. The maximum value of the TKE occurs at the first peak of the TKE at around 450 ºCA where the value is more twice than the

maximum value of the TKE at the helical intake port with the same direction and the helical intake port with the opposite direction (outward). This peak is almost four times the maximum value of the TKE at the helical intake port in the opposite direction (inward). The large maximum value at the tangential intake port of this model may be because the intake port with the tangential model causes an increase in the air velocity at the inlet, especially in volumes close to the full opening position when there is a dynamic transition from the intake valve. An increase in the velocity of incoming air indicates the collapse of falling vortices. Then, dismantling from a tumble vortex increases turbulence, and finally results in a greater TKE. The formation of the second peak of the TKE can be seen in Figure 5.6, where only the intake port with the tangential model and intake port with the helical model in the same direction clearly have a second peak. However, the second peak is not very visible and is very small in the intake port model, shared with the helical models for both the inward and outward directions. This might be due to the bifurcation area and the low pressure that occurs at the end of the compression stroke in both models of the opposite helical intake port.

Regarding the cycle-to-cycle variation of the TKE for each intake port model, the first 10 cycles are depicted in Figure 5.6. Furthermore, related to the characteristics of the intake port concept, the helical intake port in the same direction, helical intake port in the opposite direction (outward), and helical intake port in the opposite direction (inward) show similar general behavior, except only at the end of the compression stroke, where the peak occurs, which is not too big for the helical port in the same direction. However, the helical intake port in the opposite direction (inward) has more cyclic fluctuations, especially when the first TKE peak occurs. The level of the TKE in the tangential intake port model is expected to be comparably high due to the high flow of momentum during the intake process. Figure 5.6d confirms this prediction. Furthermore, related to the characteristics of the intake port concept, the helical intake port in the same direction, helical intake port in the opposite direction (outward), and helical intake port in the opposite direction (inward) show similar general behavior, except for only the end of the compression stroke, where the peak occurs. This peak is not very substantial for the helical port in the same direction. However, the helical intake port in the opposite direction (inward), has more cyclic fluctuations, especially when the first TKE peak occurs. However, the cyclic scattering of the TKE occurs in the intake port tangential model, where the first cycle is quite large while the second to tenth cycles are quite stable. This

is a concern because TKE conversions arise from various flow structures with different intensities, which can be a potential problem for combustion stability.

5.6 Summary

This study aimed to numerically and experimentally analyze the results of the in-cylinder flow of small motorcycle engines using steady flow benches for various intake port modifications based on the flow direction. This study also investigates the intake port velocity distribution, with many models of the intake port around the valve curtain for two intake valves with varied valve lifts. In addition, this study also analyzed variations of the inflow motion of the in-cylinder engine in both the horizontal and vertical planes for all intake port models. Moreover, this study also investigates the cycle-to-cycle behavior of the tumble ratio and TKE development with selected intake port models under motoring conditions to assess the stability at the beginning of the developing stage. Given the results, this study suggests the following conclusions:

1. There is a good agreement between the experimental results of the steady flow bench and simulations results of the flow coefficients for various intake port modifications based on the flow direction.

2. The velocity distribution with the tangential intake port model around the valve curtain of the two intake valves generally spreads in all directions and mostly towards the center of the cylinder with a maximum flow velocity nearly doubling compared to the other three models.

3. In the horizontal and vertical planes, the flow patterns of all intake port models are similar where the valve lift is greater. With a greater valve lift, the flow pattern will be more varies and the flow velocity will also be greater. However, the tangential intake port model has the greatest flow velocity compared to other intake port models.

4. The changes in the intake port models have a significant effect on the change in the tumble ratio. However, the tumble of the helical intake port model in the same direction has the highest tumble peak compared to other models at 460 °CA.

5. The changes in the intake port model do not have a significant effect on the process of the TKE formation. However, the effect that does occur regards the maximum value of the first

peak of the TKE, where the intake port with the tangential model gives the highest maximum TKE compared to the other models.

6. The cyclic scattering of TKE occurs in the intake port tangential model where the first cycle is quite large while the second to tenth cycle is quite stable. This needs to be a concern because TKE conversions arise from various flow structures with different intensities, which can be a potential problem for combustion stability.

6. EFFECT OF INTAKE PORT MODIFICATION BASED ON INCLINATION ANGLE ON SMALL MOTORCYCLE ENGINE

This study aimed to analyze numerically and experimentally the results of the in-cylinder flow of small motorcycle engines using steady flow benches based on the variation of the intake port inclination. The variation of intake port inclination is -15º, 0º, 11.5º(original), 15º and 30º. In addition, this study also investigates variations inflow motion in-cylinder engine in both horizontal and vertical planes on all variations of the intake port inclination. Moreover, this study also aimed to investigate the effect of the variation of the intake port inclination on the characteristics of the in-cylinder airflow which is carried out in small motorcycle engine under motoring condition. The result shows that there is a good agreement between the experiment result of steady state flow bench and simulations result in terms of flow coefficient and airflow rate at various inclination of the intake port. The result shows that the variation of intake port inclination gives effect to be an irregular shape on the swirl ratio. The bigger the inclination of intake port the smaller the tumble ratio. The biggest increase occurred in the intake port with -15º at the first peak of 8.07% and the second peak of 12.01% than the original intake port. The change in inclination of the intake port has the effect to change turbulent kinetic energy, length scale and turbulent kinematic viscosity where the maximum increases occur at the intake port with 30º with 9.55%, 4.65% and 15.25% respectively compared to the original intake port. Based on this case study, the intake port with 30º is the most optimal intake port compared to other models where this intake port has a better increase in vortices compared to other models which result in increased turbulence in the cylinder. Based on the visualization of the airflow in-cylinder engine, the airflow has the same tendency where vortices formation occurs below the intake valve. However, the change in the intake port inclination gives effect to the change of the velocity magnitude. The bigger the inclination of the intake port the bigger the velocity flow at the in-cylinder engine will be. The maximum velocity occurs in the middle of the in-cylinder engine for all intake port model. Finally, this study is expected to help in estimating air flow and optimizing internal combustion engine combustion chamber, especially in small motorcycle engine.

6.1 Comparison experiment and simulation result of flow coefficient and air flow rate

Fig. 6.1 represent the flow coefficient with valve lifts using various intake port inclination based on the experiment and simulation results. The comparison of the flow coefficient based on the experiment and simulation results with original intake port (11.5º) was shown in Fig. 6.1a. The flow coefficient seems to increase gradually with valve lift because the area of effective flow through the valve also increased until valve lift of 4 mm. From this valve lift to 6.46 mm where the valve lift reaches the maximum value, the coefficient of flow was constant. The coefficient of flow influenced the breathing capacity of the engine because of much air enter to the cylinder at the higher valve lifts. However, in the lower valve lift, this effect is quite small. There is a good agreement between experiment and simulation results. The maximum discrepancy is 17.55% at the lift valve 2,18 mm. The flow coefficient maximum is 0.76 at 6.43 mm valve lift.

As shown in Fig. 6.1b, the flow coefficient with modified intake port 0º increase with valve lift. The trend of the flow coefficient in experiment and simulation result is same where the flow coefficient increased rapidly until valve lift reached 4 mm and from this point to 6.46 mm as the maximum valve lift, the coefficient of flow become constant. This is because the cross-sectional area of the intake flow passages at the valve lift is lower than 4 mm is relatively small. Another thing is the dominance of the valve lift effect when the valve lift is lower than 4 mm. However, the cross-sectional area of the intake flow passages on the valve lift is enlarged when the valve lift is greater than 4 mm. Another factor is the dominance of the effect of intake port flow resistance when the valve lift is greater than 4 mm. The flow coefficient maximum is 0.71 at 6.46 mm valve lift. If compare with the original intake port (11.5º), this modified intake port has flow coefficient 6.58% lower than the original intake port.

Similar with the Fig 6.1b, Fig. 6.1c-6.1e show the flow coefficient with valve lifts using various intake port inclination of 15º, 30º and -15º respectively. The tendency of the flow coefficient in experiment and simulation result is similar in these three modified intake ports where the flow coefficient enlarged with valve lift until 4mm of valve lift and from this point to 6.46 mm as the maximum valve lift, the coefficient of flow become constant. The coefficient of flow influenced the breathing capacity of the engine because of much air enter to the cylinder at the higher valve lifts. However, in the lower valve lift, this effect is quite small. There is a

good agreement between experiment result in steady flow bench and numerical result. The maximum discrepancy is 16.77% at valve lift 1.42 mm, 17.22% at valve lift 5 mm and 18.43% at 4.47 mm respectively. The flow coefficient maximum is 0.78 at 6.46 mm valve lift, 0.81 at 6.46 mm and 0.68 at 6.46 mm respectively. If compare with the original intake port (11.5º), the modified intake ports with 15º and 30º have flow coefficient higher than the original intake port i.e. 2.63% and 6.58% respectively. On other side, intake port with -15º have flow coefficient lower than the original intake port 10.53%. Based on this result, the modified of intake port inclination give effect to the flow coefficient. It must be noted that although an intake port model has the highest flow coefficient, it does not guarantee that this model is the best model that can be applied for using in an engine. There are several other factors that affect an intake port model chosen as a reference, especially in improving the performance of the engine. Some of these factors will be discussed in another section of this study.

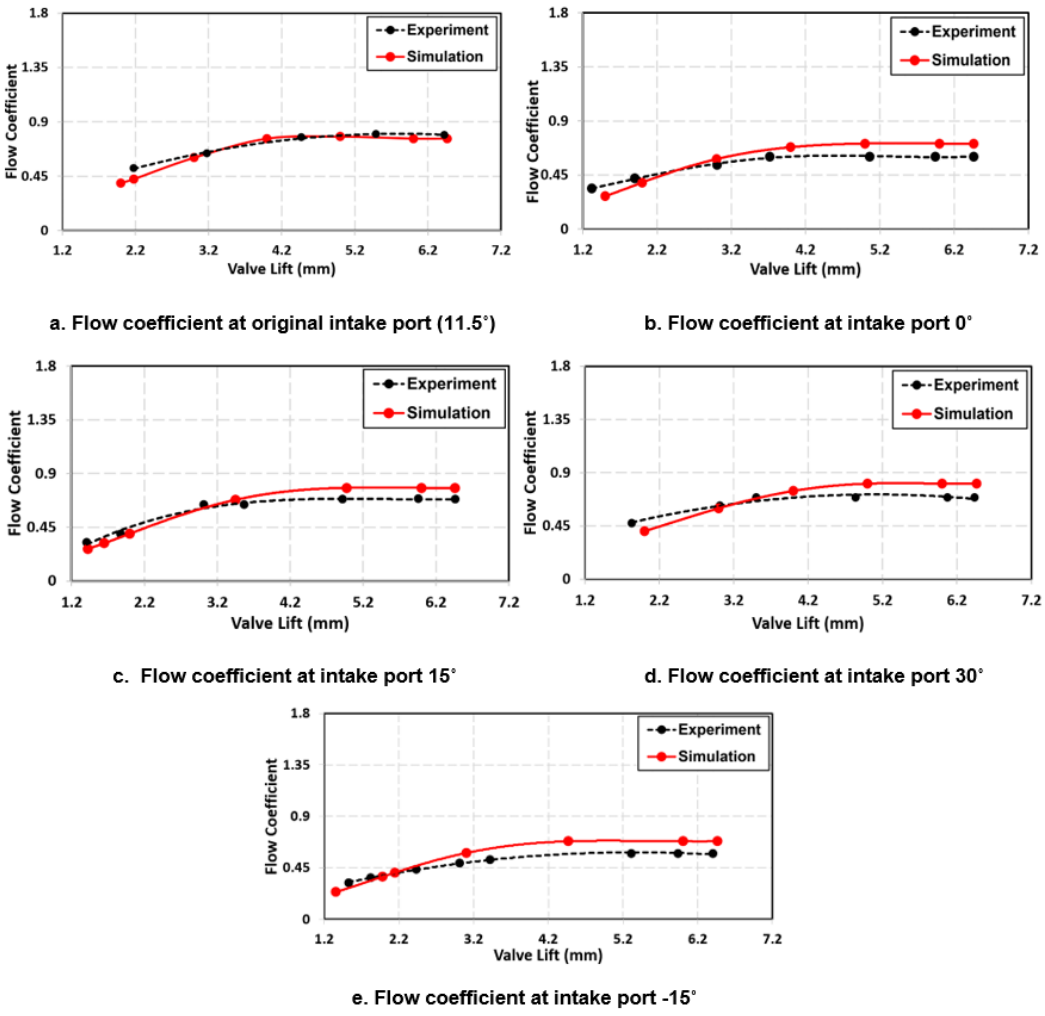

Fig. 6.1 Comparison flow coefficient in experiment and simulation at intake port 11.5˚ (original intake port), 0˚, 15˚, 30˚ and -15˚

The comparison of the intake airflow rate as a function of the valve lift between the experiments results on the steady flow bench and the simulation results at the various intake port inclination were shown in Fig. 6.2. Fig. 6.2a shows the air flow rate of engine model with original intake port (11.5º) where the intake airflow rate increases when the valve lift enlarged until 4 mm. From 4 mm to 6.46 mm as the maximum valve lift, the airflow rate becomes constant. Increasing the valve in a higher position makes more airflow into the engine cylinder and ultimately the engine's breathing capacity is higher. The results of experiments and simulations show a similar trend. The maximum discrepancy is 16.98% at the lift of 2,18 mm. The flow rate maximum is 0.021 m3/s at 6.43 mm valve lift. Fig 6.2b-6.2e also show the comparison of intake airflow rate of small motorcycle engine as a function of the valve lift between the simulation and the experiments results on the steady flow bench using various modified intake port. Similar with Fig. 6.2a, Fig. 6.2b-6.2e show that the result has same trend between experiment and simulation result where the flow rate increase with valve lift until valve lift reached 4mm and to be constant from this point to maximum valve lift of 6.46 mm. If compare with the original intake port (11.5º), the various modified intake port has flow rate lower than the original intake port except intake port with 15º and 30º. Intake port with 15º and 30º have flow rate higher than the original intake port i.e. 0.22% and 3.70% respectively. On other side, intake port with -15º and 0º have flow rate lower than the original intake port i.e. 12.70% and 8.68% respectively. Larger flow rate value does not ensure that a model is better than a model that has a lower flow rate. This is because there are many factors that can influence to make a model an option to be used as a reference in order to obtain an optimal performance engine. However, the optimal flow rate is needed to be one of the options that can be considered for designing an engine. Similar research has also been conducted by El-Adawy *et.al.* [86] where they have conducted research to determine the flow characteristics of an engine with a large bore of 92.5 mm and a maximum valve lift of 9.73 mm using two different steady state flow benches, namely the Ricardo method with an impulse torque meter and the FEV method with the paddle wheel technique. They concluded that the flow coefficient increased monotonically until the valve lift was about 6 mm and from this point up to the highest valve lift of 9.73 mm increased slightly. This occurs in both steady state flow bench models. The same thing also happened to the air flow rate where the air flow rate increased with the increase in valve lift monotonically to 6 mm and increased slightly from this point until the valve lift reached its highest point of 9.73 mm. Other researchers, Ramajo and Nigro [110], also have been done the same thing on engines with a bore stroke of 87 mm x 68 mm

and a maximum valve lift of 9 mm, where they concluded that the flow coefficient increased as the valve lift increased to 7 mm and was slightly constant until it reached the top of the valve lift. at 9 mm.

6.2 In-cylinder flow field velocity vector

6.2.1. Horizontal Plane

Comparison of flow fields of velocity vector for three different valve lifts with various intake port inclination under motoring condition, along the x-y plane (z = -4 mm) that passes the intake valves and cylinder in small motorcycle engines is shown in Fig. 6.3. Fig. 6.3a. shows the velocity vector flow field in the cylinder by using the original intake port with an angle of 11.5º. The swirl flow pattern in Fig. 6.3a clearly varies, which is caused by increased valve lifts and adjusted 300 mmH_2O of pressure drops. In addition, the flow velocity increases when the valve lift increases until the valve lift reaches a maximum value (6.46mm). When the valve lift reaches 5.7 mm, some vortices are formed around the intake valve seat and the the vortices are clearly visible on the edge of the cylinder. In the valve lifts of 6.1 mm and 6.46 mm, the flow velocity near the edge of the cylinder is clearer. However, the highest flow velocity occurs at the center of the cylinder at 60 m/s. In the center of the cylinder when the valve lift enlarges the flow velocity also increases. This is because in this area there is higher turbulence. Fig. 6.3b-6.3e shows the same thing as Fig. 6.3a. where the flow pattern and flow velocity increase when the valve lift increase. There is no significant change, especially in the position of the valve lift 5.7 mm for all intake port models except for intake ports with 30º. There is an increase in velocity magnitude at 5.7 mm position at the intake port with 30º in the area below the intake valve compared to the intake port of other models reaching 12 m/s. Moreover, the changes will be more visible when the valve lift position reaches 6.1 mm and more when the valve lift position reaches a maximum of 6.46 mm. At the maximum valve lift position, the flow pattern for all model is evenly distributed to all areas and more clearly. Moreover, the flow velocity maximum is similar result with the original model (intake port with 11.5º) where it occurs in the center of cylinder and around 60 m/s. However, the intake port with 30º and 15º have the high velocity magnitude in the side of cylinder. Another thing that distinguishes another is the distribution of the velocity magnitude in each intake port model. The intake port model with 30º has a more even distribution of velocity magnitude in all directions compared to other intake port models. This can be proven by the color index for each intake port model. From Fig. 6.3a-6.3e, it can be concluded that the flow patterns of all

intake port models are similar where the valve lift is getting bigger, the flow pattern will be more varied and the flow velocity is also getting bigger and the biggest velocity occurs at the center of the cylinder. The intake port with 30º has a slightly more even velocity distribution than the other models although the maximum flow velocity is the same as the other models. This can affect the increase in turbulence in this area. Increased turbulence results in a more homogeneous mixing of air fuel in cylinder.

Similar research has also been conducted by Binjuwair *et. al.* [111] to determine the flow structure in the engine cylinder head with a bore of 88 mm and a maximum valve lift of 10 mm and a pent roof model. They reached a similar conclusion that the flow velocity increased as the valve lift increased. It's just that this increase in flow rate only reaches the 8 mm valve lift. Meanwhile, the flow velocity does not increase when the valve lift increases from 8 mm to 10 mm valve lift. The flow velocity around the cylinder edge is also not visible. This is because in the study conducted by Binjuwair et. al., there was a lack of turbulence in the area, which could be interpreted as a small change in focus due to the need to shift the head over the endoscope for the usual liner cleaning process. Meanwhile the research authors carried out the velocity around the cylinder edge will be clearly seen. more so at the intake port with 30º. Meanwhile, another equation is that the greatest velocity flow occurs towards the center of the engine cylinder and the formation of two symmetrical opposite eddies that appear in all figures for all valve lift.

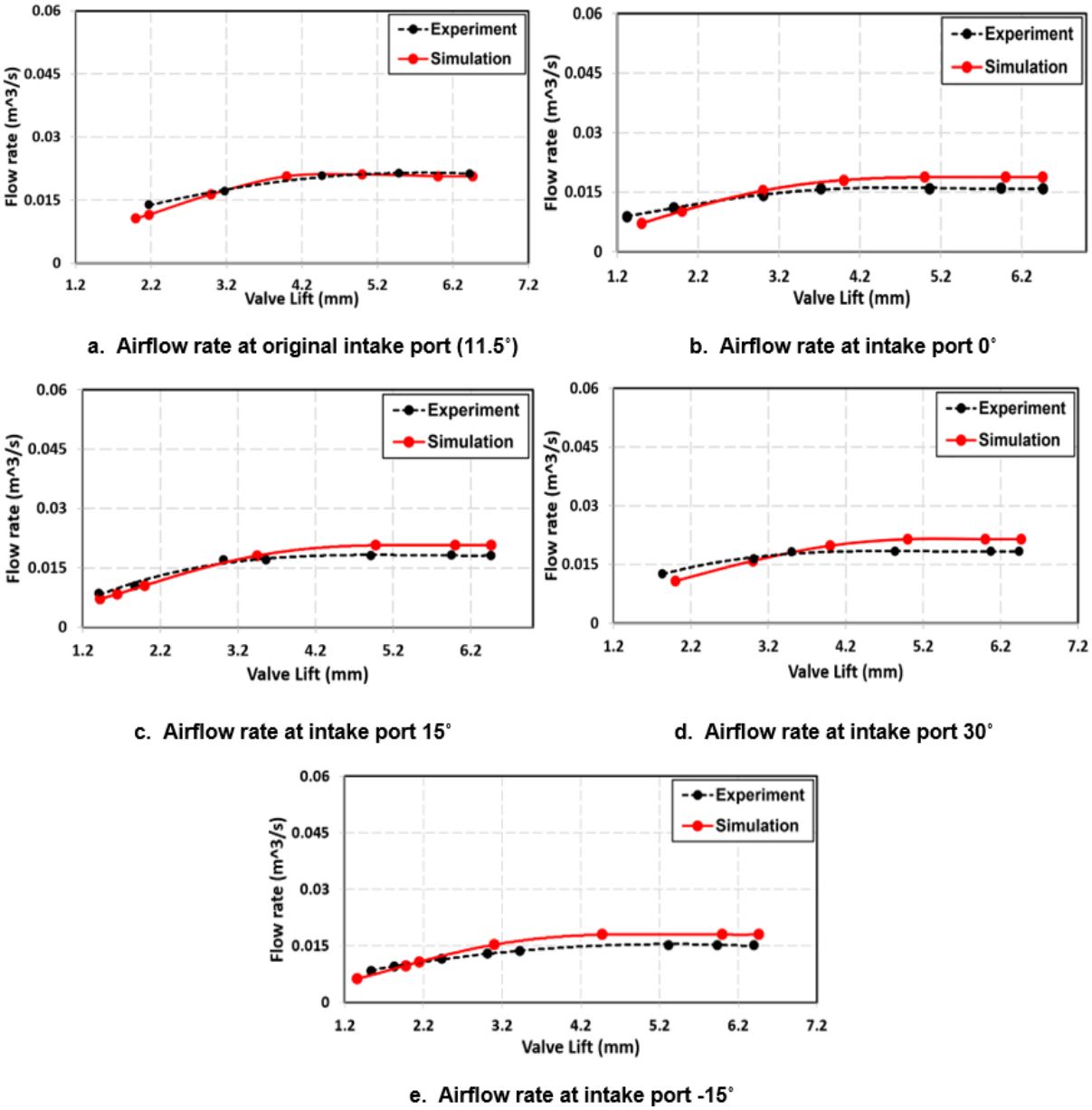

a. Airflow rate at original intake port (11.5˚)

b. Airflow rate at intake port 0˚

c. Airflow rate at intake port 15˚

d. Airflow rate at intake port 30˚

e. Airflow rate at intake port -15˚

Fig. 6.2 Comparison airflow rate in experiment and simulation at intake port 11.5˚ (original intake port), 0˚, 15˚, 30˚ and -15˚

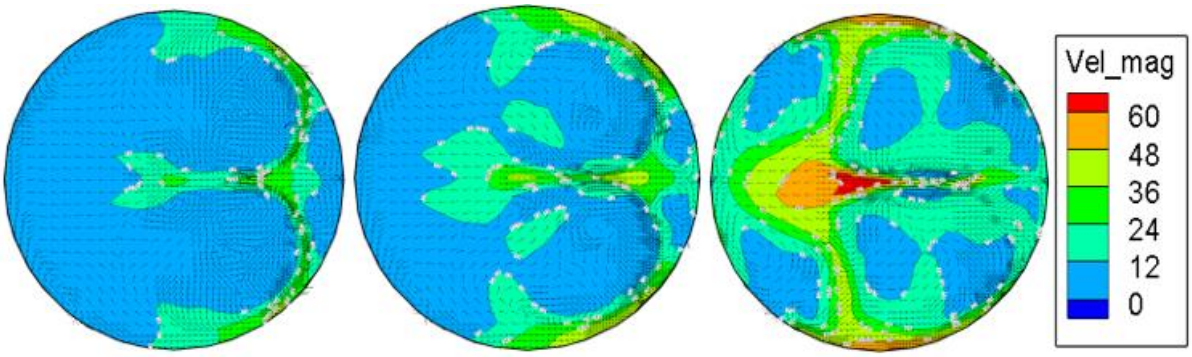

Valve lift 5.7 mm Valve lift 6.1 mm Valve lift 6.46 mm

a. Velocity vector for varied valve lifts with x-y plane (z= -4 mm) at Intake port 11.5˚

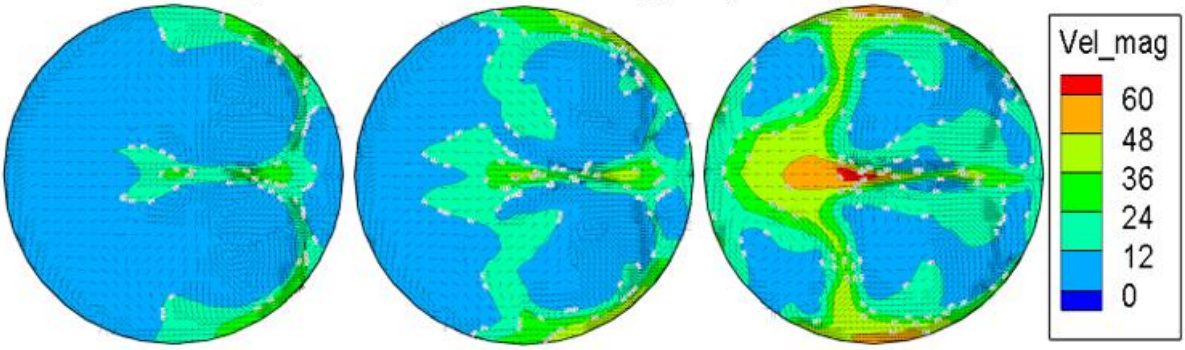

Valve lift 5.7 mm Valve lift 6.1 mm Valve lift 6.46 mm

b. Velocity vector for varied valve lifts with x-y plane (z= -4 mm) at Intake port 0˚

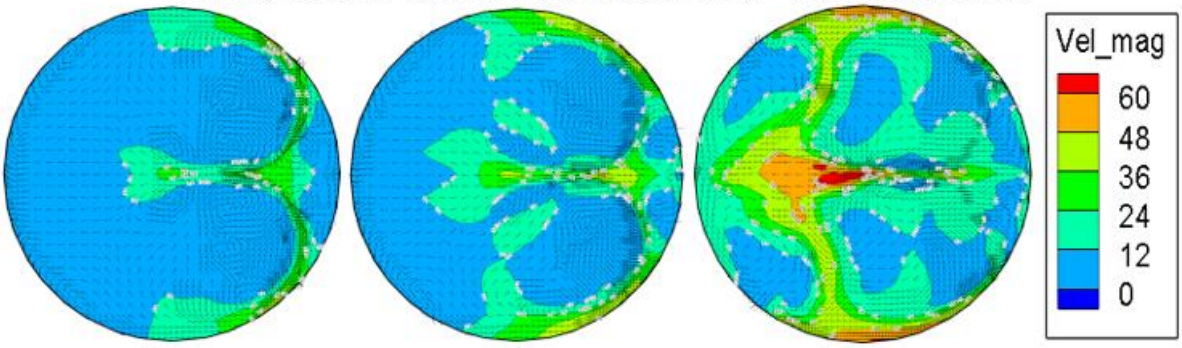

Valve lift 5.7 mm Valve lift 6.1 mm Valve lift 6.46 mm

c. Velocity vector for varied valve lifts at x-y plane (z= -4 mm) with Intake port 15˚

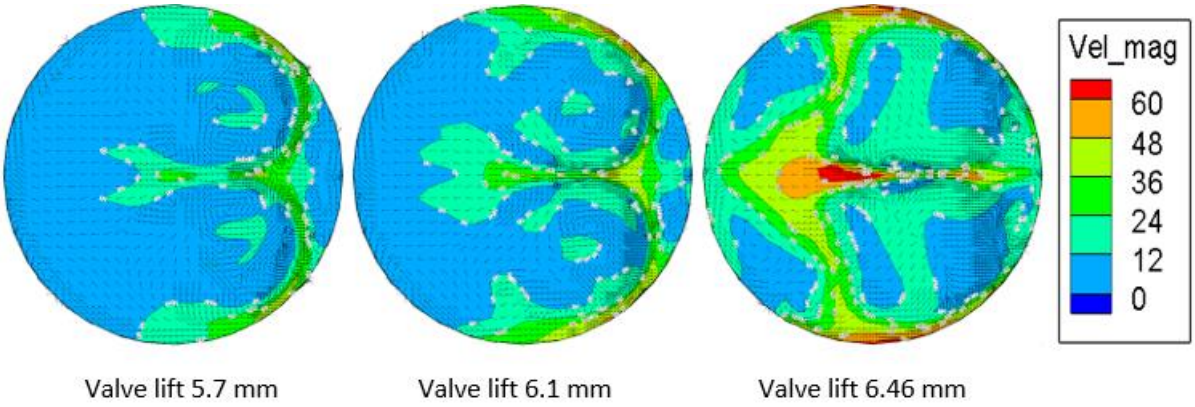

d. Velocity vector for varied valve lifts at x-y plane (z= -4 mm) with Intake port 30˚

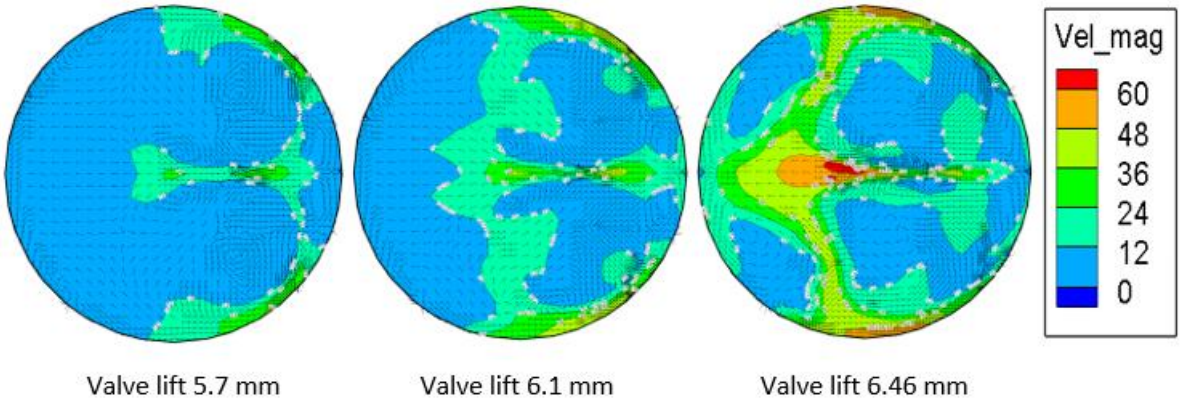

e. Velocity vector for varied valve lifts at x-y plane (z= -4 mm) with Intake port -15˚

Fig. 6.3 Velocity vector with variation of valve lifts at horizontal swirl Plane x-y plane (z= -4 mm) with intake port 11.5˚ (original intake port), 0˚, 15˚, 30˚ and -15˚

6.2.2. Vertical Plane

Comparison of flow field velocity vectors in a cylinder at three different valve lifts with 300 mmH_2O of pressure drop and varying inclination of the intake port along the x-z plane (y = 11.47 mm) that passes the in-cylinder of a small motorcycle engine shown in Fig. 6.4. Fig. 6.4a shows the flow velocity vector for three different valve lifts for a pressure drop of 300 mmH_2O with an original intake port with 11.5º. The greater the opening valve, the higher the flow pattern and flow velocity. At the beginning of the intake stroke, the air passes through the sides of the seat lips and the inside of the exhaust valve and contact with the cylinder wall. In this process a small vortex begins to form near the intake valve clockwise at the 5.7 mm valve lift. The larger the valve lift is opened the more air enters the cylinder as it does in the 6.1 mm valve lift. This results in more vortices forming in some areas in the cylinder. The climax is the formation of a large vortex in the middle of the cylinder when the valve lift reaches 6.4 mm as the maximum valve lift. The flow velocity at the valve lift is also the highest compared to the

5.7 mm and 6.1 mm valve lifts. It seems to correspond to the maximum flow velocity calculated based on the measured flow rate. The maximum flow velocity occurs at 6.46 mm valve lift of 77 m/s on the upper side of the cylinder near the intake port and 30.4 m/s at the center of the cylinder to the left.

The same thing happens in Fig. 6.4b-6.4e where the flow pattern and flow velocity increase with increasing valve lift. The difference is only the magnitude of flow velocity in the area inside the cylinder. The size of the flow velocity is marked by a color index. The index in red indicates the highest flow velocity. The greatest flow velocity occurs at the 6.46 mm valve lift at intake port 30º and 15º at 78.5 m/s on the upper side of the cylinder near the intake port and 31.4 m/s at the center of the cylinder. When compared with the original intake port with 11.5º, the flow velocity at the intake port 30º and 15º increases by 1.95% on the upper side of the cylinder near the intake port and the center of the cylinder. However, intake ports with 30º in general the distribution of flow velocity are higher in all areas in the cylinder than intake ports with 15º. In other side, decreased flow velocity occurred at intake ports with 0º and -15º on the upper side of the cylinder near the intake port and at the center of the cylinder of 3.90% (74 m/s) and 2.60% (75 m/s) respectively. The greater the flow velocity of an area shows increased turbulence in this area. Increased turbulence results in a more homogeneous mixing of air fuel in cylinder.

Similar research has also been conducted by El-Adawy *et.al.* [110] where they have conducted research to determine the flow characteristics of an engine such as the velocity vector field with variation of valve lifts with a large bore of 92.5 mm and a maximum valve lift of 9.73 mm. They reported that with the increasing of the valve lift then the vortices became more stronger and the center transferred towards the center of the engine cylinder. A similar study was carried out by Toh *et. al.* [112] where they investigated the effect of modification of the intake port section on engines with a bore stroke of 52.4 mm x 60.3 mm. There are two models of intake port cross section used in their research, namely circular cross section and elliptical cross section. They concluded that the two models have an equation where when the valve lift increases, the tumbling vortex will get bigger and go to the center of the engine cylinder. In general, the vortices tumbling is clearer in the elliptical cross section model. This proves that the elliptical port model is more conducive to tumbling than the circular model.

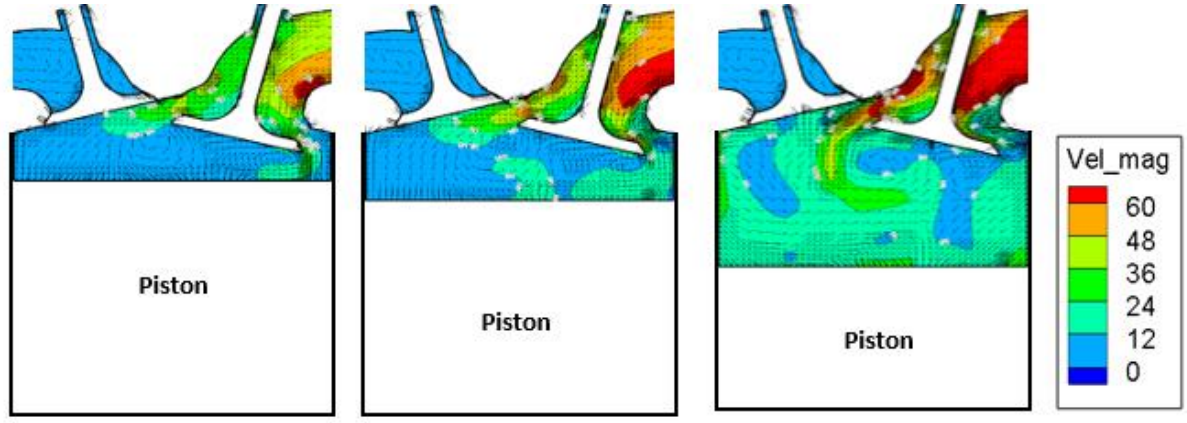

Valve lift 5.7 mm Valve lift 6.1 mm Valve lift 6.46 mm

a. Velocity vector for varied valve lifts at x-z plane (y=11.47 mm) with Intake port 11.5˚

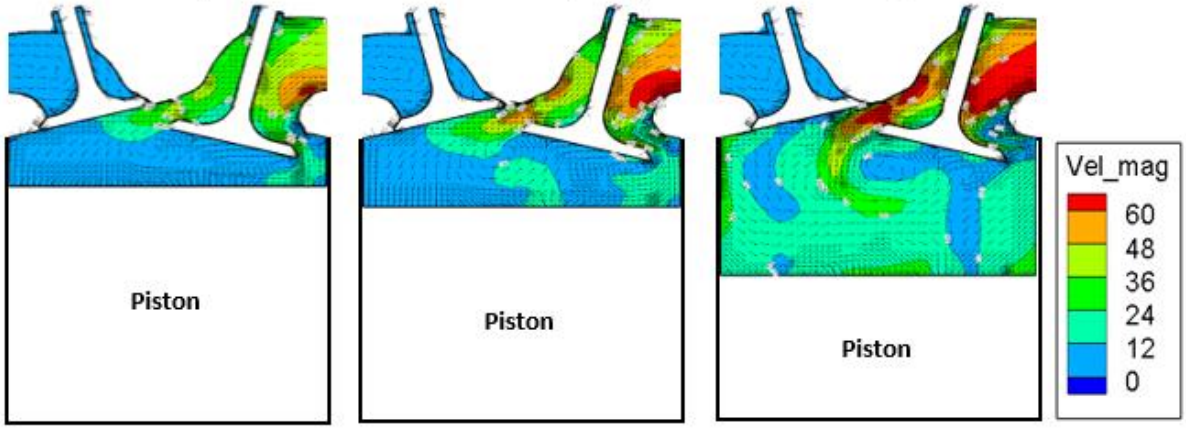

Valve lift 5.7 mm Valve lift 6.1 mm Valve lift 6.46 mm

b. Velocity vector for varied valve lifts at x-z plane (y=11.47 mm) with Intake port 0˚

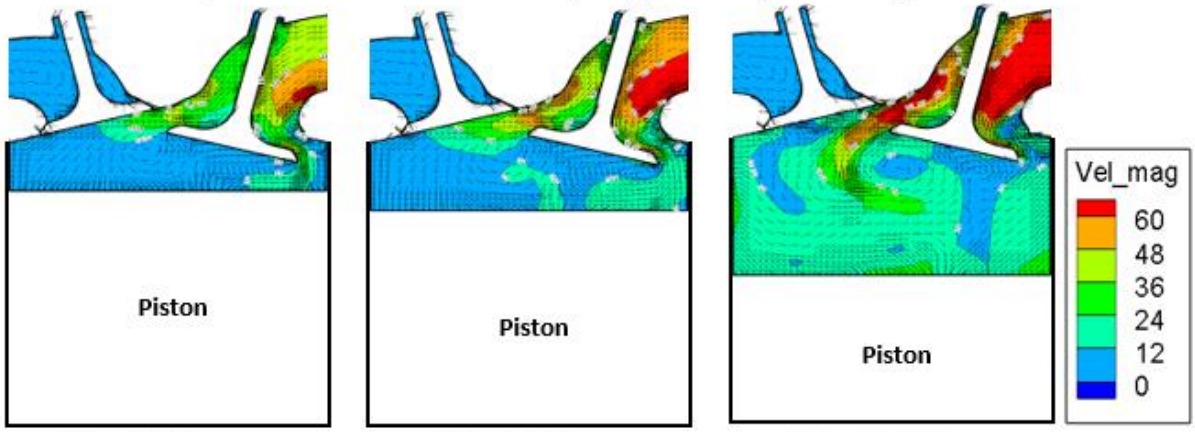

Valve lift 5.7 mm Valve lift 6.1 mm Valve lift 6.46 mm

c. Velocity vector for varied valve lifts at x-z plane (y=11.47 mm) with Intake port 15˚

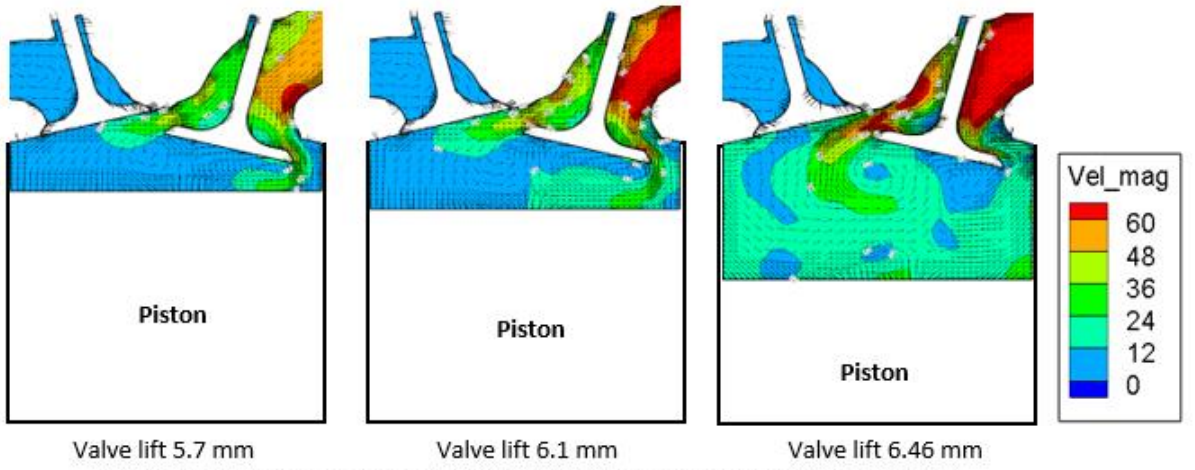

d. Velocity vector for varied valve lifts at x-z plane (y=11.47 mm) with Intake port 30˚

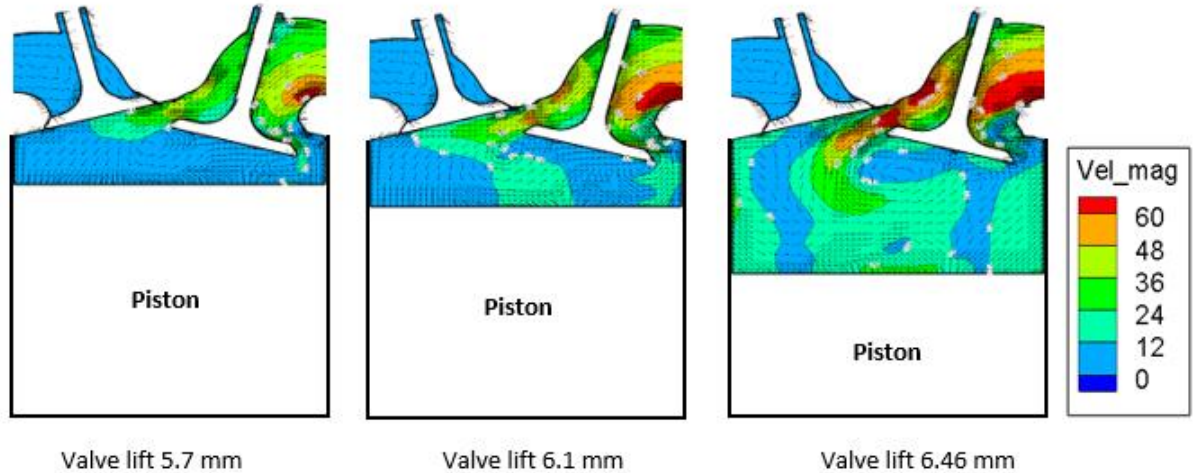

e. Velocity vector for varied valve lifts at x-z plane (y=11.47 mm) with Intake port -15˚

Fig. 6.4 Velocity vector with variation of valve lifts at vertical tumble plane x-z plane (y=11.47 mm) with intake port 11.5˚ (original intake port), 0˚, 15˚, 30˚ and -15˚

6.3 Characteristic of in-cylinder flow

6.3.1. Swirl Ratio

The formation of swirl flow due to the reaction of several components that arise after the flow from the intake port into the cylinder such as initial angular momentum, interaction between piston surface, cylinder wall and intake port. A comparison of the swirl ratio with 300 mmH_2O pressure drops at five different inclinations of intake port during the intake and compression stroke was shown in Fig. 6.5. The formation of swirl flow is started since the initial phase of the process of induction. The swirl flow enlarges and moves up and down until 495 °CA. But after the point of 495 °CA to the middle of the compression stroke around 630 °CA, the swirl ratio becomes stable. This is probably caused by the angular momentum lost to the cylinder wall and the effect of the turbulent dissipation factor that occurs in the flow. At

the end of the compression stroke, the swirl ratio turns unstable again. This is probably caused by the change in tangential velocity of the swirl flow due to interactions between the cylinder and piston walls. Based on Figure. 6.5, the change in the inclination of the intake port create an irregular shape in the swirl ratio. This irregular shape starts to appear at around 400 °CA after the intake stroke starts and the magnitude of the rise and fall of the swirl ratio increases with the increasing inclination of the intake port except for intake port with -15 because of its shape of the intake port makes the swirl flow bigger on the negative axis. However, all models show from 495 °CA to 630 °CA to become stable and at the end of the compression stroke again becomes unstable. This is caused by poor intake flow strength in the engine which is maintained during the stabilization stage.

Similar research was also conducted by Ramesh and James [105] where they conducted a study to determine the flow of a large engine with bore stroke 86 mm x 86 mm with a pent roof combustion chamber and variations in engine speed of 1000, 2000, and 3000 rpm. Their results show that the swirl ratio at all speeds produces the same tendency where at the beginning of the intake stroke the swirl ratio formation process occurs and reaches a maximum value at 390 °CA and drops to zero at 430 °CA and reaches a maximum value at 480 °CA on the negative axis and stable to the end of the axis of the compression stroke. The only difference is the maximum swirl ratio of the three variations of speed. This trend is similar to the research that the authors do, except that a significant difference occurs in the process of rising and falling of the swirl ratio, especially when the intake stroke reaches 495 °CA, while the research conducted by Ramesh and James who conducted research on large engine only occurs once the process goes up. decreased swirl ratio. This is probably because the large engine allows the airflow into the cylinder to be more flexible, and creates more interaction in the inlet, cylinder walls and piston surface.

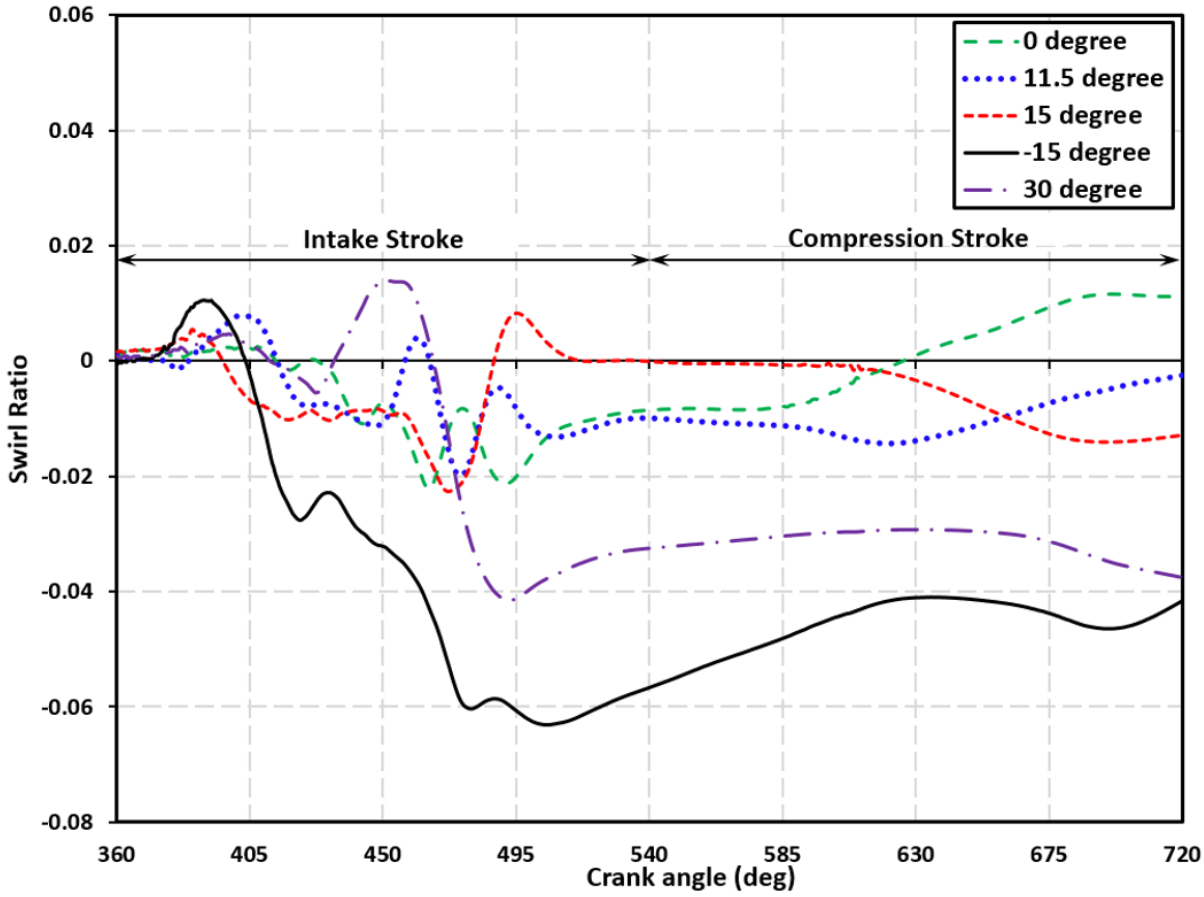

Fig. 6.5 In-cylinder swirl ratio at various intake port inclination

6.3.2. Tumble Ratio

In general, the tumble ratio is estimated under transient conditions to have a significant effect on piston movement on the tumble flow in the cylinder. A comparison of tumble ratio with pressure drop 300 mmH_2O for five different inclinations of intake port (-15˚, 0˚, 11.5˚(original), 15˚ and 30˚) under motoring condition was shown in Fig. 6.6. Generally, there are two important components of the tumble rotation in a flow field i.e. cross tumble (TRx) and normal tumble (TRy) and the total from these two tumbles was called Tumble Ratio (TR). There are three stages in-cylinder tumble flow: the production stage, the stabilization stage, and the demolition stage. The production stage appeared at the early of the intake stroke and then increased up to 380 °CA. From this point it then begins to fade, and becomes zero at 405 °CA. After this point, the tumble flow undergoes a stabilization stage and increases dramatically until reaches its peak at 470 °CA when the intake valve reaches the maximum position. Then it decreases until the intake valve closes at 560 °CA, because of the momentum of flow entering to the cylinder engine by the decreasing of valve lift and the volume of cylinder

increases to bottom death center (BDC). The tumble ratio enlarged again at the compression stroke until 640 °CA, This maybe because of the angular momentum conservation. This stage is called the stabilization stage because there is a process of up and down where the tumble ratio changes in magnitude from positive to negative and vice versa which shows changes in the direction of air motion in the cycle. The drastic reduction stage of the tumble ratio is called the demolition stage and is the last stage that occurs from 640 °CA to 720 °CA. This happens probably because of the dissipation process.

Regarding the effect of the inclination of the intake port, it can be explained that the change in the inclination of the intake port has a significant effect on the change in tumble ratio. The bigger the inclination of intake port the smaller of the tumble ratio. The biggest tumble ratio occurs at the intake port with -15º and the smallest tumble ratio occurs at the intake port with 30º. When compared with tumble ratio on the original intake port with 11.5º, tumble ratio on the intake port with -15º increased by 8.07%. While tumble ratio at intake ports with 0º, 15º and 30º was 3.77% (increasing), 2.06% (decreasing) and 25.08% (decreasing) respectively. This may be due to the intake flow strength which is getting better when the inclination of the intake port is raised especially to the point that only result in tumbling vortex, which continues throughout the stabilization stage. Based on Fig. 10, it is also shown that the variation of the intake port inclination, the flow distribution is similar, both in intake stroke and the compression stroke. However, the greater tumble ratio value on an intake port model does not guarantee that the model is the best model that can be applied to an engine. There are several other factors that affect the intake port model chosen as a reference, especially in improving engine performance. Then, this factor needs to be compared with other factors that also have effect on improving engine performance.

The tendency of the tumble ratio is similar to the results obtained by Haworth *et.al.* [113] on engines with large bore sizes and by Trigui *et.al* [114] with the geometry of the four valves pent roof of the engine. Similar results were also obtained by Ramesh and James [105] who conducted research using a large engine with bore stroke 86 mm x 86 mm. However, there is a slight phenomenon that occurs in the drop flow characteristics of a small motorcycle engine that does not occur in a large engine. This phenomenon is the initial formation of a tumble flow, at the beginning of the suction stroke until the crank angle reaches 400 °CA. This initial formation did not occur for a long time and reached a maximum value of only 0.25, then decreased again to zero, then increased again until it reached the top point at a crank angle of

approximately 460 °CA. This may be due to the zone of branching and low pressure that occurs at the start of the suction stroke in small motorcycle engines. On the other hand, the large engines started to generate flow drops from 400 °CA and soon increased significantly until they reached a peak at 460 °CA. From this point on up to the end of the compression stroke, the trend for tumble ratios on large engines has the same tendency for small motorcycle engines.

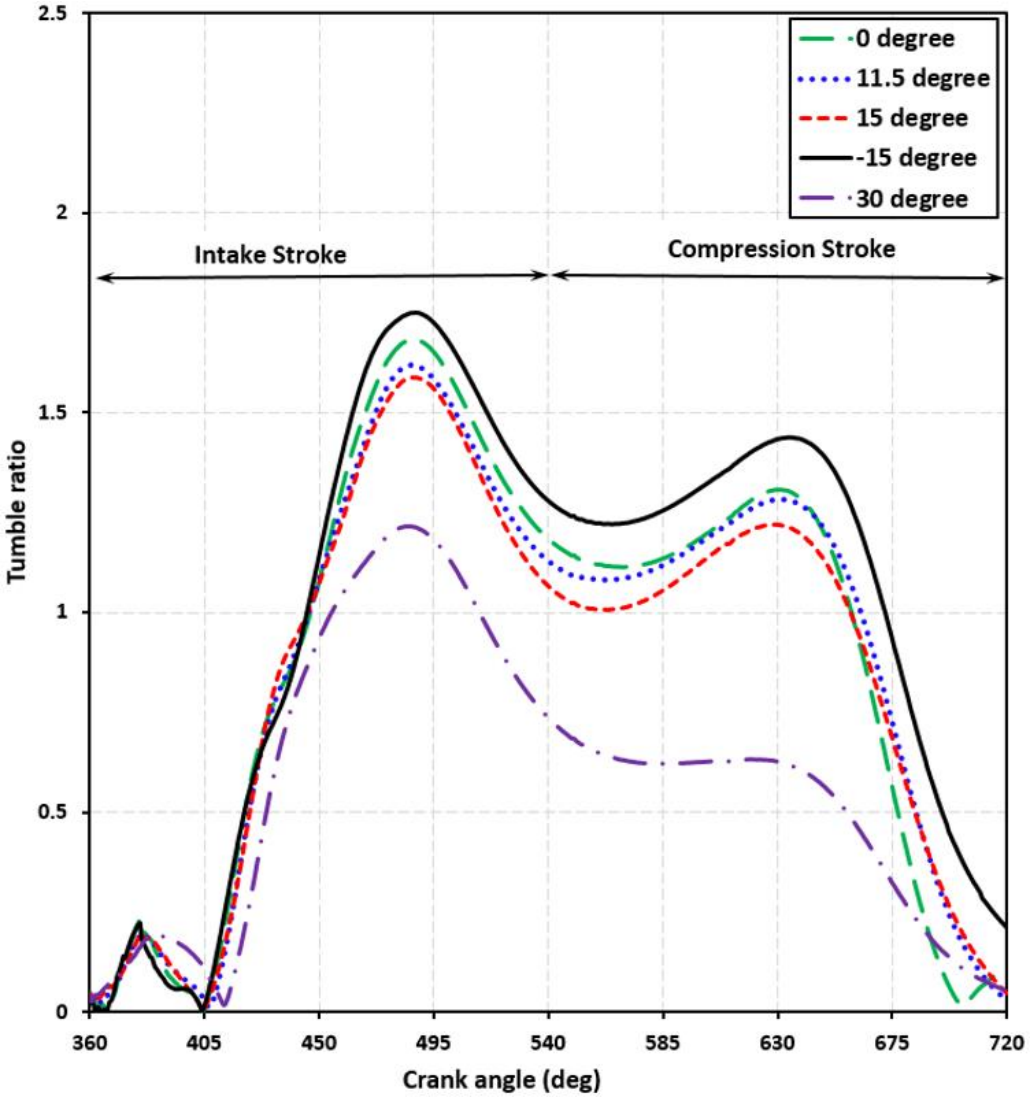

Fig. 6.6 In-cylinder tumble ratio at various intake port inclination

6.3.3. Turbulent Kinetic Energy (TKE)

Turbulent kinetic energy (TKE) is the average kinetic energy per unit of mass, which is shown by the fluctuation measure of the root mean square velocity (RMS). An important parameter for estimating turbulent viscosity is TKE. Comparison of TKE with a pressure drop

of 300 mmH_2O for five different inclination of the intake port (-15º, 0º, 11.5º (original), 15º and 30º) at intake and compression stroke and under motoring condition is shown in Fig. 6.7. In general, there are two peaks of TKE. Likewise, it can be seen in Fig. 6.7. The first TKE peak occurs at 475 °CA, that is likely to occur due to turbulence generated when air flows by mean of the curtain area of the intake valve. The second TKE peak occurs at the compression stroke around 680 °CA, which occurs due to the movement of the piston in the cylinder and falling on a narrower area. In addition, changes in the inclination of the intake port are observed to give an effect on changes in TKE both in intake stroke and compression stroke. The greater the inclination of the intake port, the greater the TKE value. The largest TKE value is reached by the intake port with 30º of 16.78 m2/s2 at the first TKE peak around 475 °CA, which is probably because the intake port with 30º causes an increase in air velocity at the inlet, especially in areas close to the full opening position when it occurs transition dynamics of the intake valve. An increase in the velocity of incoming air indicates the collapse of tumbling vortices. Then, the demolition from tumbling vortices enlarges the turbulence, and finally produce the bigger of TKE. When compared with TKE at the original intake port with 11.5º, the maximum value of TKE at intake port 30º increased by 9.55%. The increasing in the maximum value of TKE also occurred at intake ports with 15º at 16.57 m2/s2 (7.39%). However, the maximum value of TKE at intake port with 0º and -15º decreased at 14.64 m2/s2 (5.12%) and 13.64 m2/s2 (11.62%) respectively.

This study is similar to the results obtained by Addepalli and Mallikarjuna [106] where they conducted research on a large engine with a bore stroke of 87.5 mm x 110 mm and variations in engine speed of 2000, 3000, and 4000 rpm. At the three engine speeds, TKE on large engines has the same tendency as TKE on small motorcycle engine as the authors have done where there has been a significant increase in the TKE value from the start of the suction stroke until it reaches a peak point of around 460 ° CA and begins to decline from this point to the end of the compression stroke. However, there was an increase in the second TKE peak (lower than the first) at the end of the compression stroke. Related to the difference in inclination in the intake port model, it has a considerable effect on the timing of the second peak of TKE. The greater the inclination angle of the intake port, the faster the second peak of TKE will occur. This is probably due to the increasing momentum of transfer in the surrounding air as the inclination angle increases.

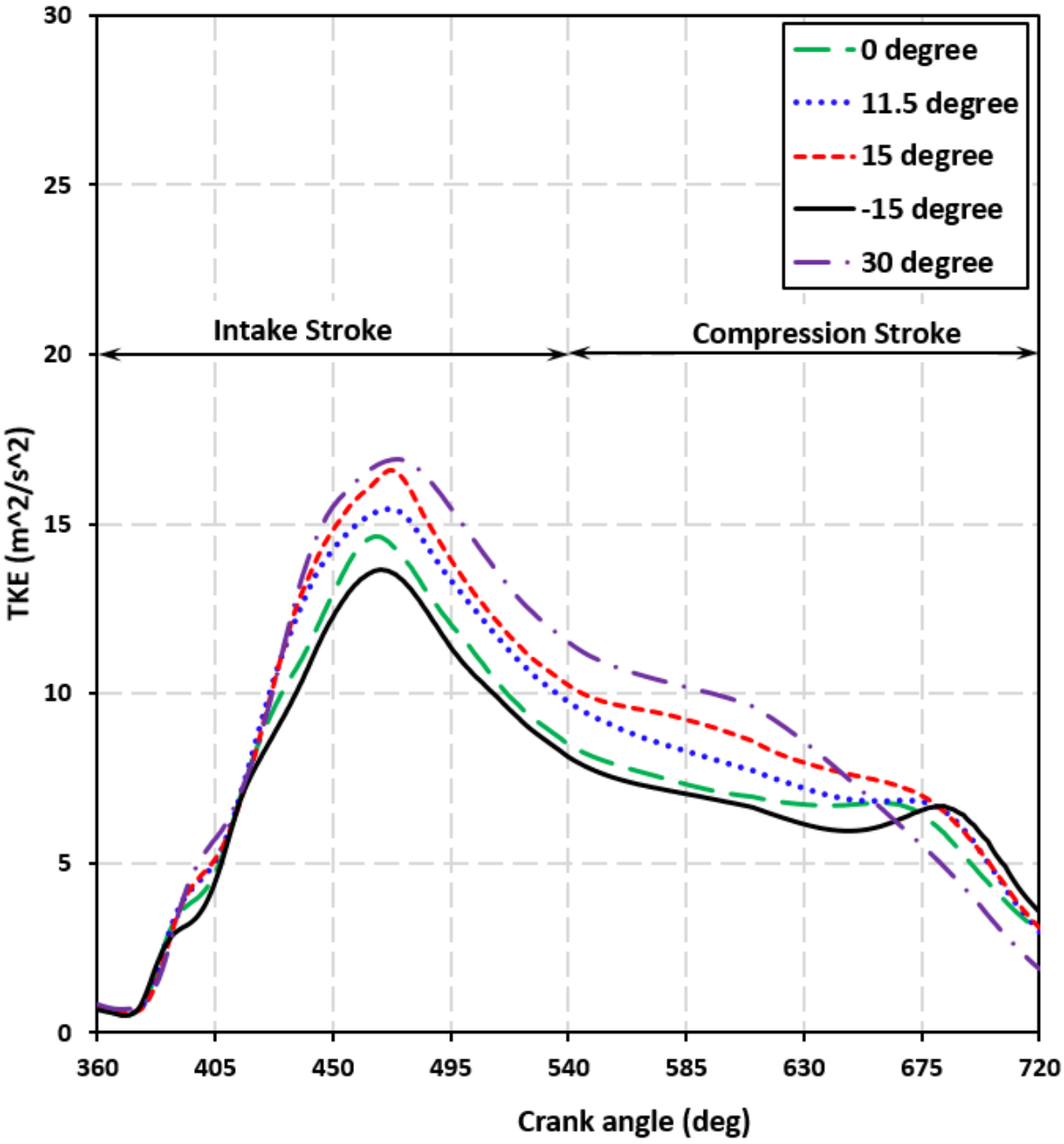

Fig. 6.7 In-cylinder TKE at various intake port inclination

6.3.4. Air Mass

Comparison of air mass in the cylinder versus the crank angle with a pressure drop of 300 mmH_2O under motoring conditions with variations in the inclination of the intake port is shown in Fig. 6.8. The mass of air that accumulates into the cylinder increases dramatically from the beginning to the end of the intake stroke around 540 ºCA and then during the compression stroke an attempt is made to stabilize. Changes in inclination from the intake port do not have much effect on changes in air mass during intake stroke. However, there is a

marginal effect of changes in the inclination of the intake port on the accumulation of air mass during the compression stroke after the image is enlarged. The intake port with 0º reaches the maximum value of the accumulated air mass of 0.000168059 kg or an increase of 1.99% compared to the original intake port. While intake ports with 30º, 15º, -15º also experienced similar increases of 1.94%, 1.37% and 1.20% respectively. This increase may be due to the inertia of air intake which is higher than the mass of air moving up close to the piston. Figure 12 also shows that the tendency of an increase in the intake port does not show a greater value than the mass of the incoming air. Similar results were also obtained by Ramesh and James [105] who conducted research using a large engine (86 mm x 86 mm). They also concluded that the mass of air that accumulates into the cylinder increases dramatically from the beginning to the end of the intake stroke around 540 ºCA and then during the compression stroke an attempt is made to stabilize. It's just that the mass of air that enters a large engine is greater than a small motorcycle engine due to the effect of its size.

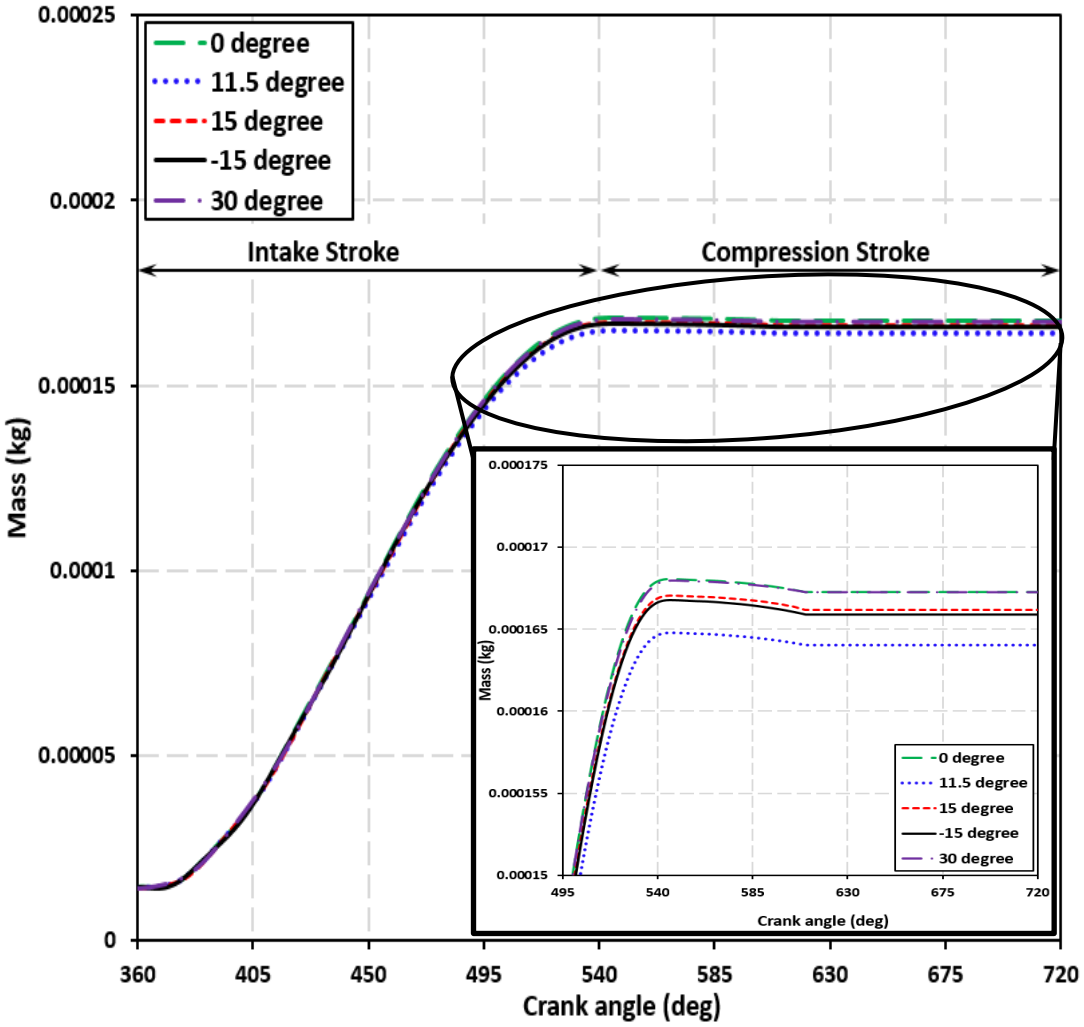

Fig. 6.8 In-cylinder air mass at various intake port inclination

6.3.5. Turbulent length scale

The turbulence length scale is one of important parameter for estimating the inlet turbulence characteristics in the numerical process. The length scale was able to predict the physical quantity of a large eddy that is loaded with energy. Each eddy scale is suitable for a certain length of turbulence scale. One of the standard eddy scales used is the integral length scale. In this study the turbulent length scale was estimated using an integral length scale. Comparison of the turbulent length scale versus the crank angle at a pressure drops of 300 mmH_2O under motoring conditions with various of the intake port inclination is shown in Fig. 6.9. In Fig. 6.9, it appears that there is no significant change in the length scale at the early of the intake stroke process up to 450 °CA. Then, there was a significant increase until it peaked at 596.5 °CA when the intake valve closes fully. Then decreases sharply until the compression stroke was complete. This process occurs in all intake port models with various inclination variations. In general, the level of dissipation is very influential on the turbulent length scale. For example, small turbulent length scales show large dissipation rates.

This is due to an increase in flow to counter the action of viscous stress. This results in an increase in the rate of dissipation. Based on Fig. 6.9, it seems that the inclination of the intake port does not significantly affect the turbulent length scale from the initial intake stage to 500 °CA and the middle until end process of the compression stroke. While an increase in the length scale from 500 °CA to 650 °CA. The largest length scale occurs at its peak at the intake port with 30º of 0.00095 m or an increase of 4.65% compared to the original intake port with 11.5º. Similar increases also occurred in intake ports with -15º of 2.40% compared to the original intake port with 11.5º. This increase occurred at 596.5 °CA when the inlet valve closed completely. As the scale length increases, the dissipation rate tends to decrease as less workflow is undertaken to counter the action of viscous stresses. Meanwhile, the decrease in length scale occurred at the intake port with 15º and 0º by 1.19% and 2.54%, respectively. Similar results were also found in a study conducted by Micklow and Gong [109] who used a large engine with a bore stroke of 137.6 mm x 165.1 mm where there was a slight increase from the start of the intake stroke to the middle of the intake stroke and increased significantly until the intake valve was closed automatically. full. The next process is a significant decrease until the end of the compression stroke. From these results it can be concluded that the difference in engine size has no effect on changes in length scale. It's just that changes to the intake port inclination modification slightly affect the length scale when the intake valve is

fully closed. This phenomenon needs attention because the length scale is an important parameter in determining turbulence. As the scale length increases, the dissipation rate tends to decrease as less workflow is done to counter the action of viscous stresses.

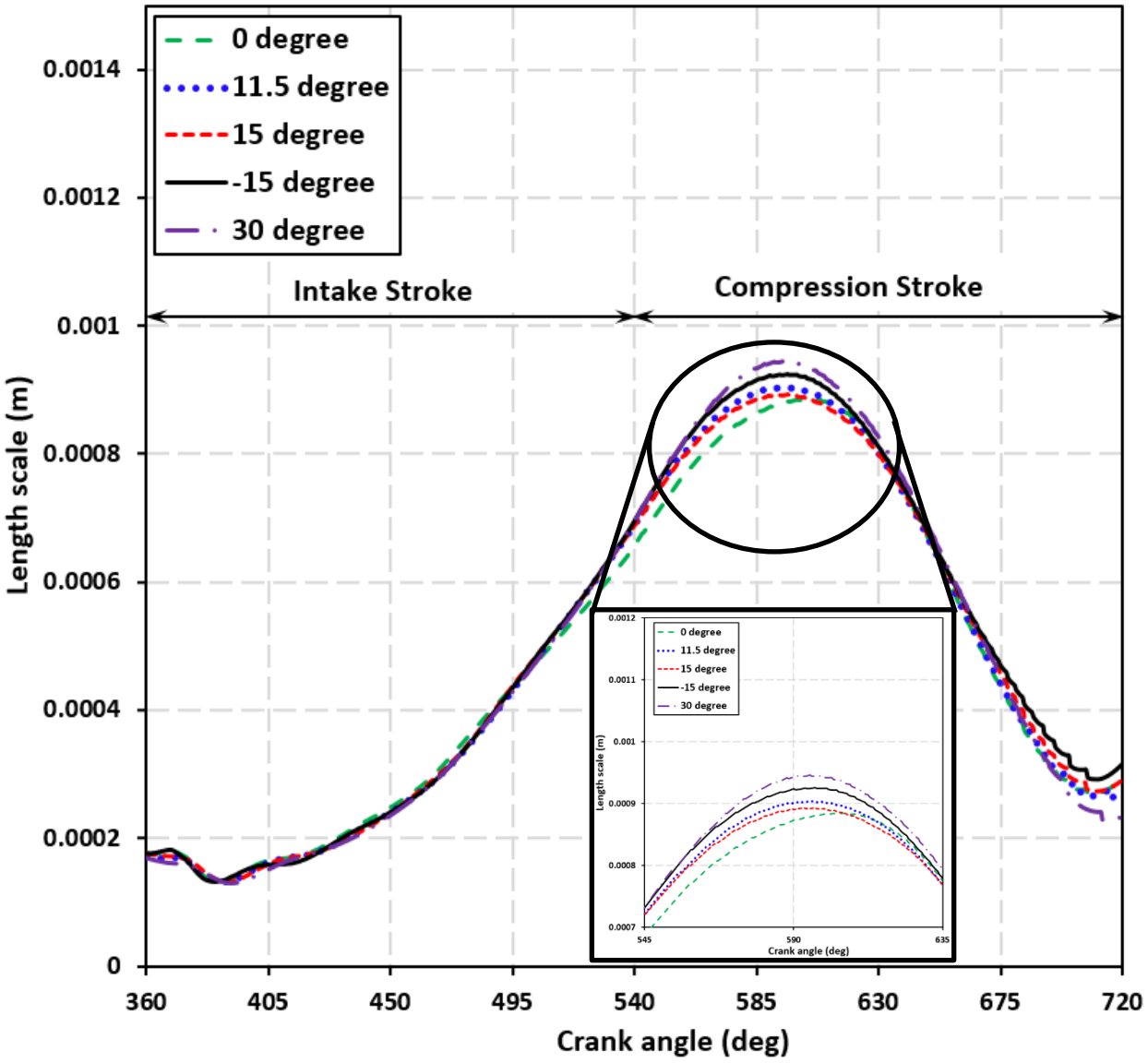

Fig. 6.9 In-cylinder length scale at various intake port inclination

6.3.6. Turbulent Kinematic Viscosity

This is a parameter for measuring inertia and fluid viscosity. This is a parameter when occurs a small vortex in the flow where the eddy momentum flux can work well. However, this is not useful when a large scales vortex occurs. Comparison of turbulent kinematic viscosity with crank angle for 300 mmH_2O pressure drop under motoring condition with the inclination variation of the intake port is shown in Fig. 6.10.

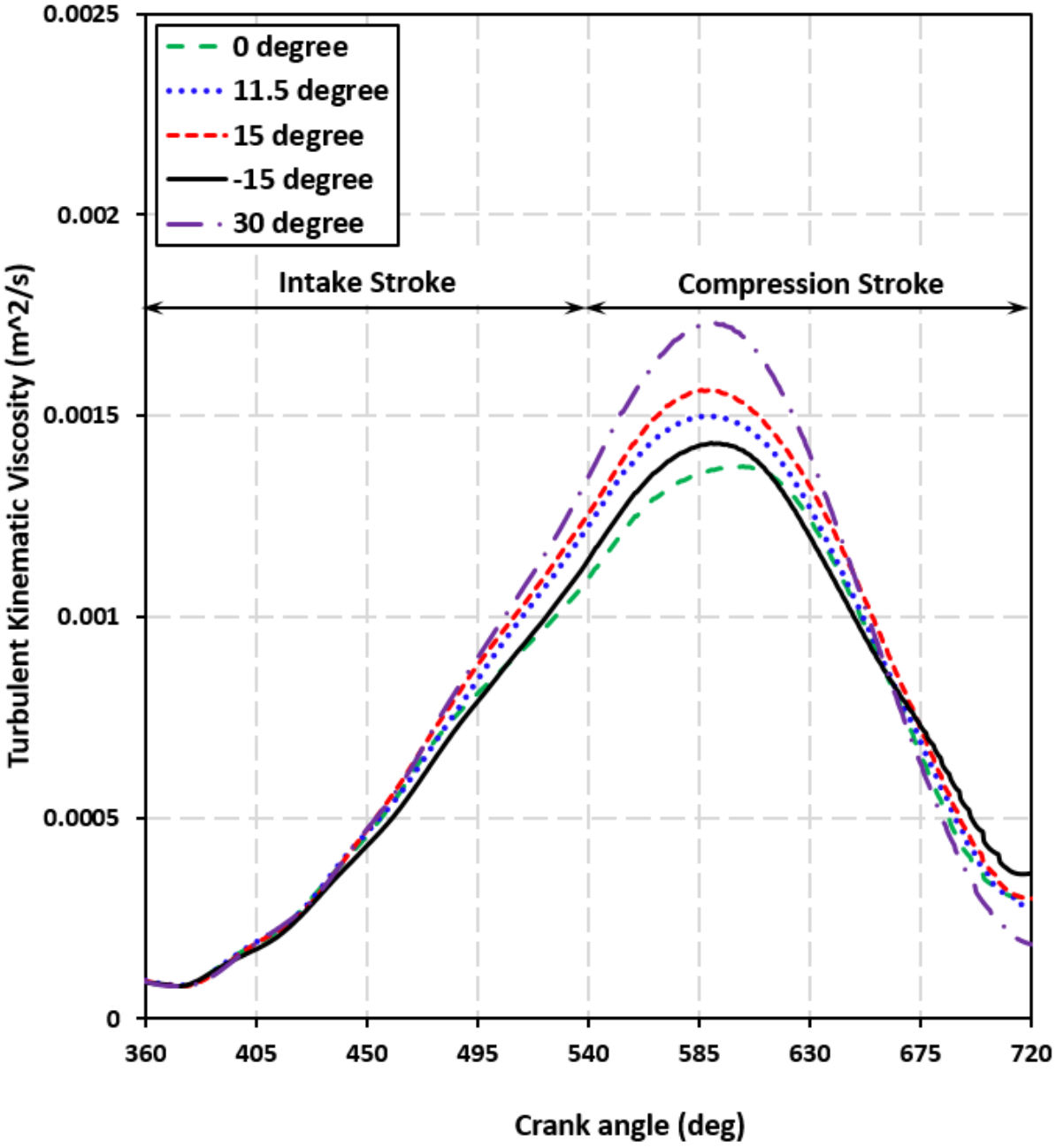

Fig. 6.10 In-cylinder of turbulent kinematic viscosity at various intake port inclination

Fig. 6.10 show that there is no significant change from this parameter at the early stage of the intake stroke until 400 °CA. However, a significant increase occurred after that point until it peaked at 590 °CA. Even this process does not last long because it immediately decreases significantly until the compression process ended. The same thing happens to all intake port models with various inclination both in the intake and compression stroke. There is no significant effect with the change in the inclination of the intake port to this parameter especially at the beginning of the intake step to 440 °CA, where the valve lift is opened

maximum. However, changes in turbulent kinematic viscosity occur after this point where the valve lift closes again. The greatest turbulent kinematic viscosity occurs at 590 °CA at the intake port with 30º where the intake port of this model has turbulent kinematic viscosity of 0.00173 m2/s or 15.25% greater than the turbulent kinematic viscosity at the original intake port of 11.5º. The increase also occurred at intake ports 15º by 4.29%. However, the decrease in turbulent kinematic viscosity occurred at the intake port with -15º and 0º by 4.49% and 8.98%, respectively. It appears from Fig. 14 that the intake port with 30º has the greatest turbulent kinematic viscosity which is probably because the intake port with 30º was able to produce more small eddies in the cylinder. This is confirmed by Figures 7 and 8. Another factor that can increase this parameter is the process of closing the valve and piston movement because in both processes will produce more small vortices in the cylinder which causes an enhancement in turbulent kinematic viscosity.

6.4 Summary

This study aimed to analyze numerically and experimentally the results of the in-cylinder flow of small motorcycle engines using steady flow benches based on the variation of the intake port inclination. The variation of intake port inclination is -15º, 0º, 11.5º(original), 15º and 30º. In addition, this study also investigating variations inflow motion in-cylinder engine in both horizontal and vertical planes on all variations of the intake port inclination. Moreover, this study also aimed to investigate the influence of the variation of the intake port inclination on the characteristics of the airflow in-cylinder which is carried out in small motorcycle engines under motoring conditions. Seeing the results, this study suggests the following conclusions:

1. There is a good agreement between the experiment results of steady flow bench and simulations results of the flow coefficients and air flow rates at various inclination of the intake port.

2. In horizontal and vertical planes, changes in the inclination of the intake port result in changes in flow velocity.

3. The change of intake port inclination gives effect to be an irregular shape at swirl ratio.

4. The bigger the inclination of intake port the smaller of the tumble ratio. The maximum increase occurred in the intake port with -15º at the first peak of 8.07% and the second peak of 12.01% than the original one.

5. The change in inclination at the intake port has the effect to change turbulent kinetic energy, length scale and turbulent kinematic viscosity where the maximum increases occur at the intake port with 30º with 9.55%, 4.65% and 15.25% respectively compared to the original intake port.

6. Based on this case study, the intake port with 30º is the most optimal intake port compared to other models where the intake port has a better increase in vortices compared to other models which results in increased turbulence in the cylinder.

7. Increased turbulence results in a more homogeneous mixing of air-fuel in cylinder engine.

7. SUMMARY AND CONCLUSIONS

A combined numerical and experimental study has been carried out to improve the characteristic of the flow field generated inside a 4 valve cylinder head of a small motorcycle engine under steady-state conditions. There are at least three steps that will be carried out in this study. Firstly, a steady-state flow bench measurements and a computational fluid dynamic (CFD) simulations have been used to investigate the flow characteristic on a single-cylinder of an original small motorcycles engine with a pent-roof head for a number of fixed valves lift at two pressure drops of 300 and 600 mmH_2O, equivalent to engine speeds of 3200 and 4600 rpm respectively. Secondly, to improve the flow characteristic of this small motorcycle engine, the modification of intake port with the variation of flow direction was designed. The modification of this intake port such as a helical intake port with the same direction, helical intake port with the opposite direction (inward), and the helical intake port with the opposite direction (outward) and the tangential intake port. The last but not the least, to more get results, the modification of intake port was developed with a variation of inclination angle based on the second step. The variation of intake port inclination is -15º, 0º, 15º and 30º. These intake port models will be compared with the original intake port (11.5º). The following conclusions are drawn from the results:

- There was a good agreement achieved between the experiment result in steady-state flow benches and simulation result of the air flow rate, flow coefficient and coefficient of discharge at 300 and 600 mmH_2O pressure drop. The modification of the intake port based on the inclination angle gives increase in some flow coefficient compared to the original intake port such as intake port with 15º and 30º of 2.46% and 6% respevtively. However, the flow coefficient for intake port with -15º and 0º decrease compared to the original intake port of 10.54% and 6.45% respevtively. On the other hand, the change in the shape of the intake port with variations in flow direction with helical port models in all models also decreased by 60.69% (helical intake port with the opposite direction (inward)), 58.96% (helical intake port with the opposite direction (outward)) and 62.27% (helical intake port with the same direction) compared to the original intake port.

- It was found that as pressure drop increases, the flow structures remain of similar orientation, however, the magnitude of the velocities within these flow structures is

increased and the vortex core found to move closer to the cylinder axis both in horizontal and vertical plane.

- In the horizontal and vertical planes, the flow patterns of all intake port models have a similar trend where the valve lift is greater, the flow pattern will be more varies and the flow velocity will also increase. However, the tangential intake port model has the greatest flow velocity compared to all helical intake port models. The tangential model with all inclination angle model has same flow velocity maximum of 60 m/s in the center of cylinder at the horizontal plane. However, the intake port with 30º and 15º have the high velocity magnitude in the side of cylinder. Moreover, the intake port model with 30º has a more even distribution of velocity magnitude in all directions compared to other intake port models. In the vertical plane, the greatest flow velocity occurs at the 6.46 mm valve lift at intake port 30º and 15º at 78.5 m/s on the upper side of the cylinder near the intake port and 31.4 m/s at the center of the cylinder. When compared with the original intake port with 11.5º, the flow velocity at the intake port 30º and 15º increases by 1.95% on the upper side of the cylinder near the intake port and the center of the cylinder. However, intake ports with 30º in general the distribution of flow velocity are higher in all areas in the cylinder than intake ports with 15º. The greater the flow velocity of an area shows increased turbulence in this area. Increased turbulence results in a more homogeneous mixing of air fuel in cylinder.

- The increase of pressure drops in the small motorcycle engine caused the swirl flow to be irregular shape during the intake stroke, until 495 °CA. However, the swirl flow had a trend of being stable and almost constant at the beginning of the compression stroke and increasing again in the end of the compression stroke. The same trend also occurs in the modification of the inclination angle of the intake port.

- The increase of pressure drop on the small motorcycle engine at the beginning of the intake stroke until the end of compression stroke has no significant effect on the tumble ratio. However, the change in intake port modification gives a significant effect on the tumble ratio where the helical intake port with the same direction has the highest tumble peak compared to other models at 460 °CA. Nevertheless, there was a significant decrease to the second peak of 56.25%. The same thing did not happen to the intake port with tangential models which only decreased 18.75% to the second peak. Moreover,

the change in the inclination of the intake port has a significant effect on the change in tumble ratio. The bigger the inclination of intake port the smaller of the tumble ratio.

- The increasing of pressure drop does not have a significant effect on the process of the TKE formation. However, the effect that occurred regards the maximum value of the peak of TKE, the highest value of around 200 % at 470 °CA at 600 mmH_2O. This may be because when the pressure drops increased from 300 to 600 mmH_2O, it caused a significant increase in the inlet air velocity in the cylinder engine. The same trend also occurred at the modification of intake port where the tangential intake port model with 30º increase 9.55% of TKE peak compared to the original models.

- The increasing of pressure drops gives a significant effect on turbulent length scale and turbulent kinematic viscosity and these two parameters have similarity trend where the biggest increase occurred at around 590 ºCA where the intake valve was almost closed. It may be because at that position the piston moves to TDC so that more vortices are formed and result in length scale and eddy viscosity increases significantly. The same trend happened when there was a modification of the intake port model where the change in inclination at the intake port has the effect to change length scale and turbulent kinematic viscosity where the maximum increases occur at the intake port with 30º with 4.65% and 15.25% respectively compared to the original intake port.

- Based on this case study, the tangential intake port with 30º is the most optimal intake port compared to other models where the intake port has a better increase in vortices compared to other models which results in increased turbulence in the cylinder.

REFERENCES

[1] Yilmaz N, Vigil FM, Benalil K, Davis SM, Calva A. Effect of biodiesel–butanol fuel blends on emissions and performance characteristics of a diesel engine. Fuel 2014;135:46–50.

[2] Tan P, Hu Z, Lou D, Li Z. Exhaust emissions from a light-duty diesel engine with Jatropha biodiesel fuel. Energy 2012;39:356–62.

[3] Swaminathan C, Sarangan J. Performance and exhaust emission characteristics of a CI engine fueled with biodiesel (fish oil) with DEE as additive. Biomass and Bioenergy 2012;39:168–74.

[4] Saravanan S. Effect of exhaust gas recirculation (EGR) on performance and emissions of a constant speed DI diesel engine fueled with pentanol/diesel blends. Fuel 2015;160:217–26.

[5] Özener O, Yüksek L, Ergenç AT, Özkan M. Effects of soybean biodiesel on a DI diesel engine performance, emission and combustion characteristics. Fuel 2014;115:875–83.

[6] Mohan B, Yang W, kiang Chou S. Fuel injection strategies for performance improvement and emissions reduction in compression ignition engines—A review. Renewable and Sustainable Energy Reviews 2013;28:664–76.

[7] Bayindirli C, Celik M. Investigation of combustion and emission characteristics of n-hexane and n-hexadecane additives in diesel fuel. Journal of Mechanical Science and Technology 2019;33:1937–46. https://doi.org/10.1007/s12206-019-0344-8.

[8] Mirzajanzadeh M, Tabatabaei M, Ardjmand M, Rashidi A, Ghobadian B, Barkhi M, et al. A novel soluble nano-catalysts in diesel–biodiesel fuel blends to improve diesel engines performance and reduce exhaust emissions. Fuel 2015;139:374–82.

[9] Gumus M, Sayin C, Canakci M. The impact of fuel injection pressure on the exhaust emissions of a direct injection diesel engine fueled with biodiesel–diesel fuel blends. Fuel 2012;95:486–94.

[10] Atabani AE, Silitonga AS, Ong HC, Mahlia TMI, Masjuki HH, Badruddin IA, et al. Non-edible vegetable oils: a critical evaluation of oil extraction, fatty acid compositions, biodiesel production, characteristics, engine performance and emissions production. Renewable and Sustainable Energy Reviews 2013;18:211–45.

[11] Thongchai S, Lim O. Investigation of the combustion characteristics of gasoline compression ignition engine fueled with gasoline-biodiesel blends. Journal of

Mechanical Science and Technology 2018;32:959–67. https://doi.org/10.1007/s12206-018-0146-9.

[12] Krishnamoorthi M, Malayalamurthi R. The influence of charge air temperature and exhaust gas recirculation on the availability analysis, performance and emission behavior of diesel - bael oil - diethyl ether blend operated diesel engine. Journal of Mechanical Science and Technology 2018;32:1835–47. https://doi.org/10.1007/s12206-018-0340-4.

[13] Costa RC, Sodré JR. Compression ratio effects on an ethanol/gasoline fuelled engine performance. Applied Thermal Engineering 2011;31:278–83.

[14] Ishiyama T, Kang J, Ozawa Y, Sako T. Improvement of performance and reduction of exhaust emissions by pilot-fuel-injection control in a lean-burning natural-gas dual-fuel engine. SAE International Journal of Fuels and Lubricants 2012;5:243–53.

[15] Yadollahi B, Boroomand M. The effect of combustion chamber geometry on injection and mixture preparation in a CNG direct injection SI engine. Fuel 2013;107:52–62.

[16] Raj ARGS, Mallikarjuna JM, Ganesan V. Energy efficient piston configuration for effective air motion–A CFD study. Applied Energy 2013;102:347–54.

[17] Naeimi H, Ganji DD, Gorji M, Javadirad G, Keshavarz M. A parametric design of compact exhaust manifold junction in heavy duty diesel engine using computational fluid dynamics codes. Thermal Science 2011;15:1023–33.

[18] Cui L, Wang T, Lu Z, Jia M, Sun Y. Full-Parameter approach for the intake port design of a four-valve direct-injection gasoline engine. Journal of Engineering for Gas Turbines and Power 2015;137:91502.

[19] Wheeler J, Polovina D, Ramanathan S, Roth K, Manning D, Stein J. Increasing EGR Tolerance using High Tumble in a Modern GTDI Engine for Improved Low-Speed Performance. SAE Technical Paper; 2013.

[20] Zhang Z, Zhang H, Wang T, Jia M. Effects of tumble combined with EGR (exhaust gas recirculation) on the combustion and emissions in a spark ignition engine at part loads. Energy 2014;65:18–24. https://doi.org/10.1016/j.energy.2013.11.062.

[21] Olsson J-O, Tunestål P, Ulfvik J, Johansson B. The effect of cooled EGR on emissions and performance of a turbocharged HCCI engine. Society of Automotive Engineers 2003;2003:21–38. https://doi.org/10.4271/2003-01-0743.

[22] Sjöberg M, Dec JE. EGR and Intake Boost for Managing HCCI Low-Temperature Heat Release over Wide Ranges of Engine Speed 2007:776–90. https://doi.org/10.4271/2007-

01-0051.

[23] Yao M, Chen Z, Zheng Z, Zhang B, Xing Y. Effect of EGR on HCCI Combustion fuelled with Dimethyl Ether (DME) and Methanol Dual-Fuels. SAE Technical Paper, 2005;2005-01–37. https://doi.org/10.4271/2005-01-3730.

[24] de Souza GR, de Castro Pellegrini C, Ferreira SL, Pau FS, Armas O. Study of intake manifolds of an internal combustion engine: A new geometry based on experimental results and numerical simulations. Thermal Science and Engineering Progress 2019;9:248–58.

[25] Cui H, Li M, Han Y. The Steady Flow Test and CFD Numerical Simulation on Improving Research of Locomotive Diesel Engine Helical Intake Port. 2010 WASE International Conference on Information Engineering, vol. 4, IEEE; 2010, p. 255–9.

[26] Kumano K, Yamasaki Y, Iida N. An investigation of the effect of charge inhomogeneity on the ignition and combustion processes in a HCCI engine using chemiluminescence imaging. Journal of Thermal Science and Technology 2007;2:200–11.

[27] Qi YL, Dong LC, Liu H, Puzinauskas P V, Midkiff KC. Optimization of intake port design for SI engine. International Journal of Automotive Technology 2012;13:861–72.

[28] Yang X, Kuo T-W, Guralp O, Grover RO, Najt P. In-Cylinder Flow Correlations Between Steady Flow Bench and Motored Engine Using Computational Fluid Dynamics. Journal of Engineering for Gas Turbines and Power 2017;139:72802.

[29] Huang RF, Lin KH, Yeh C-N, Lan J. In-cylinder tumble flows and performance of a motorcycle engine with circular and elliptic intake ports. Experiments in Fluids 2009;46:165–79.

[30] Adomeit P, Jakob M, Pischinger S, Brunn A, Ewald J. Effect of intake port design on the flow field stability of a gasoline DI engine. SAE Technical Paper; 2011.

[31] Jemni MA, Kantchev G, Abid MS. Influence of intake manifold design on in-cylinder flow and engine performances in a bus diesel engine converted to LPG gas fuelled, using CFD analyses and experimental investigations. Energy 2011;36:2701–15.

[32] Falfari S, Bianchi GM, Nuti L. Numerical comparative analysis of in-cylinder tumble flow structures in small PFI engines equipped by heads having different shapes and squish areas. ASME 2012 Internal Combustion Engine Division Spring Technical Conference, American Society of Mechanical Engineers Digital Collection; 2013, p. 715–25.

[33] Falfari S, Brusiani F, Pelloni P. 3D CFD analysis of the influence of some geometrical

engine parameters on small PFI engine performances–the effects on the tumble motion and the mean turbulent intensity distribution. Energy Procedia 2014;45:701–10.

[34] Kim Y, Han Y, Lee K. A study on the effects of the intake port configurations on the swirl flow generated in a small DI diesel engine. Journal of Thermal Science 2014;23:297–306.

[35] Rezaei R, Pischinger S, Ewald J, Adomeit P. Numerical investigation of the effect of swirl flow in-homogeneity and stability on diesel engine combustion and emissions. International Journal of Engine Research 2012;13:482–96.

[36] Wahono B, Setiawan A, Lim O. Experimental study and numerical simulation on in-cylinder flow of small motorcycle engine. Applied Energy 2019;255:113863.

[37] Rhie CM, Chow WL. Numerical study of the turbulent flow past an airfoil with trailing edge separation. AIAA Journal 1983;21:1525–32.

[38] Heywood J. Two-Stroke Cycle Engine: It's Development, Operation and Design. Routledge; 2017.

[39] Pulkrabek Willard W. Engineering fundamentals of internal combustion engine. 2nd ed. Pearson Prentice Hall; n.d.

[40] Heywood JB. Internal combustion engine fundamentals. McGraw-Hill New York; 1988.

[41] Localio D. 10 myths of cylinder head porting 2018. http://speed.academy/10-myths-of-cylinder-head-porting/ (accessed 6 April 2020).

[42] Özahi E, Çarpınlıoğlu MÖ, Gündoğdu MY. Simple methods for low speed calibration of hot-wire anemometers. Flow Measurement and Instrumentation 2010;21:166–70.

[43] Hultmark M, Smits AJ. Temperature corrections for constant temperature and constant current hot-wire anemometers. Measurement Science and Technology 2010;21:105404.

[44] Kiełbasa J. Measurement of gas flow velocity: Anemometer with a vibrating hot wire. Review of Scientific Instruments 2010;81:15101.

[45] Lomas CG. Fundamentals of hot wire anemometry. Cambridge University Press; 2011.

[46] Seffrin F, Fuest F, Geyer D, Dreizler A. Flow field studies of a new series of turbulent premixed stratified flames. Combustion and Flame 2010;157:384–96.

[47] Zhang Z. LDA application methods: laser Doppler anemometry for fluid dynamics. Springer Science & Business Media; 2010.

[48] Huisman SG, Van Gils DPM, Sun C. Applying laser Doppler anemometry inside a Taylor–Couette geometry using a ray-tracer to correct for curvature effects. European Journal of Mechanics-B/Fluids 2012;36:115–9.

[49] Kumara WAS, Elseth G, Halvorsen BM, Melaaen MC. Comparison of Particle Image Velocimetry and Laser Doppler Anemometry measurement methods applied to the oil–water flow in horizontal pipe. Flow Measurement and Instrumentation 2010;21:105–17.

[50] Anufriev IS, Anikin YA, Fil'kov AI, Loboda EL, Agafontseva M V, Kasymov DP, et al. Investigation into the structure of a swirling flow in a model of a vortex combustion chamber by laser doppler anemometry. Technical Physics Letters 2013;39:30–2.

[51] Spelter LE, Schirner J, Nirschl H. A novel approach for determining the flow patterns in centrifuges by means of Laser-Doppler-Anemometry. Chemical Engineering Science 2011;66:4020–8.

[52] Shah MS, Joshi JB, Kalsi AS, Prasad CSR, Shukla DS. Analysis of flow through an orifice meter: CFD simulation. Chemical Engineering Science 2012;71:300–9.

[53] Kaushal DR, Thinglas T, Tomita Y, Kuchii S, Tsukamoto H. CFD modeling for pipeline flow of fine particles at high concentration. International Journal of Multiphase Flow 2012;43:85–100.

[54] Liu H, Li P, Van Lew J. CFD study on flow distribution uniformity in fuel distributors having multiple structural bifurcations of flow channels. International Journal of Hydrogen Energy 2010;35:9186–98.

[55] Horvath A, Horvath Z. Application of CFD numerical simulation for intake port shape design of a diesel engine. Journal of Computational and Applied Mechanics 2003;4:129–46.

[56] Lee K, Lee C, Joo Y. Optimization of the intake port shape for a five-valve gasoline engine. Proceedings of the Institution of Mechanical Engineers, Part D: Journal of Automobile Engineering 2001;215:739–46.

[57] Yoshihara Y, Nakata K, Takahashi D, Omura T, Ota A. Development of High Tumble Intake-Port for High Thermal Efficiency Engines. SAE Technical Paper; 2016.

[58] Ye Y, Yin C-B, Li X-D, Zhou W, Yuan F. Effects of groove shape of notch on the flow characteristics of spool valve. Energy Conversion and Management 2014;86:1091–101.

[59] Modiyani R, Kocher L, Van Alstine DG, Koeberlein E, Stricker K, Meckl P, et al. Effect of intake valve closure modulation on effective compression ratio and gas exchange in turbocharged multi-cylinder engines utilizing EGR. International Journal of Engine Research 2011;12:617–31.

[60] Qin W, Xie M, Jia M, Wang T, Liu D. Large eddy simulation and proper orthogonal decomposition analysis of turbulent flows in a direct injection spark ignition engine:

Cyclic variation and effect of valve lift. Science China Technological Sciences 2014;57:489–504.

[61] Wang T, Liu D, Tan B, Wang G, Peng Z. An investigation into in-cylinder tumble flow characteristics with variable valve lift in a gasoline engine. Flow, Turbulence and Combustion 2015;94:285–304.

[62] Blair GP, Callender E, Mackey DO. Maps of discharge coefficients for valves, ports and throttles. SAE Technical Paper; 2001.

[63] Mahrous AFM, Wyszynski ML, Wilson T, Xu HM. Computational fluid dynamics simulation of in-cylinder flows in a motored homogeneous charge compression ignition engine cylinder with variable negative valve overlapping. Proceedings of the Institution of Mechanical Engineers, Part D: Journal of Automobile Engineering 2007;221:1295–304.

[64] Khalighi B. Study of the intake tumble motion by flow visualization and particle tracking velocimetry. Experiments in Fluids 1991;10:230–6.

[65] Li Y, Zhao H, Ma T. Flow and mixture optimization for a fuel stratification engine using PIV and PLIF techniques. Journal of Physics: Conference Series, vol. 45, IOP Publishing; 2006, p. 59.

[66] Richards KJ, Senecal PK, Pomraning E. Converge (v2. 3.21). Theory Manual, Convergent Science, Madison, WI 2017.

[67] Han Z, Reitz RD. Turbulence modeling of internal combustion engines using RNG κ-ε models. Combustion Science and Technology 1995;106:267–95.

[68] Claudio F, Cristian C, Giulio C, Marco BG, Stefania F, Federico B, et al. Numerical evaluation of the applicability of steady test bench swirl ratios to diesel engine dynamic conditions. Energy Procedia 2015;81:732–41.

[69] Gürbüz H, Akçay IH, Buran D. An investigation on effect of in-cylinder swirl flow on performance, combustion and cyclic variations in hydrogen fuelled spark ignition engine. Journal of the Energy Institute 2014;87:1–10. https://doi.org/10.1016/j.joei.2012.03.001.

[70] Bharathi VVP, Prasanthi G. Influence of in cylinder air swirl on diesel engine performance and emission. International Journal of Applied Engineering and Technology 2011;1:113–8.

[71] Bari S, Saad I. CFD modelling of the effect of guide vane swirl and tumble device to generate better in-cylinder air flow in a CI engine fuelled by biodiesel. Computers &

Fluids 2013;84:262–9.

[72] Stansfield P, Wigley G, Justham T, Catto J, Pitcher G. PIV analysis of in-cylinder flow structures over a range of realistic engine speeds. Experiments in Fluids 2007;43:135–46.

[73] Vucinic D, Hazarika BK, Dinescu C. Visualization and PIV Measurements of In-Cylinder Axisymmetric Flows. SAE Technical Paper; 2001.

[74] Lumley JL. Engines: an introduction. Cambridge University Press; 1999.

[75] Wang T, Li W, Jia M, Liu D, Qin W, Zhang X. Large-eddy simulation of in-cylinder flow in a DISI engine with charge motion control valve: Proper orthogonal decomposition analysis and cyclic variation. Applied Thermal Engineering 2015;75:561–74.

[76] Li Y, Zhao H, Peng Z, Ladommatos N. Analysis of tumble and swirl motions in a four-valve SI engine. SAE Technical Paper, SAE International; 2001. https://doi.org/10.4271/2001-01-3555.

[77] Li Y, Zhao H, Leach B, Ma T, Ladommatos N. Characterization of an in-cylinder flow structure in a high-tumble spark ignition engine. International Journal of Engine Research 2004;5:375–400.

[78] Kang KY, Baek JH. Turbulence characteristics of tumble flow in a four-valve engine. Experimental Thermal and Fluid Science 1998;18:231–43.

[79] Baby X, Floch A. Investigation of the in-cylinder tumble motion in a multi-valve engine: effect of the piston shape. SAE Technical Paper; 1997.

[80] Huang RF, Huang CW, Chang SB, Yang HS, Lin TW, Hsu WY. Topological flow evolutions in cylinder of a motored engine during intake and compression strokes. Journal of Fluids and Structures 2005;20:105–27.

[81] Hill PG, Zhang D. The effects of swirl and tumble on combustion in spark-ignition engines. Progress in Energy and Combustion Science 1994;20:373–429. https://doi.org/10.1016/0360-1285(94)90010-8.

[82] Ismail AR, Bakar RA, Semin. An investigation of valve lift effect on air flow and coefficient of discharge of four stroke engines based on experiment. American Journal of Applied Sciences 2008;5:963–71.

[83] Bertsch M, Schreer K, Disch C, Beck KW, Spicher U. Investigation of the Flow Velocity in the Spark Plug Gap of a Two-Stroke Gasoline Engine using Laser-Doppler-Anemometry. SAE International Journal of Engines 2012;5:34–41.

[84] Westerweel J, Elsinga GE, Adrian RJ. Particle image velocimetry for complex and turbulent flows. Annual Review of Fluid Mechanics 2013;45:409–36.

[85] Jainski C, Lu L, Dreizler A, Sick V. High-speed micro particle image velocimetry studies of boundary-layer flows in a direct-injection engine. International Journal of Engine Research 2013;14:247–59.

[86] El-Adawy M, Heikal MR, Aziz ARA, Siddiqui MI, Wahhab HAA. Experimental study on an IC engine in-cylinder flow using different steady-state flow benches. Alexandria Engineering Journal 2017;56:727–36.

[87] Mohammadebrahim A, Shafii MB, Hannani SK. The Effect of Various Test Parameters on the Steady Flow Test Results of a Four-Valve Spark Ignition Engine: A Tentative Approach toward Standardization. Advances in Mechanical Engineering 2013;5:482317.

[88] Gafoor CPA, Gupta R. Numerical investigation of piston bowl geometry and swirl ratio on emission from diesel engines. Energy Conversion and Management 2015;101:541–51.

[89] Sharma CS, Anand TNC, Ravikrishna R V. A methodology for analysis of diesel engine in-cylinder flow and combustion. Progress in Computational Fluid Dynamics, an International Journal 2010;10:157–67.

[90] Wu C, Deng K, Wang Z. The effect of combustion chamber shape on cylinder flow and lean combustion process in a large bore spark-ignition CNG engine. Journal of the Energy Institute 2016;89:240–7.

[91] Perini F, Miles PC, Reitz RD. A comprehensive modeling study of in-cylinder fluid flows in a high-swirl, light-duty optical diesel engine. Computers & Fluids 2014;105:113–24.

[92] Krishna AS, Mallikarjuna JM, Davinder K, Babu YR. In-Cylinder Flow Analysis in a Two-Stroke Engine-A Comparison of Different Turbulence Models Using CFD. SAE Technical Paper; 2013.

[93] Payri F, Benajes J, Margot X, Gil A. CFD modeling of the in-cylinder flow in direct-injection Diesel engines. Computers & Fluids 2004;33:995–1021.

[94] Fang T, Singh S. Predictions of Flow Separation at the Valve Seat for Steady-State Port-Flow Simulation. Journal of Engineering for Gas Turbines and Power 2015;137:111512.

[95] Senecal PK, Pomraning E, Richards KJ, Som S. Grid-convergent spray models for internal combustion engine CFD simulations. ASME 2012 Internal Combustion Engine

Division Fall Technical Conference, American Society of Mechanical Engineers; 2012, p. 697–710.

[96] Addepalli KS, Mallikarjuna JM. Effect of Engine Parameters on Mixture Stratification in a Wall-Guided GDI Engine-A Quantitative CFD Analysis. SAE International Journal of Commercial Vehicles 2017;10:562–71.

[97] Bella G, De Maio A, Grimaldi CN. Flow characterization of a high performance SI engine intake system-part 2: Numerical analysis. SAE Technical Paper; 2003.

[98] Nomura T, Takahashi Y, Ishima T, Obokata T. LDA and PIV measurements and numerical simulation on in-cylinder flow under steady state flow condition. 12th International Symposium on Applications of Laser Techniques to Fluid Mechanics, Lisbon, Portugal, 2004, p. 1–17.

[99] Choi W, Choi B-C, Park H-K, Joo K-J, Lee J-H. In-cylinder flow field analysis of a single cylinder DI diesel engine using PIV and CFD. SAE Technical Paper; 2003.

[100] Rabault J, Vernet JA, Lindgren B, Alfredsson PH. A study using PIV of the intake flow in a diesel engine cylinder. International Journal of Heat and Fluid Flow 2016;62:56–67.

[101] Binjuwair S, Ibrahim S. Numerical Analysis of Flow Structure inside a Single Cylinder of a 4 Valve Head under Steady-State Condition. SAE Technical Paper; 2013.

[102] Yang X, Chen Z, Kuo T-W. Pitfalls for accurate steady-state port flow simulations. Journal of Engineering for Gas Turbines and Power 2013;135:61601.

[103] Saad I, Bari S. Guide vane swirl and tumble device to improve in-cylinder air flow of CI engine using vegetable oil. Procedia Engineering 2014;90:425–30.

[104] Xu H. Some critical technical issues on the steady flow testing of cylinder heads. SAE Technical Paper; 2001.

[105] Ramesh P, Gunasekaran J. Investigation of Flow Field Pattern in a GDI Engine at Different Speeds using Numerical Techniques. SAE Technical Paper; 2013.

[106] Addepalli SK, Mallikarjuna JM. Parametric analysis of a 4-stroke GDI engine using CFD. Alexandria Engineering Journal 2018;57:23–34.

[107] Pope SB. Turbulent Flows, 771 pp 2000.

[108] Aleiferis PG, Behringer MK, Malcolm JS. Integral length scales and time scales of turbulence in an optical spark-ignition engine. Flow, Turbulence and Combustion 2017;98:523–77.

[109] Micklow GJ, Gong WD. Intake and in-cylinder flowfield modelling of a four-valve

diesel engine. Proceedings of the Institution of Mechanical Engineers, Part D: Journal of Automobile Engineering 2007;221:1425–40.

[110] Ramajo DE, Nigro NM. Numerical and experimental in-cylinder flow study in a 4-valve spark ignition engine. Mecánica Computacional 2008;27:181–205.

[111] Binjuwair S, Ibrahim S, Wigley G, Pitcher G. In-Cylinder Flow Structure Analysis by Particle Image Velocimetry Under Steady State Condition. SAE Technical Paper; 2012.

[112] Toh HT, Huang RF, Lin KH, Chern M-J. Computational study on the effect of inlet port configuration on in-cylinder flow of a motored four-valve internal combustion engine. Journal of Energy Engineering 2011;137:198–206.

[113] Haworth DC, El Tahry SH, Huebler MS, Chang S. Multidimensional port-and-cylinder flow calculations for two-and four-valve-per-cylinder engines: influence of intake configuration on flow structure. SAE Transactions 1990:647–78.

[114] Trigui N, Kent JC, Guezennec Y, Guezennec YG, Choi W-C. Characterization of intake generated fluid flow fields in IC engines using 3-D Particle Tracking Velocimetry (3-D PTV). SAE Transactions 1994:331–42.

APPENDICES

A. LIST OF PUBLICATIONS

1. **Bambang Wahono**, Ardhika Setiawan, Ocktaeck Lim, "Experimental study and numerical simulation on in-cylinder flow of small motorcycle engine", ***Applied Energy, Elsevier***, Volume 255, pp 113863, 2019. (**SCI)**
2. **Bambang Wahono,** Yanuandri Putrasari and Ocktaeck Lim, "A study on in-cylinder flow field of a 125cc motorcycle engine at low engine speeds, ***Journal of Mechanical Science and Technology, Springer***, Volume 33, Issue 9, pp 4477-4494, 2019. (**SCIE)**
3. **Bambang Wahono**, Ardhika Setiawan, Ocktaeck Lim, "The study of the Effect of Intake Port Inclination on In-Cylinder Flow of Small Motorcycle Engine Using Numerical Simulation and Experimental Investigations", ***Applied Energy, Elsevier, under review after revised*** *(Status date 2020-10-30).* (**SCI)**
4. **Bambang Wahono**, Ardhika Setiawan, Ocktaeck Lim, "Effect of the Intake Port Flow Direction on the Stability and Characteristics of the In-Cylinder Flow Field of a Small Motorcycle Engine", ***Applied Energy, Elsevier***, ***under review*** *(Status date 2020-10-27).* (**SCI)**
5. **Bambang Wahono**, Kyeonghun Jwa, Ocktaeck Lim, "A Study on In-Cylinder Flow of Small motorcycle engine Using Steady-State Flow Benches", ***Energy Procedia, Elsevier***, Volume 158, pp 1856-1862, 2019. (**SCOPUS)**
6. **Bambang Wahono,** Yanuandri Putrasari, Ocktaeck Lim, "Construction of Response Surface Model for Compression Ignition Engine Using Stepwise Method", ***The Korean Hydrogen & New Energy Society***, Volume 28, No. 1, pp. 98~105, 2017. (**KCI)**
7. **Bambang Wahono**, Ocktaeck Lim, "Effect of various design of intake port to improve the engine performance using various methods: a review", ***Applied Thermal Engineering, Elsevier***, *will be submitted (Status date 2020-11-07).* (**SCIE)**
8. **Bambang Wahono**, Ardhika Setiawan, Ocktaeck Lim, Achmad Praptijanto, Yanuandri Putrasari, "Study on the Effect of the Intake Port Configuration on the In-cylinder of Small motorcycle engine", 2019 International Conference on Sustainable Energy Engineering and Application (ICSEEA), Tangerang, Indonesia, 2019, published in **IEEE *Xplore***, pp 33-36, 2019. (**SCOPUS)**

9. **Bambang Wahono**, Ardhika Setiawan, Ocktaeck Lim, "Study on the Effect of Intake Flow by Various Intake Port Design on Small Motorcycles Engine", 2020 5th International Conference on Smart and Sustainable Technologies (SpliTech), Split, Croatia, 2020, published in **IEEE *Xplore***, pp. 1-5, 2020. (**SCOPUS)**
10. **Bambang Wahono**, Ardhika Setiawan, Muhammad Khristamto Aditya Wardana, Ocktaeck Lim, "The Effect of Intake Port Inclination on In-Cylinder Flow of Small Motorcycle Engine", 11th International Conference on Applied Energy (ICAE2019), Sweden, 2019, published in ***Energy Proceedings***, Volume 5, Part 4, 2019.
11. Ardhika Setiawan, **Bambang Wahono**, Ocktaeck Lim, "A Study of Combustion Characteristics of Two Gasoline–Biodiesel Mixtures on RCEM Using Various Fuel Injection Pressures". ***Energies, MDPI***, 13, 3265, 2020. (**SCIE)**
12. Yanuandri Putrasari, **Bambang Wahono,** Ocktaeck Lim, "DME as the next generation fuel to control NOx and particulate matter emissions from IC Engines: A review", ***Applied Energy, Elsevier****, will be submitted (Status date 2020-11-09)*. (**SCI)**

B. LIST OF CONFERENCES

International Conferences

1. **Bambang Wahono,** Yanuandri Putrasari, Ocktaeck Lim, Faculty of Industrial Technology International Congress 2017 (FoITIC 2017), Bandung, Indonesia, 2017.
2. **Bambang Wahono**, Widodo Budi Santoso, Achmad Prpatijanto and Ock Taeck Lim, International Conference on Advanced Automotive Technology (ICAT) 2018, Gwangju, Republic of Korea, 2018.
3. **Bambang Wahono,** Kyeonghun Jwa, Octaeck Lim, International Conference of Applied Energy (ICAE) 2018, Hong-Kong, 2018.
4. **Bambang Wahono**, Ardhika Setiawan, Muhammad Khristamto Aditya Wardana, Ocktaeck Lim, 11th International Conference on Applied Energy (ICAE) 2019, Västerås, Sweden, 2019.
5. **Bambang Wahono,** Ardhika Setiawan, Ocktaeck Lim, Achmad Praptijanto, Yanuandri Putrasari, the 7th International Conference on Sustainable Energy Engineering and Application 2019 (ICSEEA 2019), Serpong, Indonesia, 2019.

6. **Bambang Wahono**, Ardhika Setiawan, Yanuandri Putrasari, Widodo Budi Santoso, Ocktaeck Lim, International Conference on Advanced Automotive Technology (ICAT) 2019, Gwangju, Republic of Korea, 2019
7. **Bambang Wahono**, Ardhika Setiawan, Ocktaeck Lim, 5th International Conference on Smart and Sustainable Technologies (Splitech 2020), Virtual 2020.
8. **Bambang Wahono**, Ardhika Setiawan, Ocktaeck Lim, 12th International Conference on Applied Energy (ICAE) 2020, Bangkok, Thailand, 2020

Domestic Conferences

1. **Bambang Wahono**, Yanuandri Putrasari, Ocktaeck Lim, Korea Hydrogen & New Energy Conference 2016 Fall Conference, Gwangju, 2016.
2. **Bambang Wahono**, Yanuandri Putrasari, Ocktaeck Lim, 2017 Annual Meeting of the Korean Society of Clean Technology, Westin Chosun Hotel Busan, 2017.
3. **Bambang Wahono** and Ocktaeck Lim, KSME 2017 Spring Conference at Ulsan Division, UNIST, Ulsan, Korea, 2017.
4. **Bambang Wahono** and Ocktaeck Lim, KSAE 2018 Annual Spring Conference and Exhibition, Busan, Korea, 2018.
5. **Bambang Wahono** and Ocktaeck Lim, KSAE 2018 Annual Autumn Conference, Changwon, Korea, 2018.
6. **Bambang Wahono** and Ocktaeck Lim, KSME 2018 Spring Meeting at Ulsan Division, University of Ulsan, Ulsan, Korea, 2018.
7. **Bambang Wahono,** Ardhika Setiawan and Ocktaeck Lim, KSAE 2019 Annual Spring Conference, Jeju, Korea, 2019.
8. **Bambang Wahono** and Ocktaeck Lim, KSAE 2019 Autum Conference, Gyoengju, Korea, 2019.
9. **Bambang Wahono**, Ardhika Setiawan and Ocktaeck Lim, KSAE 2020 Annual Spring Conference, Gangwondo, Korea, 2020.
10. **Bambang Wahono**, Ardhika Setiawan and Ocktaeck Lim, KSAE 2020 Annual Autumn Conference, Jeju, Korea, 2020.
11. **Bambang Wahono**, Ardhika Setiawan and Ocktaeck Lim KSAE 2020, Busan, Ulsan, and Gyeongnam, 2020.